

Signal Conditioning for High Efficiency Wireless Transmission

By
Abdul K Mustafa

Centre for Telecommunication and Micro-electronics
School of Engineering and Science

SUBMITTED IN FULFILLMENT OF THE
REQUIREMENTS FOR THE DEGREE OF
DOCTOR OF PHILOSOPHY
AT
VICTORIA UNIVERSITY
MELBOURNE, AUSTRALIA
JULY 2010

© Copyright by Abdul K Mustafa, 2011

VICTORIA UNIVERSITY

Electrical Engineering

“I, Abdul K. Mustafa, declare that the PhD thesis entitled **Signal Conditioning for High Efficiency Wireless Transmission** is no more than 100,000 words in length including quotes and exclusive of tables, figures, appendices, bibliography, references and footnotes. This thesis contains no material that has been submitted previously, in whole or in part, for the award of any other academic degree or diploma. Except where otherwise indicated, this thesis is my own work”.

Dated: July 2010

Author: _____
Abdul K Mustafa

Research Supervisor: _____
Prof. Mike Faulkner

To My Parents

Table of Contents

Table of Contents	iv
List of Figures	vi
List of Tables	xii
1 Introduction	1
1.1 The PA Problem	3
1.2 Problem Statement	5
1.3 Research Contribution	6
1.3.1 Other Contributions	8
1.4 Organisation of the Thesis	8
2 Literature Review	10
2.1 Amplifier Non-linearities	11
2.2 PAPR of Multicarrier Signals	14
2.2.1 Problems of PAPR:	16
2.3 Various PAPR reduction schemes	17
2.3.1 Peak Clipping	18
2.3.2 Coding	19
2.3.3 Active Constellation Extension	20
2.3.4 Tone Reservation	22
2.3.5 Selected Mapping(SLM)	23
2.3.6 Partial Transmit Sequence(PTS)	25
2.4 Modern Amplifiers and Linearization Schemes	28
2.4.1 Digital Predistortion	29
2.4.2 Doherty Amplifier	30
2.4.3 Switched Mode Power Amplifier	32
2.4.4 Linear Amplification using Non-linear Components (LINC)	34
2.4.5 Envelope Tracking	36
2.4.6 Envelope Elimination and Restoration (EER)	37

2.4.7	Current Literature on Bandwidth Limitation for EER . . .	40
2.5	Simulation Parameters	41
2.6	Summary	41
3	Bandwidth Reduction Schemes for EER Transmitters	43
3.1	Minimum Power PTS Signal	44
3.2	Bandwidth Limitation	48
3.3	Iterative Bandwidth limiter (IBL)	52
3.4	Iterative BW Limitation using PTS (IBL-PTS)	54
3.5	Repetitive Bandwidth Limitation with QAM Correction (RBL)	58
3.5.1	QAM Correction	64
3.6	Bandwidth Limiter with RF drive compensation (BLDC)	69
3.7	Summary	76
4	Theoretical Analysis of Hole Punch Method	80
4.1	Hole Punch	81
4.2	Error Analysis	84
4.2.1	Theory	84
4.2.2	Derivation of In-band and Out-of-band Power of Han- ning Window Function	87
4.2.3	Theoretical and Simulation Results	88
4.3	Summary	97
5	Bandwidth Reduction Schemes on LINC	100
5.1	Introduction	100
5.2	Explanation	101
5.3	Pre-conditioning: Bandwidth Reduction on the Polar Phase . .	104
5.4	Post-conditioning: Bandwidth limit on Unwrapped Phase . . .	108
5.5	Post-conditioning: Bandwidth Limit on Polar phase component	116
5.6	Measurement Results	120
5.6.1	USRP and GNU Radio	120
5.6.2	Test Setup	122
5.7	Summary	131
6	Conclusion and Future Research	135
6.1	Future Work	137
A	Complexity Calculation for IBL, IBL-PTS and RBL Schemes	138
	Bibliography	141

List of Figures

1.1	Progress in power amplifier efficiency. Courtesy - Ericsson . . .	4
1.2	Traditional (top) and proposed (bottom) transmitter architectures.	6
2.1	AM to AM and AM to PM characteristics model of a BFR91 Class A amplifier. The amplitude axes have been normalized to 1 [7]	12
2.2	Graphical representation of Error Vector	13
2.3	Block diagram of repeated clipping and filtering technique. . . .	19
2.4	Active Constellation Extension with QPSK signals	21
2.5	SLM Block Diagram	24
2.6	PTS Block Diagram	26
2.7	Different subblock partitioning schemes for PTS technique. (a) Adjacent (b) Interleaved (c) Pseudo random	27
2.8	Different subblock partitioning schemes for PTS technique. (a) Adjacent (b) Interleaved (c) Pseudo random	28
2.9	A basic predistortion block	30
2.10	Block diagram of a basic Doherty amplifier architecture	31
2.11	Demonstrating PWM (amplitude modulation) and PPM (phase modulation) concept. Edges occur on the digital timing grid. . .	33
2.12	The LINC architecture and signal vectors	34
2.13	Block diagram of a traditional ET architecture	36
2.14	Block diagram of EER architecture	37
2.15	Spectrum of OFDM and its Envelope and Phase components . . .	39

2.16	I & Q plot of a OFDM symbol (a) without hole punching and (b) hole punching enabled.	40
3.1	Block Diagram to choose minimum OOB Power Signal using PTS. The \tilde{x}_q is goes to input of Figure 2.13	45
3.2	Spectrum of Minimum Power PTS and OFDM Symbol. Note, the RF Spectrum and EVM are not effected.	46
3.3	CCDF of OFDM Signal and Minimum OOB Power PTS signal .	47
3.4	Block diagram of BW limit process	48
3.5	Spectrum of OFDM and polar components after Envelope bandwidth limitation at $B = 1$	50
3.6	Spectrum of OFDM and polar components after Phase bandwidth limitation. The small subplot showing a zoomed version of the bigger plot. The bigger plot showing the bandwidth improvement for phase component at -50 dB	51
3.7	Mean EVM of Envelope and Phase bandwidth limitation for different bandwidth limiting values	52
3.8	Block diagram of Iterative BW limit process	54
3.9	Spectrum of OFDM and polar components after IBL on the envelope signal.	55
3.10	Block diagram of Iterative BW Limit process using PTS.	55
3.11	Spectrum of OFDM and polar components after Envelope BW limitation using PTS, $Q = 4, M = 4, S = 64$	56
3.12	CDF of EVM for envelope and phase bandwidth limitation using iterative bandwidth limitation with and without PTS technique	57
3.13	Block diagram of repetitive bandwidth reduction.	59
3.14	Spectrum of repetitive bandwidth limited polar components for $B = 1$	60
3.15	Bandwidth improvement in envelope and phase spectrum at -50 dB for different i repetitions from original phase bandwidth of 15 channels and envelope bandwidth of 3.5 channels.	60

3.16	CDF of EVM for different i repetitions at envelope bandwidth limiting value of $B = 1$ channel bandwidth	61
3.17	Spectrum of OFDM RF signal after $i = 0, 1, 4, 8$ & 14 repetitions	62
3.18	EVM vs bandwidth limitation values for different i repetitions .	62
3.19	ACI 1 and ACI 2 vs bandwidth limitation values for different i repetitions	63
3.20	QAM correction process for EVM limitation. The original constellation point is (x_d, y_d)	65
3.21	Constellation points before and after QAM correction	66
3.22	Revised block diagram of Repetitive BW limit process with QAM correction included in the loop	67
3.23	Bandwidth improvement in envelope and phase spectrum at -50 dB for $i = 10$ repetitions with QAM correction enabled in the loop.	68
3.24	CDF of EVM for $i = 10$ repetitions at envelope bandwidth limiting value of $B = 1$ channel bandwidth and QAM correction enabled.	68
3.25	Block diagram of bandwidth limiter with amplitude compensation of the RF drive signal, s_p	70
3.26	The effect of bandwidth limiting the envelope signal to 0.1 channel bandwidth	72
3.27	The effect of bandwidth limiting the envelope signal to 4 channel bandwidth	72
3.28	Spectra of the input drive signal, s_p envelope signal, a , and OFDM RF signal, x	73
3.29	Efficiency against power output. PWM curves are for $V_{dd} = 30V$ (solid) and for $V_{dd} = 10V$ (dashed) and EER (solid) [63]	74
3.30	Predicted efficiency versus envelope bandwidth for an OFDM signal using BLDC and the measured amplifier of Figure 3.29. .	75
4.1	Block diagram of hole punch process.	83

4.2	The original signal x_k is limited to a minimum amplitude a_{th} by adding a residue signal z_k . The peak of z'_k is used to scale the window function	85
4.3	Spectrum of amplitude and phase signal with and without hole punching for Hanning window length of $V = 6$	90
4.4	Spectrum of amplitude and phase signal with and without hole punching for Gaussian window length of $V = 6, V' = 1.2V$	90
4.5	CDF of EVM for 10%, 20% and 30% of hole punch for Hanning and Gaussian window of length $V = 6$	91
4.6	In-band and out of band channels of the Hanning window for window lengths of $V = 2$ and $V = 6$ in the frequency domain.	93
4.7	P_{u_k} and EVM using Hanning window for 10% and 30% of Hole Punch with increasing window length.	94
4.8	ACI 1 and ACI 2 for 10% and 30% of Hole Punch with increasing window length.	95
4.9	Envelope and Phase bandwidth improvement at -40 dB using 10% and 30% hole punch with respect to increasing window length.	95
5.1	Spectrum of EER and LINC components.	102
5.2	Spectrum of OFDM and LINC component with no Phase part and vice-versa	103
5.3	I & Q diagram of $s_1(t)$ (a) before and (b) after bandwidth limitation	105
5.4	Block diagram of the pre-conditioning scheme for BW limitation of LINC architecture	105
5.5	Spectrum of OFDM and LINC components with pre-conditioning to reduce bandwidth expansion	107
5.6	CDF of EVM using pre-conditioning scheme	108
5.7	Time domain view of wrapped and unwrapped phase of s_1	109
5.8	Block diagram of the post-conditioning bandwidth limitation scheme with unwrapped phases	110

5.9	Effect of bandwidth limitation on unwrapped θ - spectrum of OFDM ($x_{in}(t)$), modified OFDM ($x'_{out}(t)$), $s_1(t)$ and $s'_1(t)$. . .	111
5.10	Effect of bandwidth limitation on unwrapped $\theta(t)$ - CDF of EVM for modified OFDM ($x'_{out}(t)$)	112
5.11	Spectrum of OFDM and s'_1 with bandwidth limitation and OOB correction	113
5.12	Revised block diagram of post-conditioning bandwidth limitation scheme with unwrapped phases and OOB correction	114
5.13	Spectrum of OFDM and s'_1 for different i values	114
5.14	CDF of EVM for x'_{out} for different i values	115
5.15	Block diagram of bandwidth limitation on the phase polar component with OOB correction	116
5.16	Effect of bandwidth limitation on the polar phase of LINC component. Spectrum of LINC component s_1 , BW limited LINC component s'_1 , input OFDM x_{in} and resulting BW limited OFDM x'_{out}	117
5.17	Effect of repetitive bandwidth limitation on polar phase of LINC component with OOB correction for resulting OFDM signal. Spectrum of s_1 , x_{in} , s'_1 and x'_{out} for $i = 1, 2, 3, 4$	118
5.18	CDF of EVM for modified OFDM signal x'_{out} . For repetition values of $i = 1, 2, 3, 4$	119
5.19	Motherboard of USRP1	121
5.20	Block diagram of test setup 1.	123
5.21	Spectrum of OFDM at the signal analyzer generated by a single USRP daughterboard.	123
5.22	Block diagram of test setup 2.	125
5.23	A screenshot of the GRC GUI showing the process of transmitting s_1 and s_2 simultaneously.	126
5.24	Spectrum of OFDM ($s_1 + s_2$) at the signal analyzer. Yellow line showing output from the combiner with no phase correction. The blue line is when the phase imbalance is corrected.	126

5.25	Block diagram of test setup 3.	127
5.26	I & Q plot of s_1 on the signal analyzer.	129
5.27	Spectrum of a signal at 400 MHz and the carrier leak caused by USRP which is 4 MHz away from the centre.	129
5.28	Spectrum of s_1 (blue line) and s'_1 (yellow line) at the signal analyzer.	130
5.29	Spectrum x'_{out} at the signal analyzer showing the distortion caused by the bandwidth limitation process.	131
A.1	Detailed flowchart of the IBL-PTS algorithm.	139

List of Tables

2.1	Performance comparison of Amplifiers. [6]	12
2.2	PAPR values of all possible data blocks for an OFDM signal with four subcarriers and BPSK modulation.	20
2.3	Simulation parameters	42
3.1	Summary of bandwidth reduction techniques on polar drive signals for the EER architecture. Bandwidths are normalized to 1 OFDM channel.	79
4.1	EVM and Envelope, Phase improvements with respect to channels	92
4.2	Effect of hole punch on ET, EER and polar CMOS amplifiers	96
4.3	Comparison of hole punch technique with bandwidth limitation schemes from Chapter 3	99
5.1	Effect of bandwidth limit on unwrapped phase with OOB correction for different values of i	116
5.2	Effect of bandwidth limit on Polar phase component with OOB correction for different values of i	119
5.3	Summary of bandwidth reduction techniques on constant amplitude signals of LINC architecture. Bandwidths are normalized to 1 OFDM channel.	133

List of Acronyms

3G	Third Generation
3GPP	3rd Generation Partnership Project
4G	Fourth Generation
ACI	Adjacent Channel Interference
ACMA	Australian Communications and Media Authority
ACP	Adjacent Channel Power
ADC	Analog to Digital Conversion
AET	Average Envelope Tracking
AM	Amplitude Modulation
BER	Bit Error Rate
BPSK	Binary Phase Shift Keying
BW	Bandwidth
CCDF	Complementary Cumulative Distribution Function
CDF	Cumulative Distribution Function
CDMA	Code Division Multiple Access
CF	Crest Factor
CMOS	Complementary Metal-Oxide-Semiconductor
D/A	Digital to Analog
DAB	Digital Audio Broadcasting
DAC	Digital to Analog Conversion
DC	Direct Current
DPD	Digital Pre-distortion
DSP	Digital Signal Processing
EER	Envelope Elimination and Resotration
ET	Envelope Tracking
EVM	Error Vector Magnitude
FCC	Federal Communications Commission
FFT	Fast Fourier Transform
FPGA	Field-Programmable Gate Array
GRC	GNU Radio Companion
GSM	Global Standard for Mobile
GUI	Graphical User Interface

HEMT	High electron mobility transistor
HPA	High Power Amplifier
I & Q	Inphase and Quadrature
i.i.d.	Independent and Identically Distributed
IBL	Iterative Bandwidth Limitation
IBL-PTS	Iterative Bandwidth Limitation using PTS
IDFT	Inverse Discrete Fourier Transform
IFFT	Inverse Fast Fourier Transform
LINC	Linear Amplification using Nonlinear Components
LO	Local Oscillator
LTE	Long Term Evolution
MPSK	Multiple Phase Shift Keying
OFDM	Orthogonal Frequency Division Multiplexing
OOB	Out of Band
PA	Power Amplifier
PAPR	Peak to Average Power Ratio
PDF	Probability Distribution Function
PEP	Peak Envelope Power
PM	Phase Modulation
PMEPR	Peak to Mean Envelope Power Ratio
PPM	Pulse Position Modulation
PRC	Peak Reduction Carrier
PTS	Partial Transmit Sequence
PWM	Pulse Width Modulation
QAM	Quadrature Amplitude Modulation
RBL	Repetitive Bandwidth Limitation
RF	Radio Frequency
RFPA	Radio Frequency Power Amplifier
RMS	Root Mean Square
SI	Side Information
SLM	Selected Mapping
SMPA	Switched Mode Power Amplifier
USB	Universal Serial Bus
USRP	Universal Software Radio Peripheral
WBET	Wide-Bandwidth Envelope Tracking
WiMax	Wired Interoperability for Microwave Access
WLAN	Wireless Local Area Network

List of Variables

$a(t)$	Amplitude signal
a_{max}	Maximum amplitude
A_{minOOB}	Amplitude signal with minimum OOB expansion
a_{rms}	RMS amplitude
a_{th}	Amplitude of the threshold value
$b_{m,q}$	weighting factors for PTS
B	Bandwidth limiting value
C	Frequency domain vector for Tone reservation
C_{IBL}	Complexity of IBL technique
C_{bl}	Complexity of bandwidth limitation operation
$e(t)$	Error vector for LINC component calculation
G	Constant gain of composite power amplifier
i	Number of iterations
j	Imaginary number
k	Sample index in time domain
L	Oversampling rate
M	Number of phase sequences for SLM and PTS
n	Sample index in frequency domain
N	Number of Subcarriers from OFDM
N_a	Number of Valleys/sec
$p(t)$	Polar phase signal
P_{in}	Power of the input signal before amplification
P_{out}	Power of the output signal after amplification
$p_s''(t)$	Modified phase of LINC component
P_{u_k}	Power of the correction signal for Hole Punch technique
P_{minOOB}	Phase signal with minimum OOB expansion
Q	Number of weighting factors
q	Weighting factor index
S	Total number of PTS sequences
s_p	RF drive signal for BLDC architecture
s_1, s_2	LINC components with constant envelope
s'_1, s'_2	Modified LINC components

t	variable for time domain signal
T	OFDM sample period
T_s	Sample Period
u	Envelope signal with phase compensation for BLDC architecture
u_k	Correction signal for hole punch process
V	Window length
w_h	Hanning window function
w_g	Gaussian window function
x_{in}	Input time domain signal
x_{out}	Output signal
x_k	Sampled time domain input signal
x'_k	Hole punched signal
x'_{out}	Modified output of the LINC BW reduction scheme
X	Data vector
X_n	Data symbols
y_k	Peak clipped signal for hole punch process
z_k	Residue signal after peak clipping for hole punch process
z'_k	Residue signal after peak detection process
θ	Angle of the input signal
θ_u	Unwrapped phase
Θ_u	FFT of unwrapped phase
μ	index of M

Abstract

Fourth generation (4G) mobile communication systems will need wider bandwidth channels and improved spectrum efficiency to achieve the specified LTE-advanced 100Mbps (mobile) and 1Gbps (fixed) wireless transmission target rate. The next generation of wireless basestations will also need to be powered from renewable sources, particularly in developing countries. A new generation of components, circuits, algorithms and transmission structures will therefore be required to meet the wider bandwidth and the lower energy requirements. This thesis addresses the transmitter chain, which dominates the basestation power budget. In particular we consider pre-conditioning algorithms for a new generation of high efficiency radio frequency power amplifiers (RFPA). Many 3G and post 3G architectures use orthogonal frequency division multiplexing (OFDM) modulation with high density transmission constellations to achieve high data rates. However, OFDM suffers from high peak to average power ratio (PAPR) problems. High efficiency power amplifiers and signal conditioning is required to operate effectively. Modern amplifier architectures using switch mode power amplifiers (SMPA) can achieve high efficiency and linearity (e.g. envelope elimination and restoration (EER) and linear amplification with nonlinear components (LINC)). However, the nonlinear operations involved with these architectures cause the bandwidth of the input OFDM signal to expand. This poses problems to some of the analogue processing blocks, and limits the modulation bandwidth of these very promising high efficiency schemes. The bandwidth expansion problem is the main focus of this thesis.

In this thesis, we firstly consider the EER architecture: originally proposed

by Khan. The Cartesian to polar conversions causes high bandwidth expansion for the envelope and phase drive signals. Five novel bandwidth limitation schemes are proposed in this thesis. The techniques are based on both distortionless and distortion based schemes. Among the schemes, the bandwidth limitation with RF drive signal compensation performs the best. The technique reduces the envelope bandwidth by 71%.

Secondly, we look at the only other technique that is available in current literature: the ‘hole punch’ scheme proposed by D. Rudolph. An in depth theoretical analysis of the hole punch method is described and important omissions from Rudolph paper are addressed and solutions to the omissions are provided. It is found that, most of the novel bandwidth limitation schemes proposed in this thesis perform similar or better than the hole punch method.

Lastly, the bandwidth expansion problem associated with the LINC architecture is discussed. Here, we identify the modulated signal’s phase component as the dominant cause of bandwidth expansion in the LINC architecture. Three novel bandwidth limitation schemes are proposed. The post-conditioning scheme outperforms other methods and manages to reduce the bandwidth of the constant amplitude LINC component by 69% with an acceptable inband distortion level. The thesis also provides measurement results for the best technique. The measured results are shown to be within 2 dB of the simulation predictions.

Acknowledgement

First of all, I thank Allah for giving me strength and ability to complete this thesis.

I would like to express my deep and sincere gratitude to Prof. Mike Faulkner for his unreserved guidance and support throughout the whole process of my thesis. I would also like to give thanks to Dr Roman Malyniak, he has spent lots of time to review and critique my thesis.

Initial stage of this research was partially funded by L.M. Ericsson (Sweden). I would like to thank Dr. Peter O'Landers for his support.

During this work I have collaborated with many colleagues for whom I have great regard, and I wish to extend my warmest thanks to all those who have helped and encouraged me with my work in the Centre for Telecommunication and Microelectronics. I would like to personally thank my good friends and colleague Waqas, Shabbir, Faizan, Rizwan, Micheal, Robabeh, Shahryar, Vandana and Mohammadreza.

Finally, the deepest gratitude would go to my beloved parents, two brothers and sister-in-law for their loving support. Without their encouragement and understanding it would have been impossible for me to finish this work.

Chapter 1

Introduction

From the end of last century, wireless communication has been a rapidly growing area. The rapid advances in multimedia applications involve more and more transmissions of data, audio and graphical files like images and video. In response to this demand the third Generation (3G) of wireless architectures has already been deployed, more and more wireless local area networks (WLAN) are being set up, and planning for the data centric wide area extensions, also known as long term evolution (LTE) or 3.8G, is well advanced .

Fourth generation (4G) mobile communication systems further advance these trends and will need wider bandwidth channels and improved spectrum efficiency to achieve the specified LTE-advanced 100Mbps (mobile) and 1Gbps (fixed) wireless transmission target rate. Hence, next generation systems need wider bandwidths and more sophisticated modulation schemes with a higher data carrying capacity. A new generation of components, circuits and transmission structures will therefore be required to meet the resulting tighter requirements on signal purity and wideband operation. All this must be achieved

with ever increasing expectations for a ‘green’ solution of low energy consumption. This thesis addresses one of the key components in the transmitter chain, the radio frequency power amplifier (RFPA).

Many 3G and post 3G architectures use orthogonal frequency division multiplexing (OFDM) modulation with high density transmission constellations such as 64-QAM (quadrature amplitude modulation with 64 points), important examples being LTE, LTE advanced and wired interoperability for microwave access (WiMax). OFDM uses a large number of sub-channels, and like any other multicarrier systems, suffers from a high Peak to Average Power Ratio (PAPR). Sometimes this is also called Peak to Mean Envelope Power Ratio (PMEPR) or Crest Factor (CF). PAPR, PMEPR and CF of an OFDM signal are defined as the ratio of the peak voltage to RMS voltage [1].

When an OFDM signal with high PAPR goes through a power amplifier (PA) it causes a significant amount of non-linear distortion since the PA works in the saturation region to get good power conversion efficiency. The non-linear distortion causes in-band distortion and out-of-band (OOB) radiation, for which we find performance degradations in the form of error vector magnitude (EVM) and adjacent channel interference (ACI) respectively. A linear PA with a large dynamic range is required to reduce the signal distortion. However, this linear PA has poor efficiency and is very expensive.

1.1 The PA Problem

The PA is an important component in the transmission chain. The linearity of the amplifier often defines the maximum data rate for the system and its power output defines the basestation coverage area. In addition, the PA often accounts for more than 40% of the whole transceiver power budget, forcing the use of larger and heavier batteries for a given talk time, and in some basestations, the use of air conditioners and bulky heat dissipating units [2]. Increasing the energy efficiency of power amplifiers is a key requirement of next generation wireless systems.

PAs have been well studied and developed since the early days of vacuum tubes and continued on throughout the modern era of solid-state transistors. Many classes of operation have been proposed, and the efficiency-linearity trade-off has been well understood.

Most of the early studies on PAs were for low frequency operation, from a few kHz to tens of MHz. With the exponential growth in cellular and wireless communications, modern power amplifier designers face a difficult task. Firstly, the carrier frequencies are now much higher (many GHz). Secondly, the linearity requirement has been significantly increased to accommodate many new and intricate modulation techniques and thirdly, the efficiency becomes much more critical with the smaller and lighter trend towards portable devices.

Figure 1.1 shows the efficiency graph of different amplifier structures over

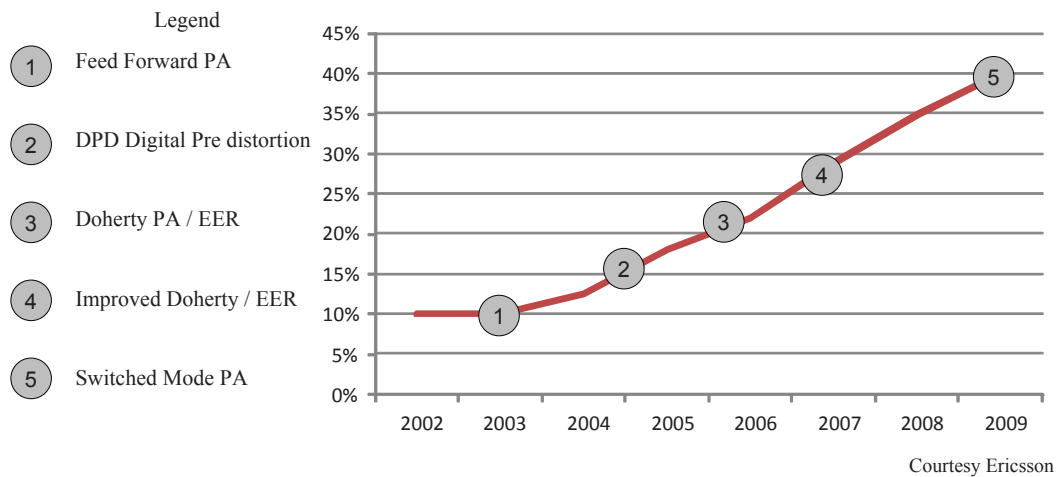


Figure 1.1: Progress in power amplifier efficiency. Courtesy - Ericsson

the last 8 years. The early designs allow non-linear operation of class AB amplifiers in order to improve power efficiency. The distortion products are then corrected by signal processing methods. Feed-forward amplifiers subtract the distortion products from the amplifier output in the RF domain. Digital predistortion (DPD) applies the correction signal to the input baseband signal in the DSP domain. The more recent techniques use less traditional amplifier structures such as Doherty, which uses two amplifiers, one of which is activated only on signal peaks, and envelope elimination and restoration (EER) and envelope tracking (ET). The latter two operate the amplifier in saturation over a wide dynamic range by modulating the amplifier's power supply. Further in the future there is the possibility of switching amplifiers that use pulse width modulation to eliminate all losses (theoretically). There is also the linear amplification with nonlinear components (LINC) and outphasing Chireix structures, which are attracting considerable research interest. These use the

sum of two constant envelope signals to reconstruct the desired transmission. Constant envelope signals have low distortion, because their 0 dB PAPR avoids the generation of AM to PM and AM to AM distortion.

Two of the emerging high efficiency amplifier structures, EER and LINC require specialised drive signals. These signals are a result of a non-linear transform, which is normally performed in the DSP and outputted to the amplifiers through the normal D/A process. The non-linear nature of these drive signals mean that they can have a bandwidth much larger than the original input signal, posing problems to some the following analogue processing blocks, and limiting the modulation bandwidth of these very promising high efficiency schemes. The bandwidth expansion problem is the focus of this thesis.

This work formed the preconditioning section of an all new digital basestation architecture using EER and LINC high efficiency (switching) amplifiers. The project was partially funded by L.M. Ericsson (Sweden) with the requirements of 1) 100W output power 2) 100 MHz bandwidth and 3) 100% efficiency! for a basestation system. Figure 1.2 shows the all new digital architecture (bottom) compared to the traditional structures (top). The work in this thesis is on the first block, the signal preconditioning unit.

1.2 Problem Statement

In order to reduce the bandwidth expansion problem, we have formulated different ways of preconditioning the input signal so it has less bandwidth at

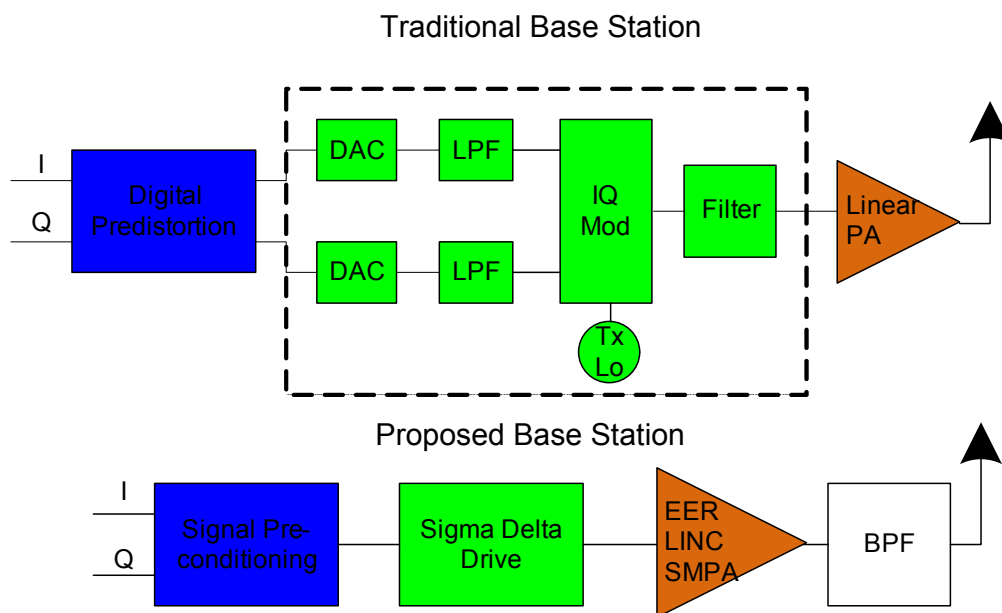


Figure 1.2: Traditional (top) and proposed (bottom) transmitter architectures.

the power amplifier. All the signal conditioning is done in the DSP part of the transmitter. The resulting tradeoff of bandwidth reduction and distortion caused by preconditioning has also been investigated thoroughly. The inband distortions are quantified as EVM and out of band distortions are quantified as adjacent channel interference (ACI).

1.3 Research Contribution

This research has led to the following contributions:

1. A. K. Mustafa and Mike Faulkner, "Theoretical Analysis of Hole Punch Signal Conditioning for High Efficiency EER Power Amplifiers," *EURASIP Journal on Wireless Communications and Networking*, vol. 2010, Article ID 250949, 8 pages, 2010.

2. V. Bassoo, K. Tom, A. K. Mustafa, E. Cijvat, H. Sjoland, M. Faulkner, "A potential transmitter architecture for future generation green wireless base station," *EURASIP Journal on Wireless Communication and Networking*, vol. 2009, Article ID 821846, 8 pages, 2009.
3. A. K. Mustafa, M. Faulkner, "Bandwidth limitation for the constant envelope components of a LINC architecture", in preparation for journal submission.
4. A. K. Mustafa, M. Faulkner, "Repetitive Fixed Bandwidth Limitation and QAM correction for EER Power Amplifier," *2010 IEEE Wireless Communications and Networking Conference (WCNC)*, pp.1-5, 18-21 April 2010.
5. A. K. Mustafa, V. Bassoo, M. Faulkner, "Reducing the Drive Signal Bandwidths of EER Microwave Power Amplifiers," *International Microwave Symposium Digest, 2009. MTT '09. IEEE MTT-S*, pp.1525-1528, 7-12 June 2009.
6. A. K. Mustafa, M. Faulkner, "Iterative Bandwidth Limitation for High Efficiency EER Power Amplifier," *4th International Symposium on Wireless Pervasive Computing, 2009. ISWPC 2009*, pp.1-5, 11-13 Feb. 2009.
7. V. Bassoo, K. Tom, A. K. Mustafa, E. Cijvat, H. Sjoland, M. Faulkner,

“Potential Architecture for Future Generation ‘Green’ Wireless Base Station,” *4th International Symposium on Wireless Pervasive Computing, 2009. ISWPC 2009*, pp.1-5, 11-13 Feb. 2009.

1.3.1 Other Contributions

Although it is not directly related to this thesis, it is worth mentioning the following publication which was published in an international conference:

1. V. Bassoo, A. K. Mustafa, M. Faulkner, ”Distortion Arising from Polar to PWM/PPM Conversion in an All Digital Upconverter for Switching RF Power Amplifier,” *International Microwave Symposium 2009*, June 2009.

1.4 Organisation of the Thesis

In Chapter 2, the background knowledge needed for this thesis is provided. The chapter describes the basic nonlinearities in the power amplifier, PAPR issues associated with the modern modulation schemes, and brief description of the current literature in bandwidth reduction schemes for EER architectures.

Chapter 3 describes four novel bandwidth reduction techniques developed in this thesis. These techniques were inspired by popular schemes used for PAPR reduction. The work in this chapter was responsible for five publications.

Chapter 4 looks in more detail at the hole punch method presented by

other authors. The contributions from this chapter include the performance of different window functions and a thorough mathematical analysis of the EVM and ACI generated by the correction signal in the hole punch process. The work from this chapter resulted in one journal publication.

The work in Chapter 5 is related to the LINC architecture. The architecture is more suitable for wideband signals because there is no high power envelope modulation. However, the two phase modulated drive signals still have bandwidth expansion and limit the modulation bandwidth. This chapter introduces different bandwidth limitation schemes and shows measurement results.

Finally, the findings from this thesis are summarized in Chapter 6. The best scheme is identified and future research is proposed.

Chapter 2

Literature Review

In this chapter, we review the background knowledge needed for this thesis. There are few publications: only three to my knowledge ([3, 4, 5]) directly related to signal conditioning for the new switch-based power amplifier architectures currently being researched. All three are based on the ‘Hole punch technique’ and none of them contain any theoretical analysis or measurement results. The hole punch scheme will be discussed later in this chapter and also in Chapter 4: where the provided mathematical analysis is one of the contribution of this thesis. However most of the schemes proposed in this thesis borrow heavily from existing PAPR reduction methods and so these will be reviewed along with the new amplifier structures being considered.

In the next section, a brief review of basic amplifier non-linearities is provided and it is shown how the distortion they generate can be minimised by reducing the envelope variations of the signals they work on. Reduction of signal dynamic range is key to high efficiency operation of RF PA’s. This is followed (Section 2.2) by a more comprehensive study of peak to average ratio

and various PAPR reduction schemes (Section 2.3) , that can be applied to multi-carrier / multi-code modulations. PAPR signal conditioning schemes are not the only method for reducing the signal dynamics in an amplifier. Amplifier topologies can be altered such that the amplifier is always operated in saturation (its most efficient state), and two of these structures will be discussed in detail in Section 2.4.

2.1 Amplifier Non-linearities

Radio frequency power amplifiers are separated into different classes of operation, based on the biasing conditions and circuit topologies. Table 2.1 [6] shows a comparison of fidelity and efficiency of very well known analog amplifiers and Class D digital switched mode amplifier. They are all subject to the same distortion mechanisms which to a first approximation can be modelled as an AM to AM distortion and an AM to PM distortion, Figure 2.1. Saturation of the output voltage leads to a signal dependant gain (AM to AM) and the compression at high signal level is clearly visible. A non-constant phase indicates the generation of AM to PM distortion [7]. These distortions cause in-band errors in the transmitted signal, measured by the error vector magnitude (EVM) and out-of-band interference which shows up as adjacent channel interference (ACI). Figure 2.2 and the following equation explains the EVM calculation.

Table 2.1: Performance comparison of Amplifiers. [6]

Class	Fidelity	Efficiency	Volume
A	Excellent	25%-30%	X-Large
B	Fair	70%-80%	Large
AB	Good	Between A and B	Fair
D	Bad	100% (Theoretical)	Small

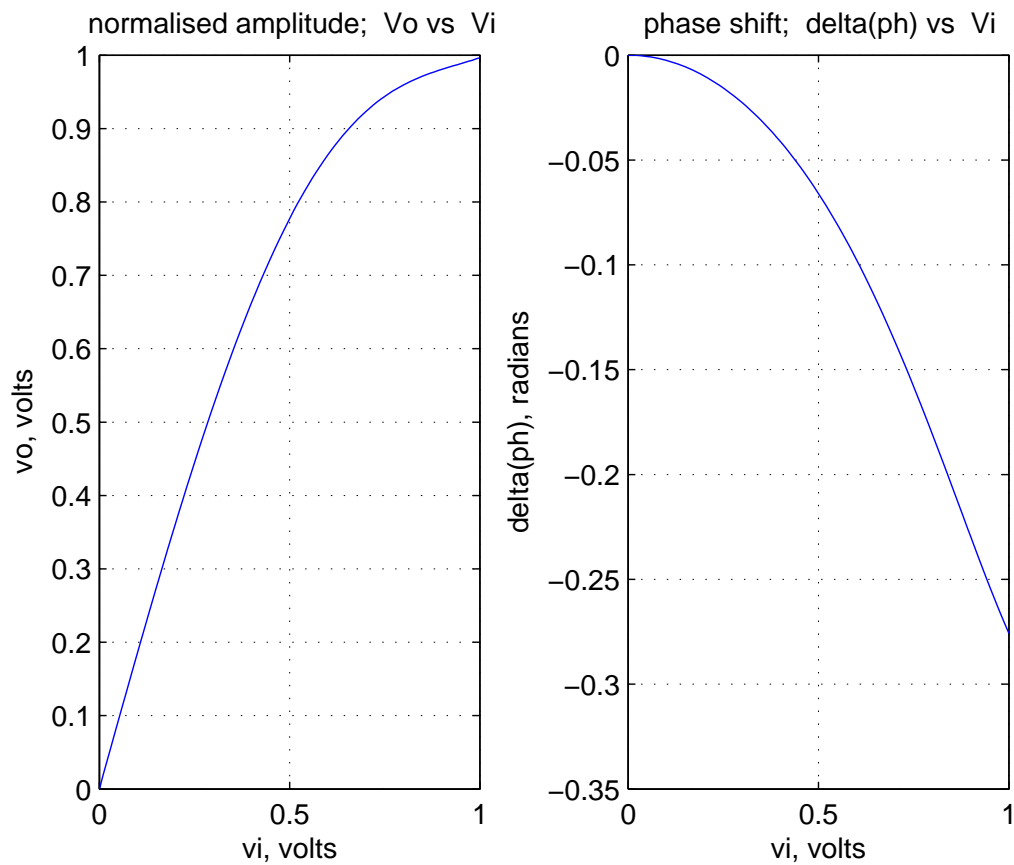


Figure 2.1: AM to AM and AM to PM characteristics model of a BFR91 Class A amplifier. The amplitude axes have been normalized to 1 [7]

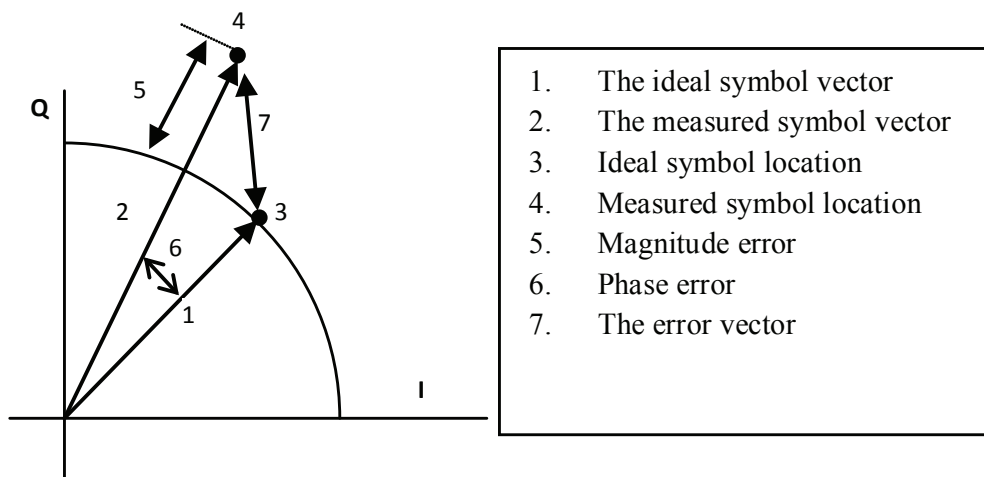


Figure 2.2: Graphical representation of Error Vector

$$EVM = \frac{\frac{1}{N} \sum_{n=1}^N |X_n - X'_n|^2}{\frac{1}{N} \sum_{n=1}^N |X_n|^2} \quad (2.1)$$

where X_n is the ideal symbol and X'_n is the measured symbol with total N number of unique symbols in the constellation.

EVM and ACI requirements are defined by the appropriate wireless standard. An additional requirement is a high dc power conversion efficiency ($\frac{P_{out}(rf)}{P_{in}(dc)}$). Amplifiers operating at saturation are normally in their most efficient state. Modulated signals are hardly ever in this state, since their average power is much less than their peak power. Efficiency reduces with signal back-off from peak (saturated) power, which presents a problem for signals with high PAPR.

A number of techniques have been developed to meet the wireless standards while maintaining high efficiency.

- Constant envelope modulations can be used. They carry their information in the signal phase and so have no AM component, and do not generate distortion in the amplifier. FM radio and GSM mobile standards use this approach. Unfortunately they have low spectral efficiency.
- Linearisation can be used. Amplifiers are allowed to generate distortion, which is then cancelled using external circuits.
- Signal conditioning schemes can be used for reducing the PAPR
- New PA architectures structure the signal in such a way that the amplifier operates in saturation all the time. The processing of these signals are nonlinear and this generates other problems: discussed in the last section of this chapter.

2.2 PAPR of Multicarrier Signals

Any multicarrier signal, for example, OFDM, with a large number of subchannels has a large peak to average power ratio (PAPR); sometimes also known as peak to mean envelope power ratio (PMEPR), or a crest factor (CF)¹. These are defined as the ratio of the peak voltage to the RMS voltage.

A multicarrier signal is a sum of many independent signals modulated onto subchannels of equal bandwidth. A data block is a collection of data

¹For a baseband signal, PAPR, PMEPR and CF are the same. However, for a bandpass signal with a carrier frequency larger than signal bandwidth, PAPR and PMEPR is 3 dB less than CF

symbols $X_n, n = 0, 1 \dots N - 1$, described as a vector $X = [X_0, X_1 \dots X_{N-1}]^T$ [8]. The complex baseband representation of a *multicarrier* signal, consisting of N subcarriers in the time domain, is given by

$$x(t) = \frac{1}{\sqrt{N}} \sum_{n=0}^{N-1} X_n e^{j2\pi\Delta f t}, 0 \leq t \leq NT, \quad (2.2)$$

where $j = \sqrt{-1}$, Δf is the subcarrier spacing, and NT denotes the useful data block period. In OFDM the subcarriers are orthogonal, i.e., $\Delta f = 1/NT$ and T is the sample period.

In this thesis uniform oversampling is used. The oversampling rate is denoted by L , giving rise to NL equidistant samples in an OFDM symbol. The time domain signal samples are represented as a vector $x = [x_0, x_1, \dots, x_{NL-1}]^T$ and is given by [8].

$$x_k = x(kT/L) = \frac{1}{\sqrt{N}} \sum_{n=0}^{N-1} X_n e^{j2\pi kn\Delta f T/L}, k = 0, \dots, NL - 1 \quad (2.3)$$

The PAPR of a signal is the ratio of the maximum peak power and the average power of the signal. The PAPR can be described as

$$PAPR = \frac{\max_{0 \leq t \leq NT} |x(t)|^2}{\frac{1}{NT} \int_0^{NT} |x(t)|^2 dt} \quad (2.4)$$

Theoretically, the difference between a multicarrier signal and single carrier signal in terms of PAPR is denoted as

$$\Delta(dB) = 10 \log N \quad (2.5)$$

When the number of subcarriers, N is 1000, The equation 2.5 makes the difference in PAPR 30 dB. But as OFDM data is well scrambled, it is very rare for the above value to reach this limit [9, 10]. OFDM signals can be treated as a series of independent and identically distributed (i.i.d) modulated carriers. Therefore, it follows from the central limit theorem [11] that the OFDM signal distribution tends to be Gaussian when N is large. When N is greater than 20, the OFDM distribution resembles a Gaussian distribution.

2.2.1 Problems of PAPR:

- To prevent spectral growth of the multicarrier signal in the form of inter modulation among subcarriers and out of band (OOB) radiation, the transmit PA should operate in a linear region, which requires a large input backoff at the PA. This is not a desirable feature for mobile devices, as, it reduces the battery life significantly [8]. Consequently, in some applications the effect of a high PAPR might overshadow the benefits of the multicarrier transmission technique.
- Due to the high peak power of the OFDM signals, the dollar cost of PA increases. The cost of the PA is set by the peak power, not the average power.
- The high peak-to-average power ratio of the OFDM modulation scheme also requires highly linear upconverters that must handle the peak signal without producing distortion. This means that the upconverters

must have a high-level compression point, which results in larger devices, higher supply voltage, and higher quiescent currents. Subsequently, DC power consumption also increases.

- Regulatory bodies, such as ACMA² and FCC³ can force a reduction in transmit power when power limits for the band are based on the maximum peak power of the signal.

2.3 Various PAPR reduction schemes

There has been a lot of published work on PAPR reduction. The PAPR reduction schemes can be classified in two categories: those that generate distortion and those that are distortionless. The simplest form of PAPR reduction is amplitude clipping, where the signal is clipped at some certain amplitude thresholds. Deliberate clipping of the signal results in signal distortion. A problem of this technique is that it results in peak regrowth after filtering [1, 12]. Well known distortionless techniques include the use of coding, partial transmit sequence (PTS) and selected mapping (SLM). Coding can be used for PAPR reduction where a limited set of code words are chosen with low PAPR from the set of all possible code words. This requires an extensive search to find the codes that have low peaks [13, 14]. In SLM, a set of different sequences are produced which represent the same information as the input data block: one

²Australian Communications and Media Authority

³Federal Communications Commission

with the lowest PAPR is transmitted. The disadvantage of this technique is that it requires more inverse fast Fourier transform (IFFT) operations and also the receiver needs to receive side information (SI) in order to select the correct decoding signal [15, 16]. PTS method is similar to the SLM technique, except the sequences are generated in the time domain rather than the frequency domain as in SLM [17]-[21]. The performance of both schemes are similar, but PTS is simpler and often used as reference for different PAPR reduction proposals. The above techniques are discussed in more details in the following subsections.

2.3.1 Peak Clipping

Amplitude clipping is one of the most basic PAPR reduction schemes. In this method, the amplitude is forced to saturate when it goes above a certain threshold value [22]. Mathematically, it can be visualized from the following equation:

$$x'(t) = \begin{cases} x(t), & |x| \leq a_{th} \\ a_{th}e^{j\theta(t)}, & |x| > a_{th} \end{cases} \quad (2.6)$$

where, $x(t)$ is the input signal and a_{th} is the threshold value above which the clipping occurs. However, peak clipping causes in-band distortion as well some out of band spectral regrowth. This distortion is often quantified as the signal to clipping noise ratio. To mitigate this problem, a filtering operation is performed. Although, the filtering reduces the OOB emissions and smoothens the in-band clipping noise, it results in some peak regrowth. To compensate for

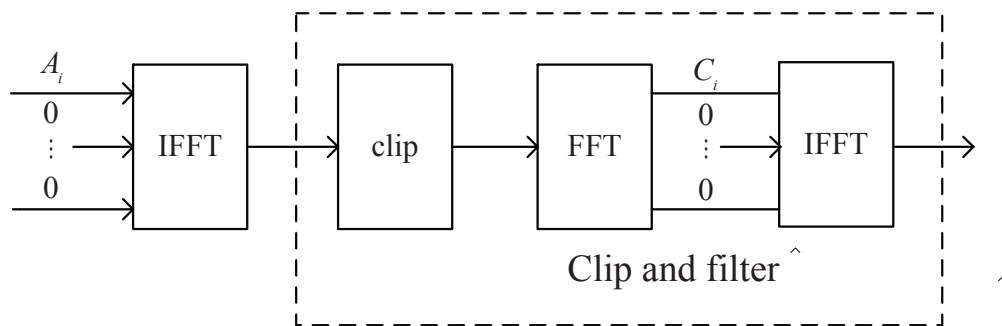


Figure 2.3: Block diagram of repeated clipping and filtering technique.

this a repetitive clip-filter-clip structure is employed in [1, 12]. Figure 2.3 shows the block diagram of the process. The results show that, with repetition the signal to clipping noise ratio is improved; although the improvement saturates after a certain number of repetitions. This architecture inspired some of the techniques that have been proposed in this thesis for bandwidth reduction.

2.3.2 Coding

Coding technique can also be used on the data signals to decrease PAPR. The idea is to select the code-words that have low PAPR [13, 14]. As an example: the peak envelope power (PEP) for all possible data blocks of an OFDM signal with four subcarriers and binary phase shift keying (BPSK) modulation is shown in Table 2.2. It can be seen from this table that four data blocks result in a PAPR of 6.0 dB, and another four data blocks result in a PAPR of 3.7 dB. It is clear that coding can reduce PAPR by avoiding transmitting those sequences: in which case the PAPR will remain constant at the minimum level of 2.3 dB.

Table 2.2: PAPR values of all possible data blocks for an OFDM signal with four subcarriers and BPSK modulation.

Data Block X	PAPR (dB)	Data Block X	PAPR (dB)
$[1, 1, 1, 1]^T$	6.0	$[1, 1, 1, 1]^T$	2.3
$[1, 1, 1, -1]^T$	2.3	$[1, 1, 1, 1]^T$	3.7
$[1, 1, -1, 1]^T$	2.3	$[1, 1, 1, 1]^T$	6.0
$[1, 1, -1, -1]^T$	3.7	$[1, 1, -1, -1]^T$	2.3
$[1, -1, 1, 1]^T$	2.3	$[-1, -1, 1, 1]^T$	3.7
$[1, -1, 1, -1]^T$	6.0	$[-1, -1, 1, -1]^T$	2.3
$[1, -1, -1, 1]^T$	3.7	$[-1, -1, -1, 1]^T$	2.3
$[1, -1, -1, -1]^T$	2.3	$[-1, -1, -1, -1]^T$	6.0

The main problems of coding are:

- The approach suffers from the need to perform an exhaustive search to find the best codes.
- The approach requires a large lookup tables for encoding and decoding, especially if there is a high number of subcarriers.
- It is possible to obtain some error correction capability from the coding scheme, but the performance is well below par.

2.3.3 Active Constellation Extension

The technique extends some of the outer signal constellation points of the data block. The process is done dynamically such that the PAPR of the data block is reduced. For explanation purposes, consider a a multicarrier signal which is quadrature phase shift keying (QPSK) modulated. Each subcarrier has four

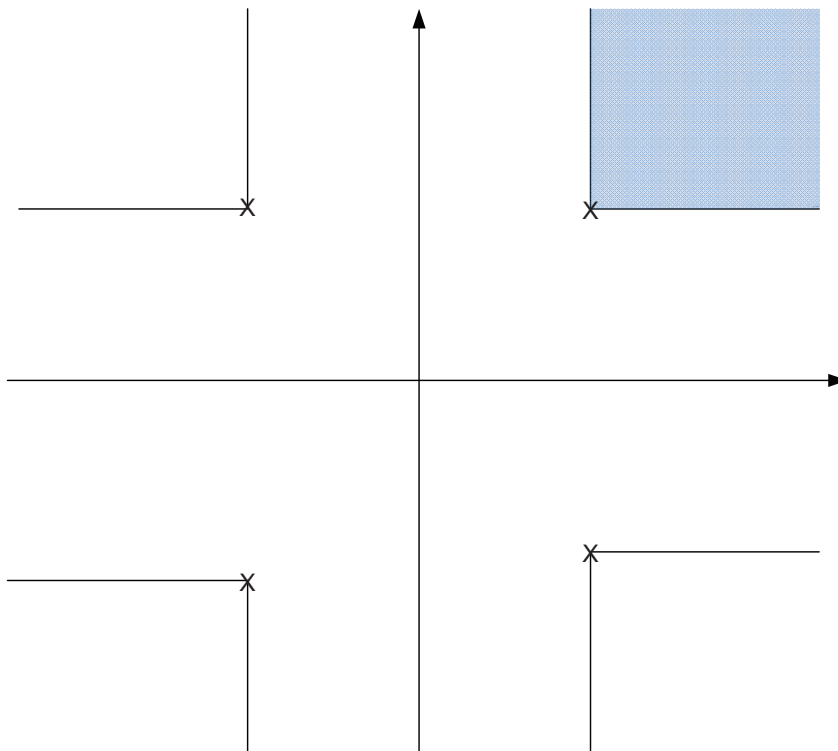


Figure 2.4: Active Constellation Extension with QPSK signals

possible constellation points that lie in each quadrant on the complex plane and are equidistant from the real and imaginary axes. Assuming white Gaussian noise, the maximum likelihood decision regions are bounded by the real and imaginary axes. Any point that is farther from the decision boundaries than the nominal constellation point will offer increased noise margin and lower bit error rate (BER). From this concept, it is understood that there will be no degradation in performance by modifying the constellation points within the quarter -plane outside of the nominal constellation points [8, 23].

This process can be viewed from Figure 2.4, where the shaded region represents the region of increased noise margin for the data symbol in the first

quadrant. If the process is done properly, a combination of these additional signals can be used to partially cancel time domain peaks in the transmit signal. The same principle can be applied not only to QPSK, but also to other modulation schemes, such as QAM and MPSK. This scheme simultaneously decreases the BER slightly while reducing the peak magnitude of a data block. In addition, there is no loss in the data rate and no additional information is required for the data decoding purpose. The only drawback is that the modification increases the transmit signal power and the usefulness of this scheme is rather restricted for a modulation with large constellation size.

2.3.4 Tone Reservation

Tone reservation is a technique to reduce the PAPR by adding a data-block-dependent time domain signal to the original signal. The time domain signal can be easily computed at the transmitter and stripped off at the receiver. In this technique, the transmitter does not send data on a small subset of subcarriers that are optimized for PAPR reduction [24]; instead it tries to find the time domain signal to be added to the original signal x such that the PAPR is reduced. By adding a frequency domain vector $C = [C_0, C_1, \dots, C_{N-1}]^T$ to X , the new time domain signal can be represented as $x + c = IDFT\{X + C\}$, where c is the time domain signal due to C and IDFT stands for inverse discrete Fourier transform. The tone reservation technique restricts the data block X and peak reduction vector C to lie in disjoint frequency subspaces

(i.e., $X_n = 0, n \in i_1, i_2, \dots, i_K$ and $C_n = 0, n \notin i_1, i_2, \dots, i_K$). The K nonzero positions in C are called peak reduction carriers (PRCs). Since OFDM has orthogonal subcarriers, the additional signals do not cause any distortion to the data bearing subcarriers. The procedure to solve the values of $C_n, n \in i_1, i_2, \dots, i_K$ is a complex optimization problem that can be easily cast as a linear programming problem. To reduce the complexity of linear programming, a simple gradient algorithm is also proposed in [24]. In wireless systems, there are unused subcarriers (eg. WLAN 802.11g has 48 data tones out of 64 subcarriers) that can be utilized for tone reservation scheme.

2.3.5 Selected Mapping(SLM)

In SLM, the transmitter generates a different set of candidate data blocks, all representing the same information as the original data block, and selects the best one for transmission [8].

In other words, M statistically independent sequences are generated from the same information. The sequence with the lowest PAPR is chosen for transmission.

Let $X = [X_0, X_1, \dots, X_{N-1}]$ represent a data block and there are M number of phase sequences of length N such that $Q^{(\mu)} = [Q_0^{(\mu)}, Q_1^{(\mu)}, \dots, Q_{N-1}^{(\mu)}], \mu = 1 : M$ where $Q_k^{(\mu)} = e^{j\phi_k^{(\mu)}}$, $k = 0, 1, \dots, N - 1$ with $\phi_k^{(\mu)}$ is uniformly distributed over $[0, 2\pi)$. Multiplying X element wise with $Q^{(\mu)}$ produces M candidates.

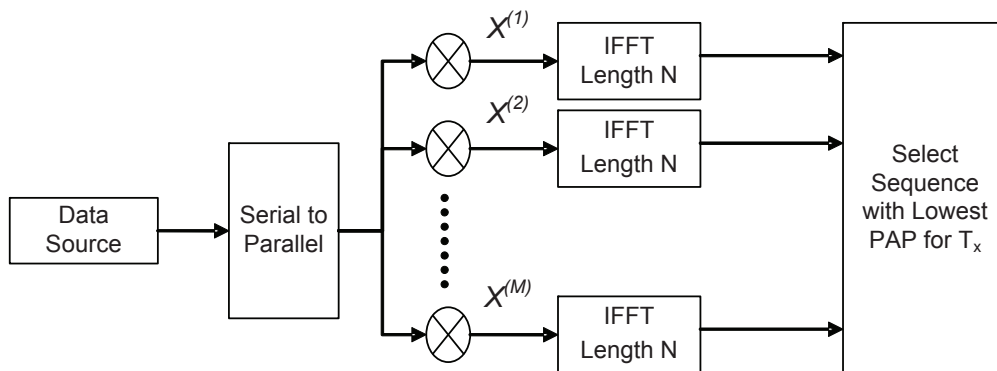


Figure 2.5: SLM Block Diagram

$$X^{(\mu)} = [Q_0^{(\mu)} X_0, Q_1^{(\mu)} X_1, \dots, Q_{N-1}^{(\mu)} X_{N-1}], \mu = 1 : M \quad (2.7)$$

Using M , N point inverse discrete Fourier transform (IDFT) yields the time domain signal:

$$x^{(\mu)} = [x_0^{(\mu)}, x_1^{(\mu)}, \dots, x_{N-1}^{(\mu)}], \mu = 1 : M \quad (2.8)$$

Then from all the M different frames the one with the lowest PAPR is selected for transmission. The process can be viewed from Figure 2.5.

Problems with SLM:

- It requires more IDFT operations. Normally it would require a N -point IDFT operation for OFDM signal. But this case requires M number of N -point IDFT operations, i.e. $M.N$ number of IDFT operations.
- The technique also requires some side information (SI) to send to the receiver side in order to decode the signal. For SLM, the SI is the sequence that the transmitter has used in order to determine the lowest

PAPR. Recent studies have tried to overcome this by using scrambling operation [25].

2.3.6 Partial Transmit Sequence(PTS)

Similar to SLM, the PTS technique reduces PAPR by introducing some redundancy. Here the input data is partitioned into disjoint subblocks or clusters. Then these subblocks are combined with different phase rotations to generate multiple sequences of the same data stream. The stream with the lowest PAPR is chosen for transmission [17]-[21].

We defined the data block, $X_n, n = 0, 1, \dots, N - 1$, as a frequency domain vector. Then we partition the data into M disjoint sub-blocks of $X_{n,m}$ such as in [17, 19]. After the IFFT a new set of signal vectors can be generated using a set of complex weighting factors, $b_{m,q}$, where m is the sub-block index and $q = 1 : Q$ is the weighting factor index.

$$x_k = \sum_{m=1}^M b_{m,q} x_{k,m}, \text{ where } b_q = \exp\{j\phi_q\}, \phi = [0, 2\pi) \quad (2.9)$$

Q is the number of possible phase rotations weighting each sub-block, giving a total of $S = Q^{M-1}$ number of waveforms or trials. In the simulations we use $M = 4$ sub-blocks and a set of $Q = 4$ ($[\pm 1, \pm j]$) phase rotations which yields 64 trials.

$$X' = \sum_{m=1}^M b_m X_m, m = 1, 2, \dots, M \text{ where } b^{(k)} = e^{j\phi^{(k)}} \quad (2.10)$$

Figure 2.6 shows the block diagram of PTS scheme. The PAPR can be minimized by exhaustive search for an appropriate combination of each subblock

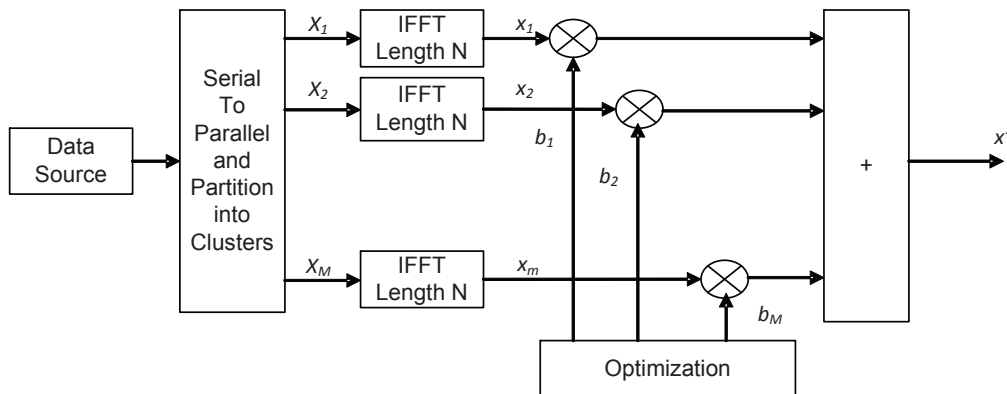


Figure 2.6: PTS Block Diagram

with the phase rotation factors. So, in the time domain, the optimized signal can be expressed as

$$x' = \sum_{m=1}^M b_m x_m \quad (2.11)$$

Different Subblock Partitioning scheme for PTS:

The sub-vector segmentation method has three types: adjacent segmentation, interleaved segmentation and pseudo-random segmentation. Segmentation methods are depicted in Fig 2.7. They all follow the principle: every sub-carrier can only appear in one PTS subblock, and all subblocks contain an equal number of sub-carriers.

The different subblocking scheme results in different PAPR reductions. The reduction is mainly decided by autocorrelation of each sub-vector. An Interleaved and adjacent subblocking scheme has higher autocorrelation which causes a mutual disturbance when the peak value is eliminated. However, for

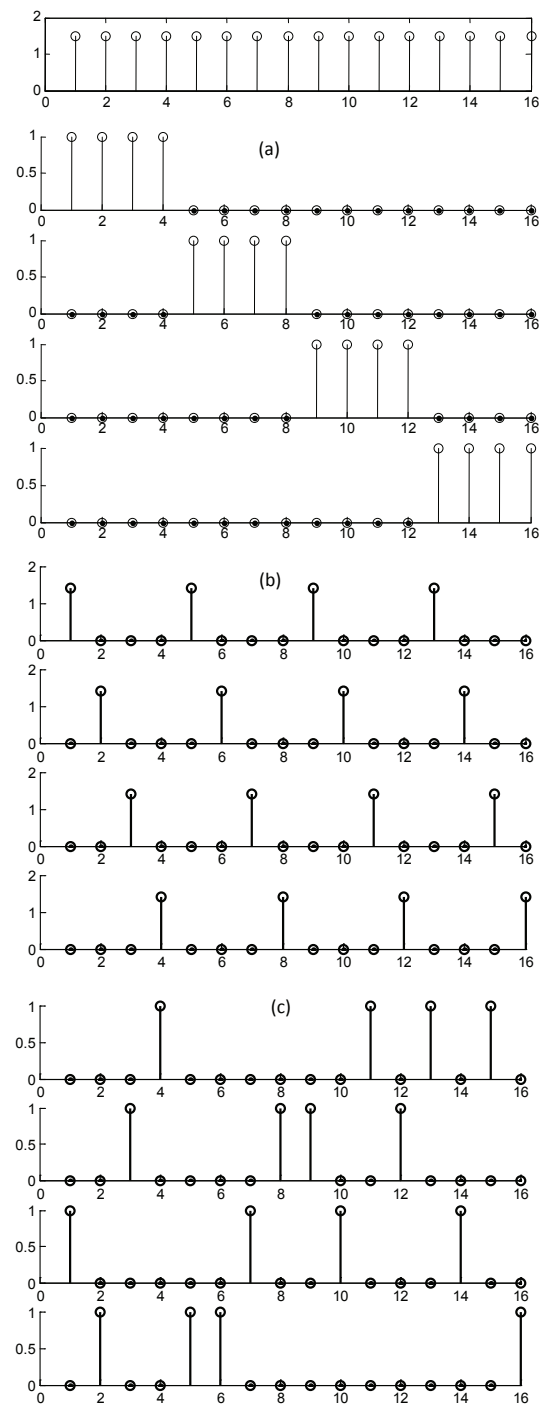


Figure 2.7: Different subblock partitioning schemes for PTS technique. (a) Adjacent (b) Interleaved (c) Pseudo random

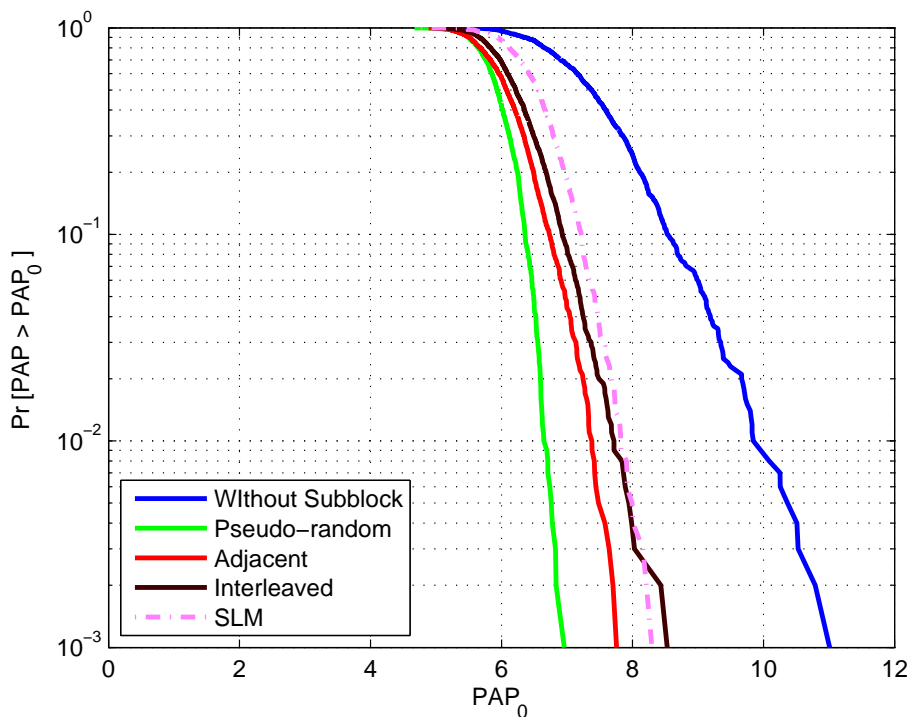


Figure 2.8: Different subblock partitioning schemes for PTS technique. (a) Adjacent (b) Interleaved (c) Pseudo random

the pseudo-random scheme the autocorrelation is lowest after the IFFT computation, therefore, the PAPR reduction is better than the other two techniques.

Figure 2.8 shows the complementary cumulative distribution function (CCDF) of PAPR for SLM and three different schemes of PTS. The SLM technique is on par with the adjacent segmentation scheme. Extensions to the basic PTS scheme include, the addition of cyclic phase shifting [17] to further increase the number of phase variations.

2.4 Modern Amplifiers and Linearization Schemes

Linearization schemes can be divided into two categories based on the PA used.

Firstly, the schemes based on the conventional PAs. These PAs are linear in

nature over a large output range where it is most efficient. Power amplifiers of Class -AB, -B and -C are included in this category. The popular linearization schemes for these types of PAs are polar and cartesian feedback [26, 27, 28], feedforward [29, 30] and predistortion techniques [31, 32].

On the other hand, the second category of linearization employs switching power amplifiers that are highly non-linear, for their inherently higher efficiency, while manipulating the overall system to achieve the required linearity. This category includes envelope elimination and restoration (EER) [28, 33, 34], envelope tracking (ET) [35, 36, 37, 38] and linear amplification using nonlinear components (LINC) [2], [28], [39]-[49]. This category is the main focus of this thesis and will be discussed at the end of this chapter.

The current state of the art for cellular basestation transmitters is based on digital predistortion (DPD) using the Doherty amplifier architecture [50]-[55]. This amplifier setup uses a combination of the linear amplifiers to get high efficiency over a large dynamic range. This structure along with the DPD will be briefly described in the next subsections.

2.4.1 Digital Predistortion

The digital predistortion (DPD) is a popular technique that allows minimizing output distortion and spectral regrowth. The scheme also maximizes power efficiency by digitally processing the input signal to produce a highly linear output [31, 32]. In theory, the nonlinear behaviour of the PA can be modelled

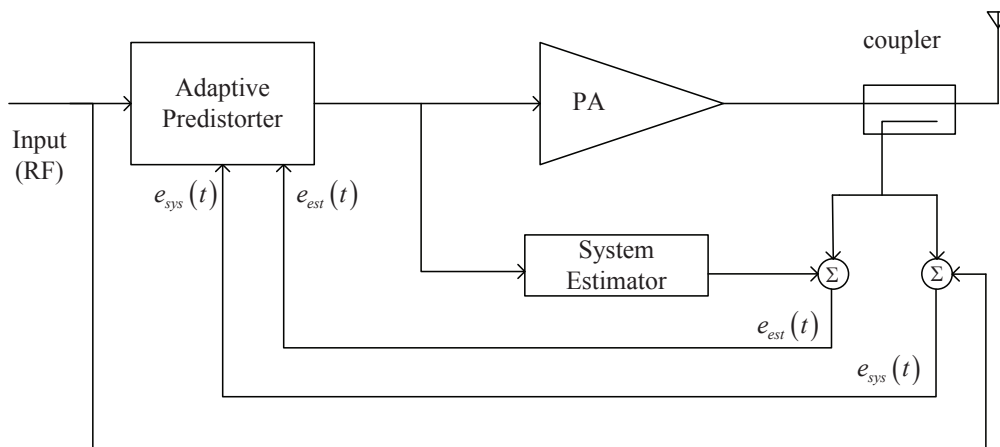


Figure 2.9: A basic predistortion block

and cancelled by a process of using predistortion prior to entering the power amplifier. However, this kind of setup is vulnerable to variation in system settings which include operating temperature and environment changes. As such, the popular techniques include a feedforward technique, look-up-table technique and polynomial technique. The latter two requires a feedback loop, an adjuster and a complex look-up-table or polynomial block. Figure 2.9 shows a block diagram of a basic predistortion scheme which uses two feedback signals to manage the non-linearity of PA as well as cater for system variations.

2.4.2 Doherty Amplifier

The Doherty amplifier is known to improve the efficiency at high output back-off power. The results of using Doherty amplifier structures have been well studied in literature. A classic Doherty amplifier consists of two amplifiers: a carrier amplifier biased to operate in Class AB mode, and a peaking amplifier biased to operate in Class C mode. The basic block can be viewed from

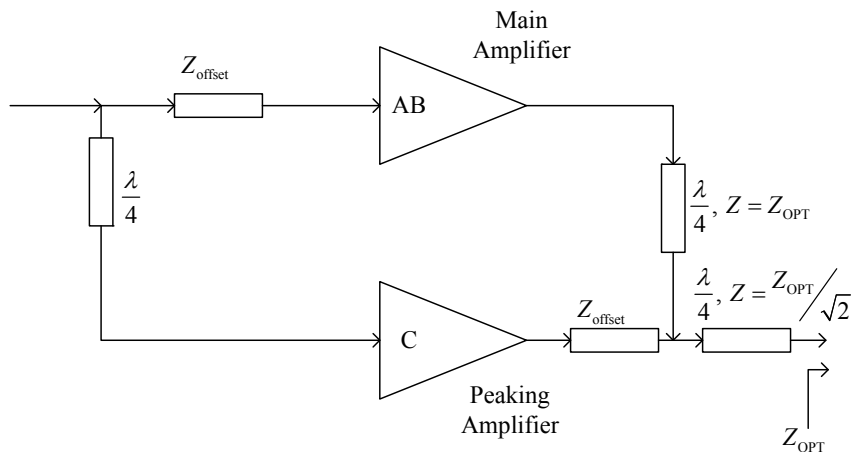


Figure 2.10: Block diagram of a basic Doherty amplifier architecture

Figure 2.10. A power splitter is used to divide the input signal equally to each amplifier with a 90-deg. difference in phase. After the amplification, the signals are recombined using a power combiner. The peaking amplifier is biased such that it only conducts when the drive level is greater than a specific value. Only the Class AB main amplifier provides amplification when the signals are less. In this way the amplifier structure produces high efficiency and gain [50]. There are a few types of amplifier structures using Doherty. They are symmetric [51], asymmetric structures [52] with uneven power transistors and as an N-way structure using multi-paralleled transistors [53]. The symmetric structure has a maximum efficiency point at 6 dB back-off power from peak output power. The asymmetric Doherty amplifier can obtain a high efficiency at various back-off powers using a combination of uneven power device sizes for the main and peaking amplifier. As there are differences in terms of matching circuits and delay between the two amplifiers (main and peaking amplifiers), it is quite

difficult to optimize the gain and output power for the asymmetric structure. The N-way Doherty has better efficiency compared to the conventional 2-way by using multiple parallel transistors that are identical. The only drawback of the system is the total gain depends on the N-way power splitter for the input. Under low gain situations this will increase the power dissipation of the driving amplifier. There has been some proposed work to mitigate this problem [54, 55].

In the following subsections alternate high efficiency amplifying structures are described. These are based on a switching philosophy.

2.4.3 Switched Mode Power Amplifier

Switched mode power amplifiers (SMPA) are becoming increasingly popular due to their high efficiency. They are progressively replacing the traditional linear power amplifiers in mainstream applications such as home entertainment systems, automotive sound systems, and professional installations where high quality is needed.

The main idea behind the switch mode power amplifier technology is to operate the transistor in saturation, so that either the current or voltage depending on the amplifier class is switched ON or OFF. Subtle differences in topology and how the switch is modulated has led to a variety of switching amplifier classification such as “Class D”, “Class E”, and “Class F” [56].

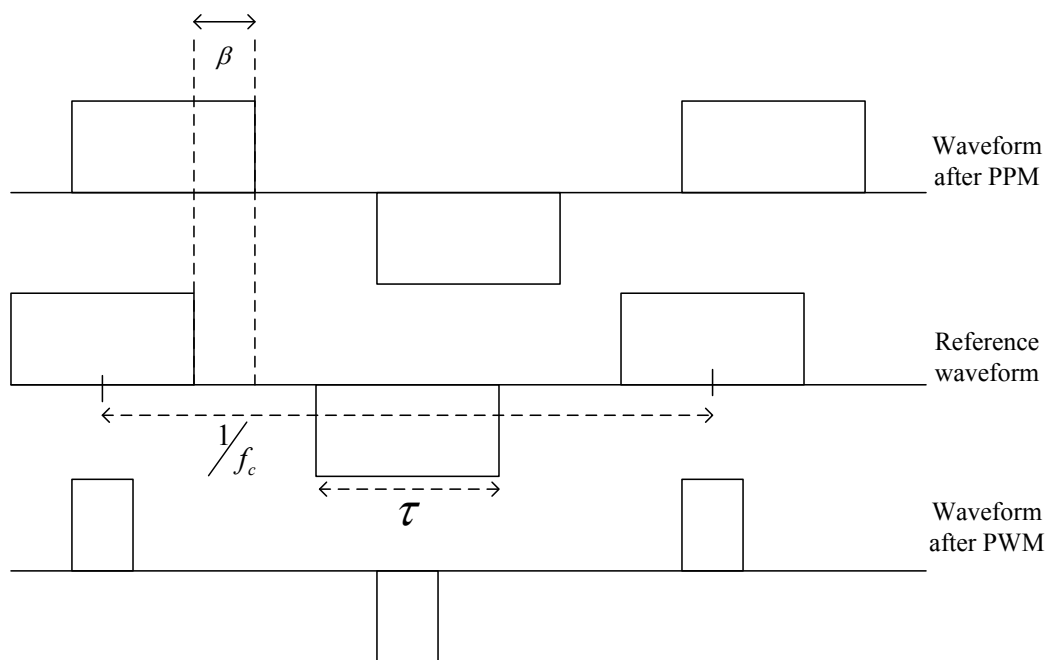


Figure 2.11: Demonstrating PWM (amplitude modulation) and PPM (phase modulation) concept. Edges occur on the digital timing grid.

Variation of the duty ratio (pulse width) of a class-D PA produces an amplitude modulated carrier. The envelope of the output signal is proportional to the sine of the pulse width; hence the pulse width is varied in proportion to the inverse sine of the desired envelope. A signal with amplitude and phase variation can be represented by a combination of a pulse width modulation (PWM) and a pulse position modulation (PPM) respectively (Figure 2.11).

The process can be established in DSP. RF PWM can accommodate a significant RF bandwidth with only a simple, low-loss output filter. Ideally, the efficiency is 100 percent. In practice, switching losses occur, because of finite switching times and the charging and discharging of the parasitic capacitances within the switching transistors. Switching losses tend not to change with pulse

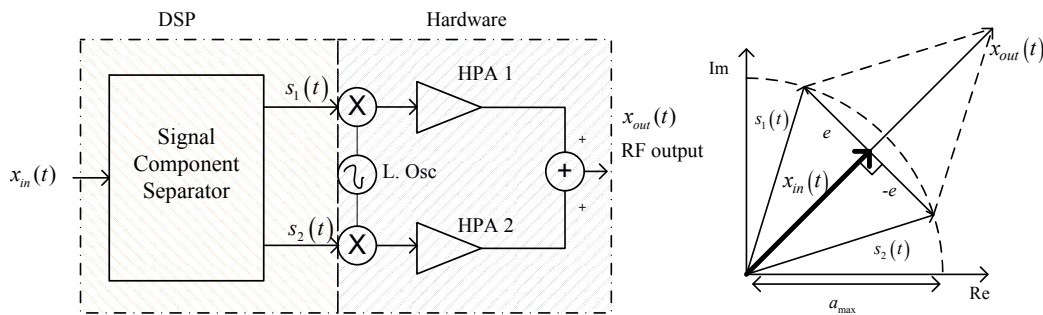


Figure 2.12: The LINC architecture and signal vectors

width. Low duty cycle wave-forms therefore have low efficiency [57]. The next sub-sections consider switching architectures with constant 50% duty cycle.

2.4.4 Linear Amplification using Non-linear Components (LINC)

The concept of outphasing power amplifiers surfaced around the 1930s. It was proposed to perform a simultaneous realization of high efficiency and high linearity amplification [39]. It has been attracting a lot of interest recently for wireless communication applications under the name of LINC [40]. Many recent publications have enhanced the concept further [41, 42], including a variation called CALLUM [43, 44]. The principle of this technique can be explained from Figure 2.12. An amplitude and phase modulated signal ($X_{in}(t)$) is divided into two separate phase modulated signals ($s_1(t)$ and $s_2(t)$), each with a constant amplitude. Then each signal is amplified by nonlinear but highly efficient amplifiers. The PAs' outputs are then recombined to yield the RF output [45, 46, 28] as depicted in Figure 2.12). We note that the amplitude of the recombined signal is determined by the outphasing angle

(angular difference) between s_1 and s_2 . The advantage of this approach is that each amplifier can be operated in a very power-efficient mode, and yet the final output can be highly linear and free of intermodulation products: which is a key consideration for bandwidth efficient wireless communication. The process can be understood from the following set of equations:

$$\begin{aligned}
 x_{in}(t) &= a(t) \cdot e^{j\theta(t)} \\
 s_1(t) &= x_{in}(t) + e(t) \\
 s_2(t) &= x_{in}(t) - e(t) \\
 e(t) &= j \cdot x_{in}(t) \cdot \sqrt{\frac{a_{max}^2}{x_{in}^2} - 1}
 \end{aligned} \tag{2.12}$$

a_{max} is the amplitude of the s_1 and s_2 components' envelope which is always constant. Hence,

$$s_1(t) = a_{max} e^{j\angle s_1(t)} = a_{max} p_s(t) \tag{2.13}$$

where, $p_s(t)$ is the polar phase of the $s_1(t)$.

Ideally, for a signal to be suitable for linear amplification, the output needs to be a linear scale of the original input, where G is the constant gain of the composite power amplifier.

$$x_{out}(t) = G \cdot x_{in}(t) \tag{2.14}$$

In addition, in order for the highly efficient, non-linear power amplifiers to be employed, the decomposed signals $s_1(t)$ and $s_2(t)$ can not have amplitude modulation. Furthermore, the decomposition has to be such that its inverse

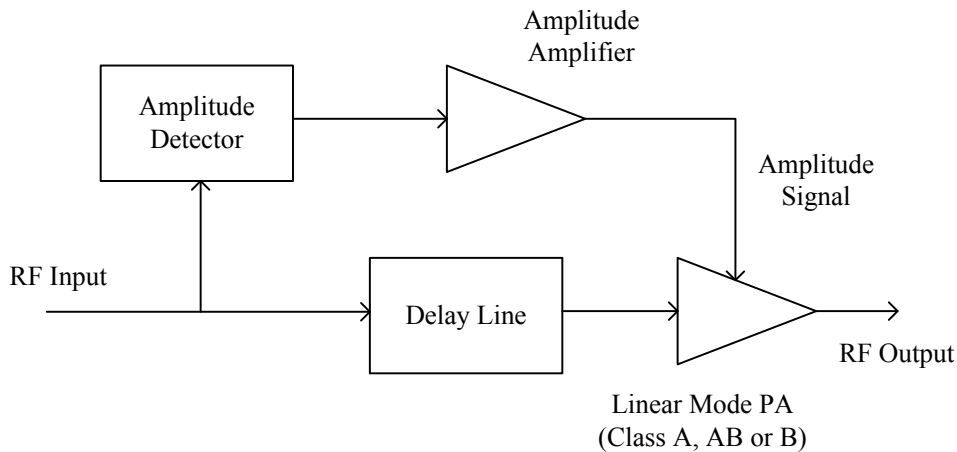


Figure 2.13: Block diagram of a traditional ET architecture

function, which is performed at the re-combiner block, can be efficiently implemented using analog circuitry [2]. The constant envelope drive signals are generated through nonlinear equations and therefore have a significantly larger bandwidth. This limits the applicability of the system to narrowband signals.

2.4.5 Envelope Tracking

The ET utilizes a linear PA and a supply modulation circuit: where the supply voltage tracks the input envelope. There are two known ET schemes. One is the wide-bandwidth envelope tracking (WBET) [35, 36] and the second one is the average envelope tracking (AET) [37]. Figure 2.13 shows the block diagram of a traditional ET system. The difference between WBET and AET are the WBET tracks the instantaneous wide bandwidth input envelope signal power, whereas the AET technique tracks the long-term average input envelope signal power. The second approach is useful for systems like code division multiple access (CDMA) as it uses dynamic power control [38].

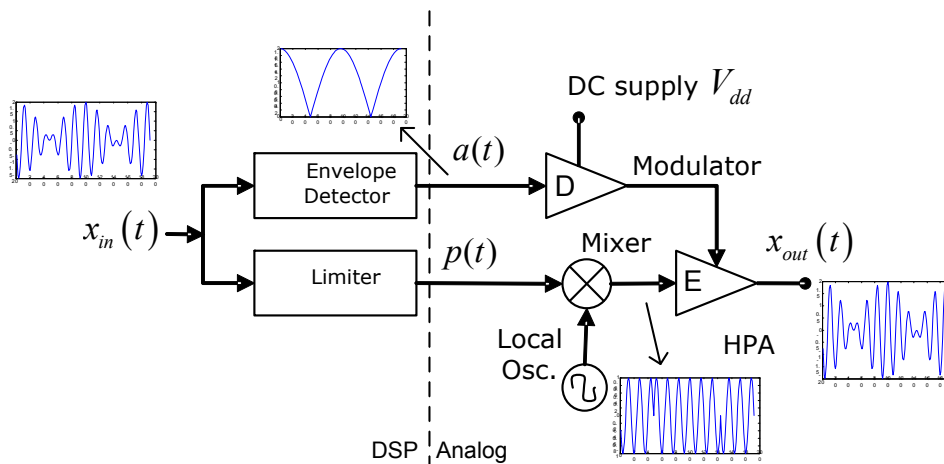


Figure 2.14: Block diagram of EER architecture

2.4.6 Envelope Elimination and Restoration (EER)

The EER architecture using SMPA can achieve high efficiency for modulation schemes like OFDM and CDMA [34]. This section provides an overview of EER architecture and the BW expansion problem. EER is quite similar to the ET technique. Here, the technique converts the cartesian signal to amplitude $a(t)$ and phase $p(t)$ polar components. The phase, $p(t)$ is then upconverted and transmitted directly to the PA's RF input. The amplitude, $a(t)$, controls PA output stages supply voltage, V_{dd} , using a switched mode supply modulator. The process is depicted in Figure 2.14. The PA architecture can work as a non linear switch (Class E), and can theoretically obtain 100% efficiency [33, 28].

$$\begin{aligned}
 a(t) &= |x_{in}(t)| \\
 p(t) &= 1 \cdot e^{j\theta(t)} \text{ where } \theta(t) = \angle x_{in}(t) \\
 x_{out}(t) &= a(t)e^{j\theta(t)}
 \end{aligned} \tag{2.15}$$

The phase and amplitude information have to arrive at the same time. To achieve this, $p(t)$ is normally delayed to match the time difference between two paths [28, 33], as shown in Figure 2.14. The supply signal is now modulated and this requires a variable voltage high efficiency class D switching power supply if energy gained in the RF HPA is not to be lost in the supply driver. Class D supplies must have a switching frequency of the order of ten times the modulation bandwidth so that low pass filtering can remove the switching artifacts. Class D supplies lose efficiency as the switching frequency rises. It is therefore important that the bandwidth of the modulation envelope is as small as possible.

OFDM is a noise like signal which describes an almost random path in the inphase and quadrature (I & Q) plane. Any near zero crossings cause large dips in the envelope signal and a large rate of phase change (instantaneous frequency) for the phase drive signal. The coordinate transform of this signal from Cartesian to polar results in signal components that have wider bandwidth than that of the input signal. For the coordinate transform the signal goes through nonlinear components like a diode (for an envelope detection) and a hard limiter (for phase) and thus suffers bandwidth expansion. The amount of bandwidth expansion depends on the modulation scheme. Modulations with limited envelope dynamic range such as $\frac{\pi}{4}$ shift QPSK have less bandwidth expansion than the wider dynamic range modulation schemes such as multi-carrier modulation (OFDM or WCDMA).

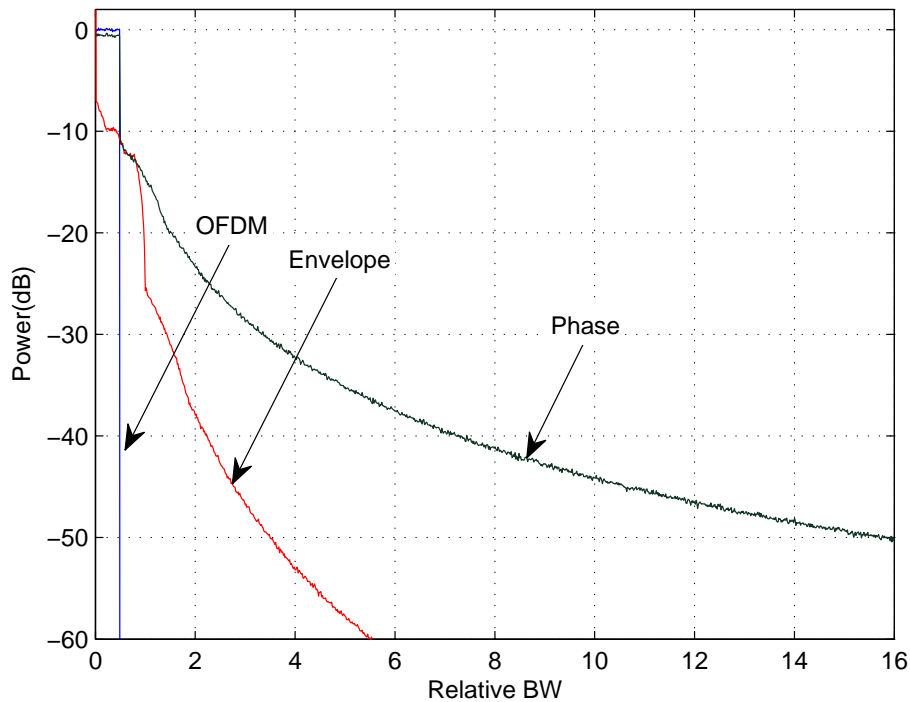


Figure 2.15: Spectrum of OFDM and its Envelope and Phase components

Figure. 2.15 shows the spectrum of OFDM and its polar components. The x-axis is normalized such that the bandwidth of the original signal is unity. The envelope and phase components have much wider bandwidth than that of the original OFDM signal. At the -50 dB level the envelope BW is at 3.5 relative channels and the phase BW is around 15 channels. This spectrum figure will be used as a reference for the various bandwidth reduction schemes proposed in Chapters 3 and 4.

This bandwidth expansion poses some difficulties for the DSP and the DAC circuits if the polar conversion is done digitally. As such some bandwidth limitation technique is required. There are very few papers currently available which are directly relevant to bandwidth limitation of the polar signals. In the

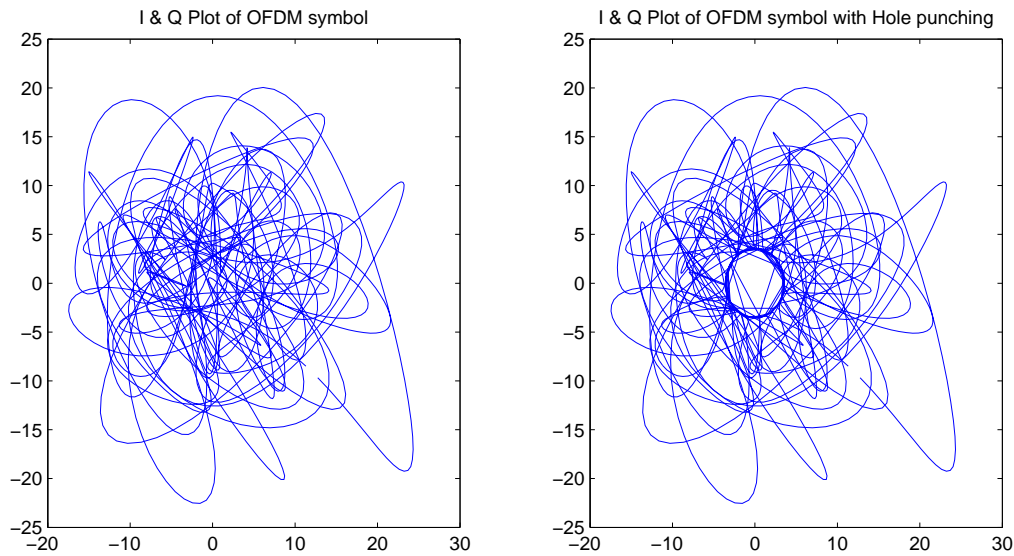


Figure 2.16: I & Q plot of a OFDM symbol (a) without hole punching and (b) hole punching enabled.

next subsection, a brief description is provided.

2.4.7 Current Literature on Bandwidth Limitation for EER

In the current literature, the only technique used to reduce the bandwidth of the polar drive signals is based on the hole punch scheme originally proposed by Rudolph [3]. He showed the bandwidth expansion can be reduced by preventing zero crossings in the I & Q plane (Figure 2.16). The process involves the addition of a bandwidth limited correction signal to keep the signal envelope from going to zero. His paper confirmed that any adjacent channel power generated by the process was minimal. However, he did not consider in band distortion which, we show later, degrades the EVM of the transmitted signal to an almost unusable level.

Hunton [4] proposed to eliminate near-zero values by adding offsetting vectors to the signal constellation: in order to stop trajectories passing origin. This can be thought of a variation of hole punching process. However, due to the process, phase and magnitude of the signal are changed, which leads to considerable distortion. The process shows some OOB filtering to reduce the spectral splatter; but the EVM still remains quite dominant.

In [5] Wang et al. showed a similar technique to that of Rudolph. They used a technique based on a combination of direct clipping, circle-tangent shifting, and the use of unused tones. Although the main goal of the paper was to achieve improved linearity for PA, the paper manages to reduce the bandwidth expansion of the polar drive signals marginally. The technique uses a Gaussian window with many taps and involves many iterations (example: 300 tap Gaussian window and 20 iterations for LTE signal) to find a perfect hole in the constellation.

2.5 Simulation Parameters

Table 2.3 shows the simulation parameters for this thesis unless mentioned otherwise.

2.6 Summary

In this chapter, the technical background for this thesis has been overviewed. In the first section amplifier modulation was shown to be the dominant cause of amplifier non-linearity. PAPR reduction schemes can reduce the dynamics of

Table 2.3: Simulation parameters

OFDM specification:	
Number of subcarriers, N	64 or 128
Oversampling rate, L	16-64
Number of active tones	48 for WLAN $N = 64$
Modulation	QPSK
PTS:	
Number of subblocks, M	4
Number of trials, S	64
Subblock partitioning scheme	Adjacent
Spectral Mask Standard	IEEE 802.11g WLAN
EVM requirement	-25 dB
Number of OFDM symbols	100 – 500 (depending on complexity)

the envelope signal (AM component and popular methods for reducing PAPR are discussed). In particular, the PTS and the clip-filter-clip schemes were discussed in details since they have relevance to the approach taken in this thesis. PAPR reduction is not enough to stop the amplifier distortion. Linearization schemes are needed. DPD is the most common linearization scheme and it has been briefly described. Switched mode power amplifier architectures are potential candidates for achieving higher efficiency and linearity. Two of these architectures, LINC and EER/ET, were discussed and are the main focus of this thesis. The final section of the chapter reviewed the hole punching scheme, the only published method for reducing the bandwidth of the polar signals in EER architecture. There has not been any attempt to reduce the bandwidth expansion on LINC components.

In the next chapter, novel polar bandwidth limitation schemes for EER architecture will be shown.

Chapter 3

Bandwidth Reduction Schemes for EER Transmitters

In the case of EER, the RF PA supply voltage needs to be modulated by a highly efficient variable voltage switching (Class D) power supply. As previously described, the efficiency of such supplies drops with switching frequency. Class D supplies must have a switching frequency of the order of ten times the modulation bandwidth so that low pass filtering can remove the switching artifacts. Class D supplies lose efficiency as the switching frequency rises. These problems effectively limit the EER amplifier structure to narrowband modulations and thus making the system less suitable for future 4G wireless systems. The bandwidth of the envelope should be as small as possible. In the following sections, a number of novel techniques for reducing the bandwidth expansion of the EER signal components are discussed.

Section 3.1 describes bandwidth reduction using the minimum power PTS approach. This work was presented at the IEEE International Microwave Symposium (IMS) 2009 [58]. The next section introduces a method of direct polar

bandwidth limitation. This is the core process for a number of novel schemes described in the rest of the chapter. Section 3.3 and Section 3.4 describe the iterative bandwidth limiter (IBL) technique which was presented at the 4th International Symposium on Wireless Pervasive Computing (ISWPC), 2009 [59]. Section 3.5 describes a repetitive bandwidth limitation (RBL) scheme that also corrects the in-band distortions using a QAM correction method. This was presented at the WCNC 2010 [60]. The final technical section of the chapter (Section 3.6) describes a new bandwidth limitation scheme that combines the PWM and PPM switched mode power amplifier with the EER technique. This work was part of a collaborative research project with Lund University: which targeted the next generation digital basestation architectures. This section formed a major contribution in the publication that was presented at the ISWPC 2009 [61] and also published in the EURASIP Journal on Wireless Communications and Networking [62].

3.1 Minimum Power PTS Signal

We have already learnt that the PTS method generates multiple sequences of a signal and then chooses the ones with the lowest PAPR (Section 2.3.6). Here, we modify the technique to reduce the bandwidth expansion of the envelope and/or the phase drive signal in an EER architecture (Figure 3.1), by:

1. increasing the inverse fast Fourier transforms (IFFT) oversampling rate, L , for accurate measurement of the out-of-band spectrum.

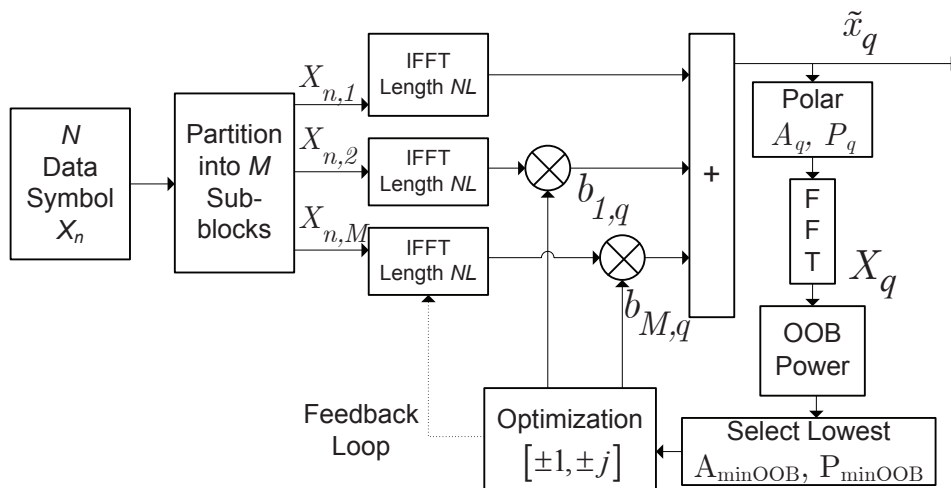


Figure 3.1: Block Diagram to choose minimum OOB Power Signal using PTS. The \tilde{x}_q is goes to input of Figure 2.13

2. altering the trial selection criterion, i.e. instead of choosing the signal with minimum PAPR, the signal is chosen on the basis of minimum out of band power for the selected polar component (A_{minOOB} or P_{minOOB}). This involves an additional FFT operation to calculate the power spectrum of the amplitude ($A_{n,q}$) or phase ($P_{n,q}$) of the EER drive signals.

$$A_{\min OOB} = \arg \min_{1 \leq q \leq Q^{M-1}} \int_{n=0.5N}^{1.5N} A_{n,q} \quad (3.1)$$

$$P_{\min OOB} = \arg \min_{1 \leq q \leq Q^{M-1}} \int_{n=0.5N}^{1.5N} P_{n,q} \quad (3.2)$$

Most of the signal power resides in the first adjacent channel. It is found that, limiting the OOB power calculation in the frequency range $0.5N$ to $1.5N$ (instead of $0.5N$ to $NL/2$), the computational complexity is reduced without affecting the BW improvement. The results from these two selection criteria

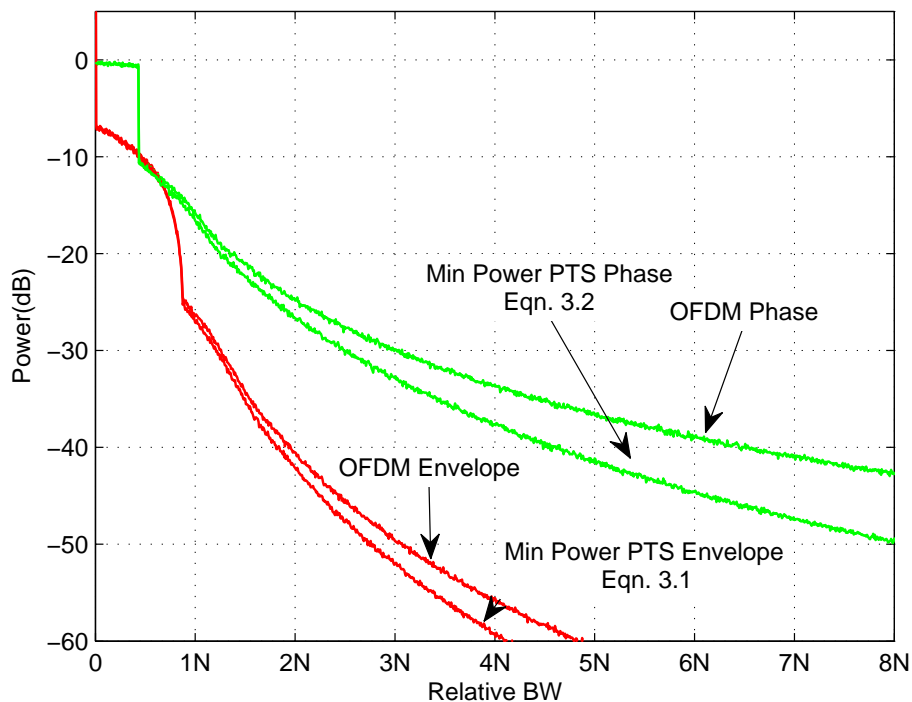


Figure 3.2: Spectrum of Minimum Power PTS and OFDM Symbol. Note, the RF Spectrum and EVM are not effected.

are shown in Figure 3.2. The effect of choosing the trial, q , with the minimum OOB phase power (eq. 3.2) results in a bandwidth reduction of approximately 31% at -40 dB level, with a minimal impact on the envelope spectrum. However, when the minimum OOB envelope power (eq. 3.1) is chosen as the selection criterion, the bandwidth reduction is around 7% for the envelope signal with phase bandwidth also improves by 20%. From the above discussion, it is fairly obvious that the bandwidth of the phase signal is more responsive to the PTS method.

It is also interesting to see whether the selected waveform based on the eq 3.1 and eq 3.2 has any effect on the PAPR of the OFDM signal. Figure 3.3

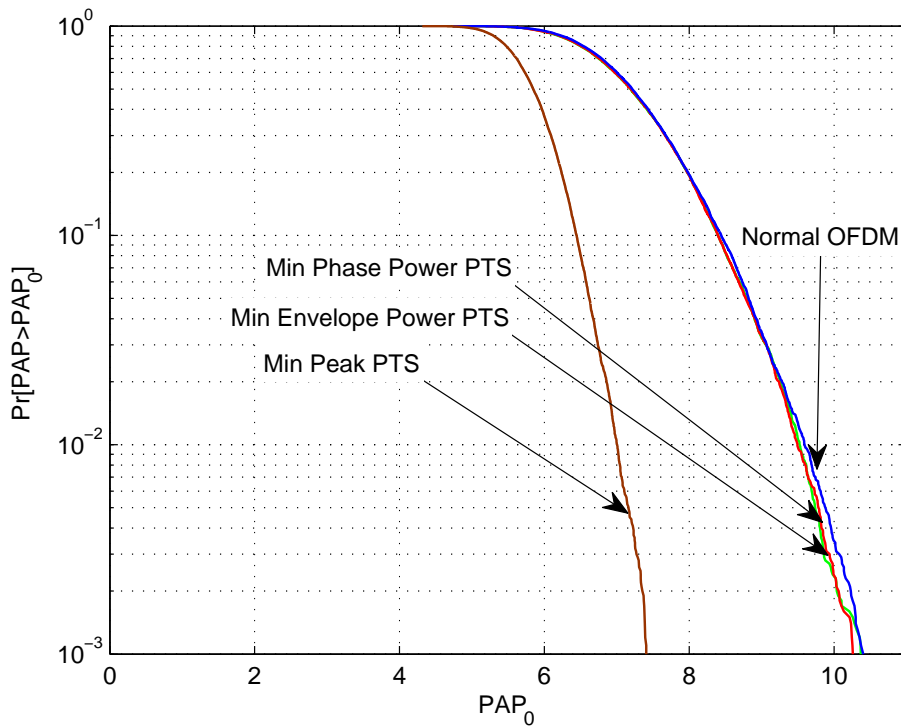


Figure 3.3: CCDF of OFDM Signal and Minimum OOB Power PTS signal shows the complementary cumulative distribution function (CCDF) of PAPR of OFDM signal and the recombined signal, \tilde{x}_q , using A_{minOOB} and P_{minOOB} . In both cases, the \tilde{x}_q is almost identical to that obtained from normal OFDM. Also shown is the CCDF of PAPR of the minimum peak power PTS selection criteria based on [19]. When choosing conventional PTS signal for reducing PAPR, there is a 3 dB improvement. However, these waveforms show no improvements in the bandwidth expansion of the polar components. From this it can be concluded that there is no correlation between PAPR and the bandwidth of its polar components.

This technique manages to reduce the bandwidth expansion to some extent. In addition, it does not result in any EVM buildup as PTS is a distortionless

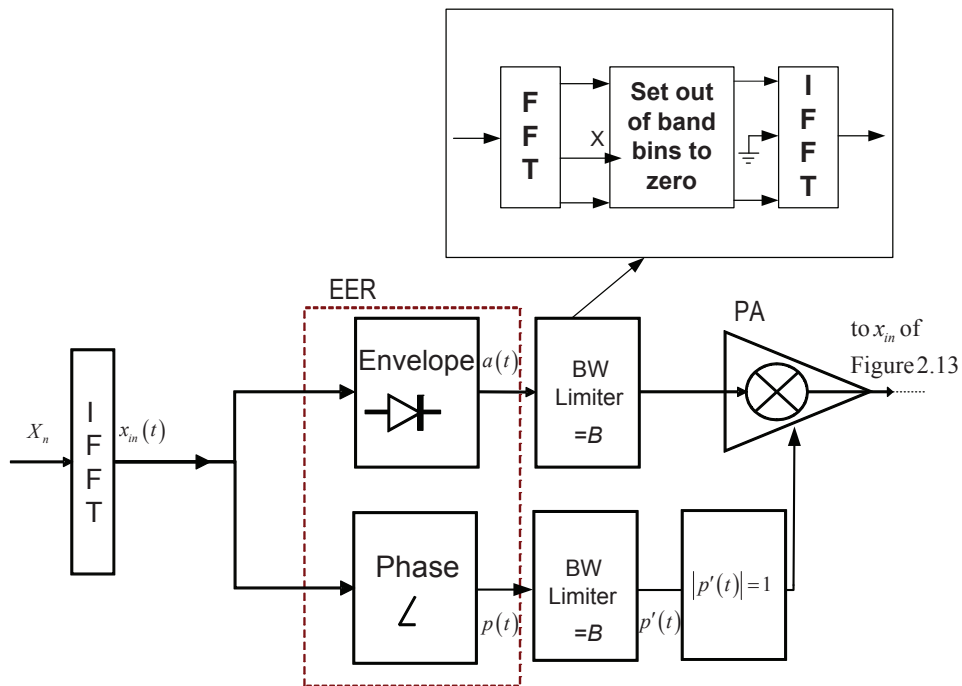


Figure 3.4: Block diagram of BW limit process

scheme. However, the complexity increases with more IFFT operations and some additional data needs to be transmitted as SI for receiver decoding purposes.

3.2 Bandwidth Limitation

In order to reduce the bandwidth expansion further, some distortion in the signal is required. The envelope and phase drive signals have infinite bandwidth. The bandwidth of the OOB bins are forcibly limited by setting them to zero in the frequency domain. Which requires an additional FFT and IFFT operation. The process can be depicted from Figure 3.4. Bandwidth limitation is performed on either the envelope or the phase drive signal. It is not done

on both signals at the same time as the EVM produced by the procedure is impractical. The following equations explain this process:

$$A_{n_{\text{BW Limit}}} = \begin{cases} A_n & 0 \leq n \leq BN, \\ & NL - BN \leq n \leq NL - 1 \\ 0 & BN + 1 \leq n \leq NL - 1 - BN \end{cases} \quad (3.3)$$

$$P_{n_{\text{BW Limit}}} = \begin{cases} P_n & 0 \leq n \leq BN, \\ & NL - BN \leq n \leq NL - 1 \\ 0 & BN + 1 \leq n \leq NL - 1 - BN \end{cases} \quad (3.4)$$

where B is the bandwidth relative to the OFDM channel width (also equals to critical sample rate f_s). The phase bandwidth limitation process requires an additional hard limiter. The bandwidth limitation on the phase signal introduces an amplitude component to the constant envelope phase signal. In order for the EER architecture to work properly, the amplitude variation must be removed.

The distortion caused by the bandwidth limitation results in some EVM buildup depending on the value of B . The EVM caused by the bandwidth limitation has an inverse relationship to B : i.e. as the B value gets lower, the EVM gets higher (worse).

Figure 3.5 shows the spectrum of the OFDM signal and its two polar components when the envelope BW is limited to 1 channel bandwidth ($B = 1$). Here, the black line is the reference spectral mask of WLAN 802.11g. The bandwidth limitation technique manages to reduce the envelope bandwidth.

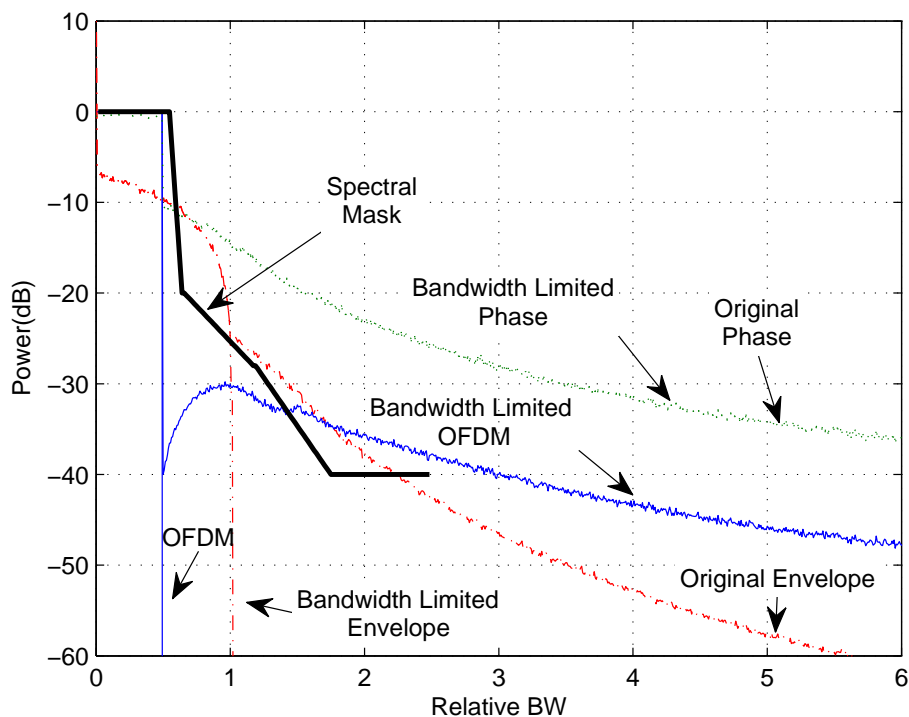


Figure 3.5: Spectrum of OFDM and polar components after Envelope bandwidth limitation at $B = 1$

However, there is almost no improvement for the phase component. In addition, the OFDM signal also deteriorates; the RF signal does not follow the spectral mask criteria. The OFDM inband signal is also affected by a buildup in EVM. However, a level of -43 dB (figure 3.7 with $B = 1$) is unlikely to cause a problem.

If the phase bandwidth is limited (Figure 3.6), the phase improves to 8.9 channel bandwidths¹ at -50 dB level which is an improvement of 43.3%. The envelope bandwidth does not improve². Again the OFDM-RF signal suffers spectral splatter and does not follow the spectral mask. Envelope is a high

¹The bandwidth of the original phase component is at 15 channel bandwidth at -50 dB

²The bandwidth of the original envelope component is at 3.5 channel bandwidth at -50 dB

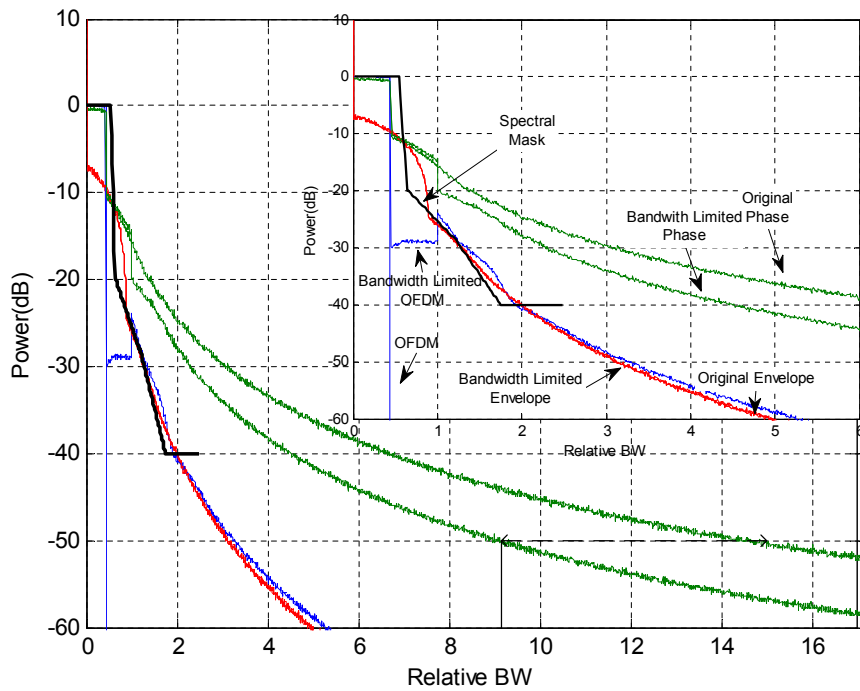


Figure 3.6: Spectrum of OFDM and polar components after Phase bandwidth limitation. The small subplot showing a zoomed version of the bigger plot. The bigger plot showing the bandwidth improvement for phase component at -50 dB

power signal (power supply modulated) and as the envelope component of the EER architecture drives the supply modulator it is important that the bandwidth of the envelope signal is as low as possible in order for the high frequency components to amplify without distortion. As such envelope bandwidth reduction is more important than phase bandwidth reduction. Keeping this in mind, the rest of the schemes in this chapter will only employ envelope bandwidth limitation.

The distortion from the bandwidth limitation process causes EVM buildup. Figure 3.7 shows the EVM of both envelope and phase bandwidth limitation processes with different bandwidth limiting values, B . For $B > 0.6$, envelope

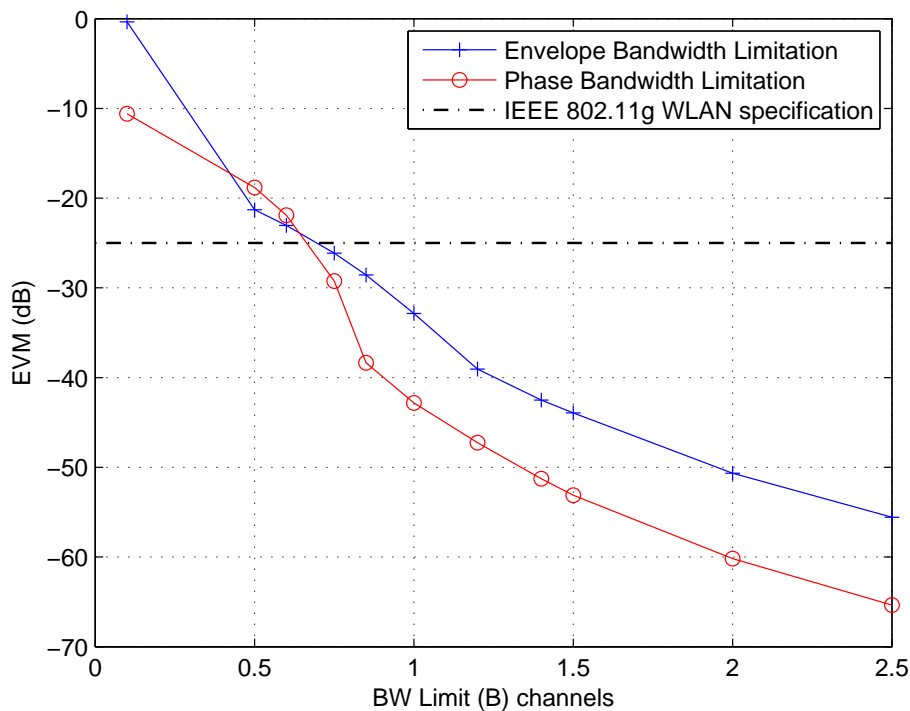


Figure 3.7: Mean EVM of Envelope and Phase bandwidth limitation for different bandwidth limiting values

bandwidth limitation yields less EVM buildup than phase bandwidth limitation.

From these simulations, an optimum bandwidth limiting value can be chosen, that can satisfy the EVM specifications. Here, $B = 0.75$ will meet the -25 dB EVM specification for WLAN standard. However, it still does not guarantee the OFDM-RF spectrum is below the spectral mask. This issue is addressed in the next bandwidth reducing scheme.

3.3 Iterative Bandwidth limiter (IBL)

In this section an iterative bandwidth limitation (IBL) technique is introduced: this is based on the bandwidth limitation scheme proposed in the last section.

The process is applied on envelope component. The scheme allows us to find the minimum bandwidth limiting point for each symbol; from which we can specify design bandwidth for the envelope hardware. It is explained as follows:

1. The process first sets $B = 3.5$ channels out of maximum bandwidth of $B = L/2$, where L is the oversampling rate. So $B = L/2$ means effectively no bandwidth limitation for polar components. The value of B was set to 3.5 as for greater value of B the OFDM-RF signal stays well below the spectral mask. In addition, starting from $B = 3.5$ reduces unwanted complexity.
2. After this, the bandwidth of the envelope is limited to B using Eqn. 3.1.
3. Then the signal is recombined from the polar components and goes through a decision block. In this block, the signal is compared with the OOB criteria of the spectral mask.
4. Then the process goes through an iterative loop with B being reduced by a stepsize. The process is continued until a value for B is found; for which the signal fails to match the spectral mask.
5. Once this condition is achieved, the stored signal of the previous iteration is chosen for transmission as it is the last modified signal that is below the spectral mask.

The process can be depicted in Figure 3.8.

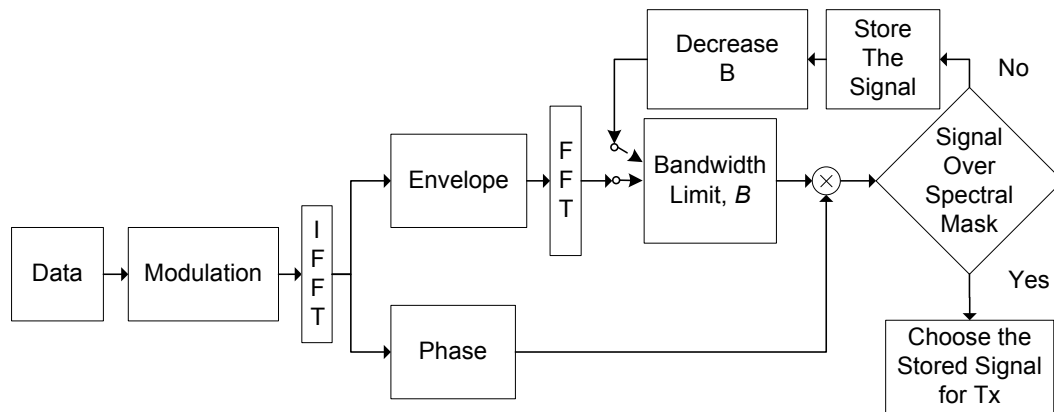


Figure 3.8: Block diagram of Iterative BW limit process

For this simulation, the parameters are chosen from the IEEE 802.11g WLAN standard. The iterative BW limitation is performed on the envelope A_n component. Figure 3.9 shows the simulation results for the envelope BW limitation. The spectrum of the signal stays within the IEEE 802.11g mask and the envelope BW is at 2.55 channels (at -50 dB level) which is a reduction of 28%. In the next section, the bandwidth reduction is further increased using the PTS method.

3.4 Iterative BW Limitation using PTS (IBL-PTS)

The PTS technique can be added to IBL (Figure 3.8) and can be used to achieve further reduction in BW. The process is depicted in Figure 3.10. The details of the incorporation is as follows:

1. The IFFT's oversampling rate is increased for accurate measurement of out-of-band spectrum.

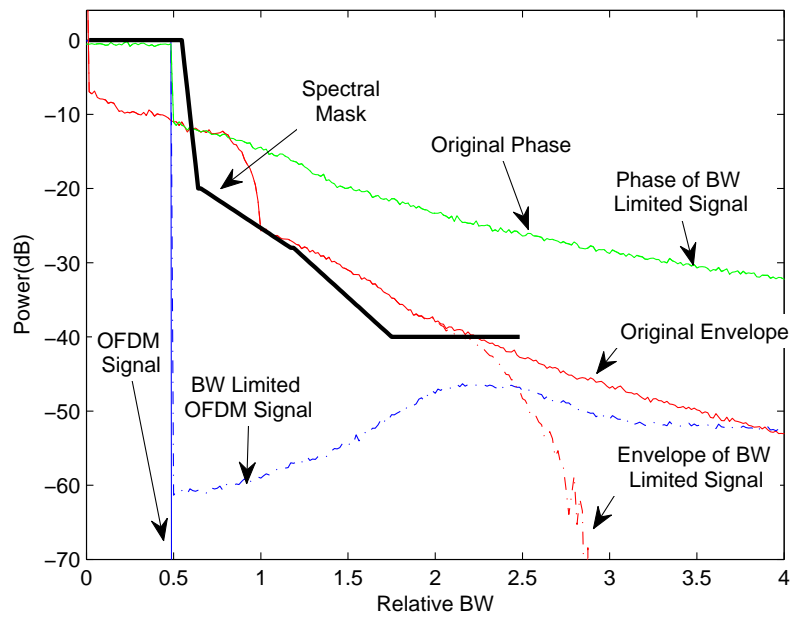


Figure 3.9: Spectrum of OFDM and polar components after IBL on the envelope signal.

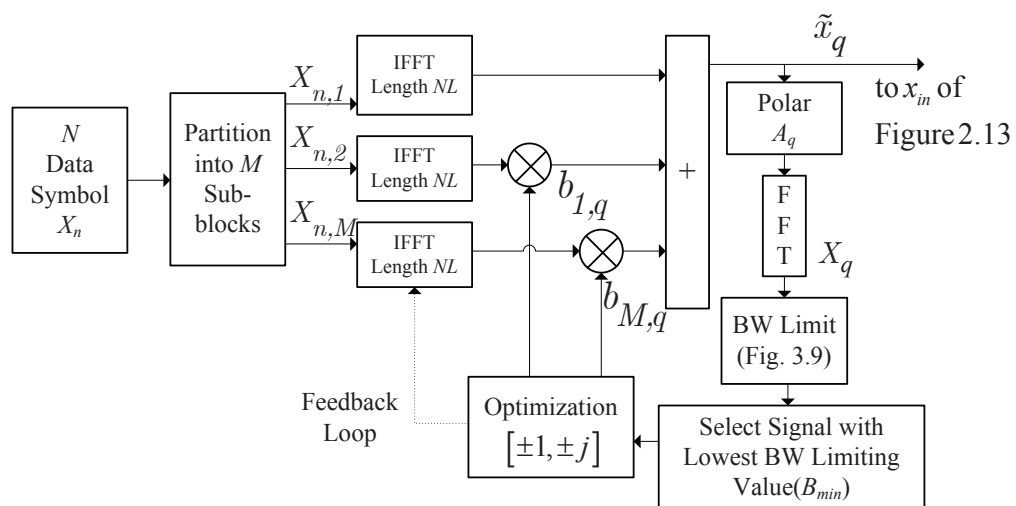


Figure 3.10: Block diagram of Iterative BW Limit process using PTS.

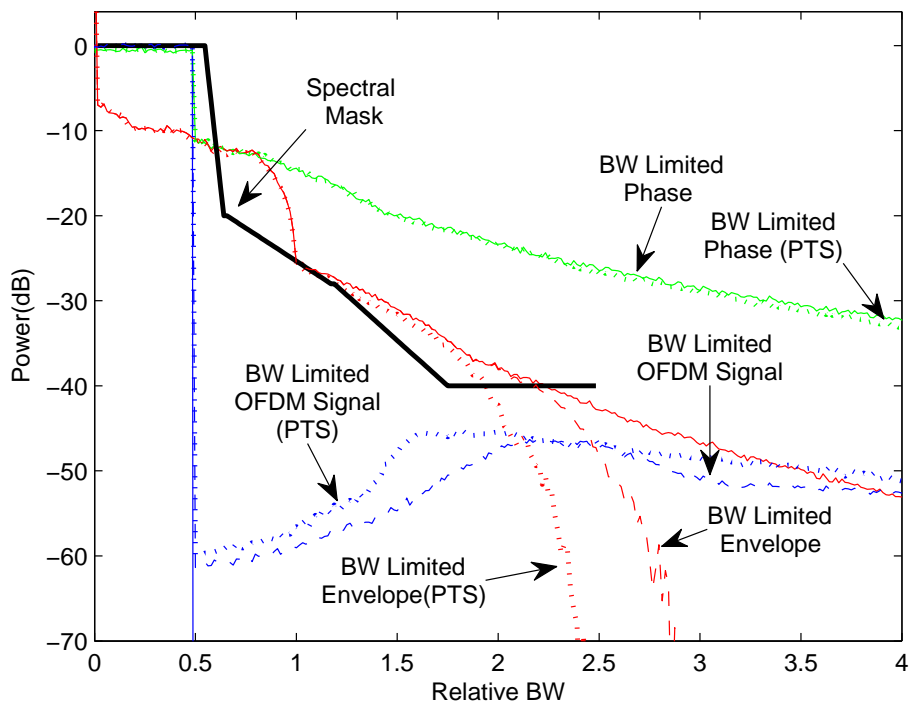


Figure 3.11: Spectrum of OFDM and polar components after Envelope BW limitation using PTS, $Q = 4, M = 4, S = 64$

2. The IBL process described in the previous section is applied to all S PTS waveforms. As such, there will be $S = Q^{M-1}$ number of BW limited envelope($A_{n_{\text{BW Limit}}}$) components. As the BW reduction is proportional to the number of bins set to zero, the trial selection criterion is changed from the minimum PAPR to the lowest BW limiting value (B_{\min}).

Choosing B_{\min} from PTS sequences results in BW reduction of the polar drive signals. In Figure 3.11, IBL-PTS reduces the envelope bandwidth by 37% (28% for IBL). Also as a bonus, the bandwidth of the phase signal is also reduced by 16% compared to no reduction for IBL.

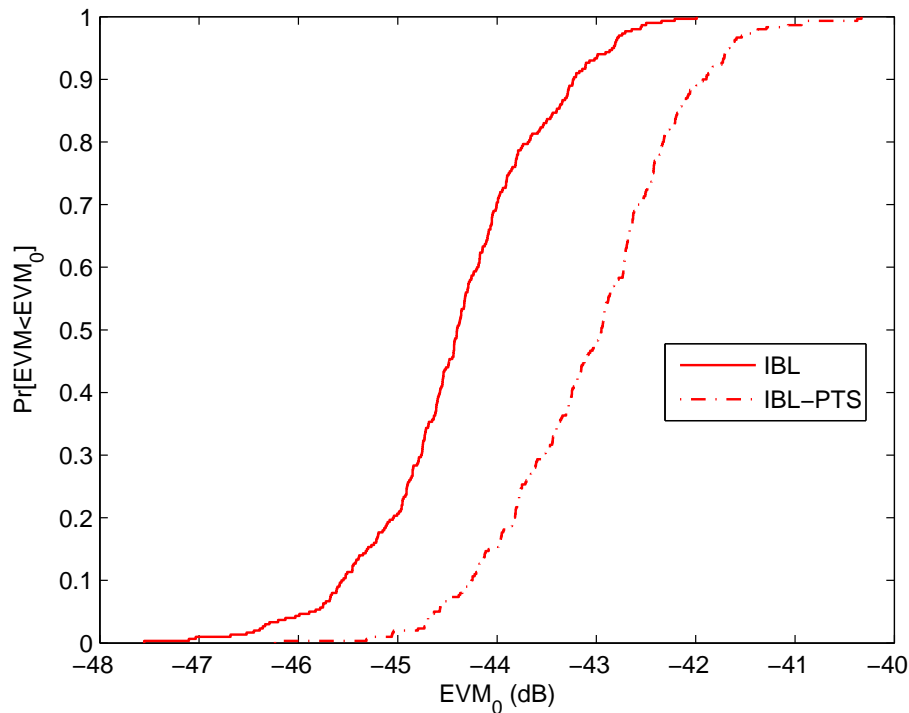


Figure 3.12: CDF of EVM for envelope and phase bandwidth limitation using iterative bandwidth limitation with and without PTS technique

As BW limitation introduces distortion, it results in EVM buildup. Figure 3.12 shows a CDF of the EVM for envelope bandwidth limitation using IBL and IBL-PTS. At 50 percentile, the envelope BW limitation has -44.4 dB EVM while the same method using PTS results in -43 dB EVM. The PTS incorporation manages the extra bandwidth reduction with only 1.4 dB extra EVM loss.

In this section the IBL technique managed to reduce the bandwidth of the polar drive signals. The EVM buildup and spectrum splatter is within the specification of the IEEE 802.11g standard. It requires some additional filtering to reduce the OOB spectral splatter. In addition, the PTS method is incorporated with the IBL and is showing further improvement in bandwidth

reduction. This however, comes with a cost of at least an order of magnitude increase in computational complexity to choose the sequences and the requirement of sending side information. The calculation of the complexity is shown in Appendix A. The complexity of IBL and IBL-PTS are as follows

$$C_{\text{IBL}} = 0.95NC_{\text{bl}} \quad (3.5)$$

$$C_{\text{IBL-PTS}} = ((3.5 - 2.21)N + S) C_{\text{bl}} \quad (3.6)$$

where, C_{bl} is the approximate complexity of the envelope bandwidth limitation operation.

3.5 Repetitive Bandwidth Limitation with QAM Correction (RBL)

The IBL technique managed to keep the OFDM signal spectrum within the specifications of the spectral mask. However, it did not take full advantage of the ‘unused’ (don’t care bands are at the edge of the channel) tones. To address this issue, a new technique is proposed. The process is shown in Figure 3.13. Here, the envelope bandwidth is reduced and recombined with the phase signal to give x'_k .

$$x'_k = a_{k_{\text{BWLlimit}}} \cdot p_k \quad (3.7)$$

There is some spectral regrowth in the OFDM RF signal due to the envelope BW limitation process. This is removed by converting to the frequency

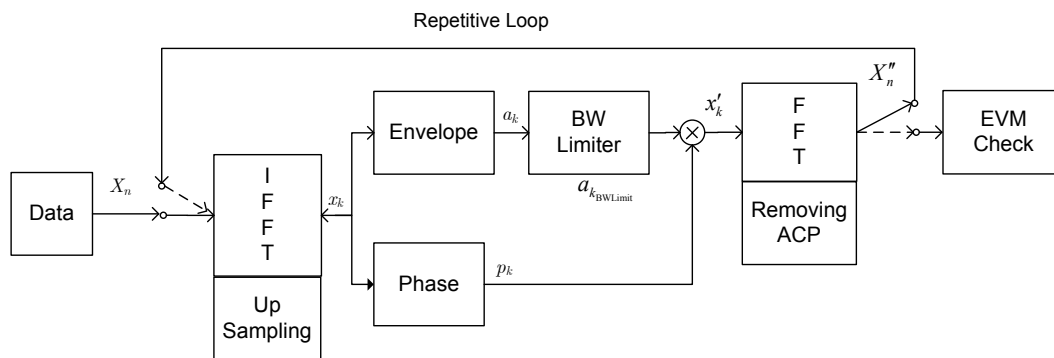


Figure 3.13: Block diagram of repetitive bandwidth reduction.

domain (FFT operation) and setting the power of the adjacent channels to zero. The modified data, $X_{n_{\text{BWLimit}}}$ is fed back to the IFFT block. The process³ is repeated i times and the bandwidth limiting value, B , is kept the same for each repetition.

$$\begin{aligned}
 X'_n &= \text{FFT} \{x'_k\} \\
 X''_n &= \begin{cases} X'_n & 0 \leq n \leq N/2, \\ 0 & NL - N/2 \leq n \leq NL - 1 \\ 0 & N/2 + 1 \leq n \leq NL - 1 - N/2 \end{cases} \quad (3.8)
 \end{aligned}$$

Figure 3.14 shows the spectrum of the envelope and the phase component when the repetitive process is completed. The simulation has the same parameters from Figure 3.5; here the repetition is done 5 times ($i = 5$). As the process limits the envelope signal at the same value for each repetition, the envelope signal does not improve any further. However, the phase bandwidth reduces to 9.3 channels at -50 dB level, which is an improvement of 42% from the original phase signal.

Figure 3.15 shows the effect of bandwidth improvement with increasing

³The technique is inspired by the clip-filter-clip method for PAPR reduction [12]

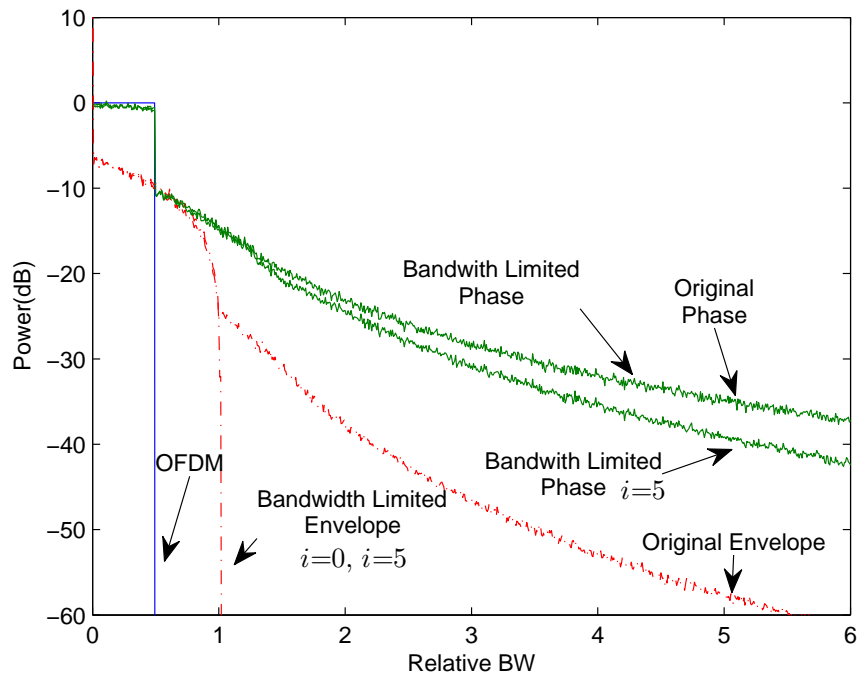


Figure 3.14: Spectrum of repetitive bandwidth limited polar components for $B = 1$.

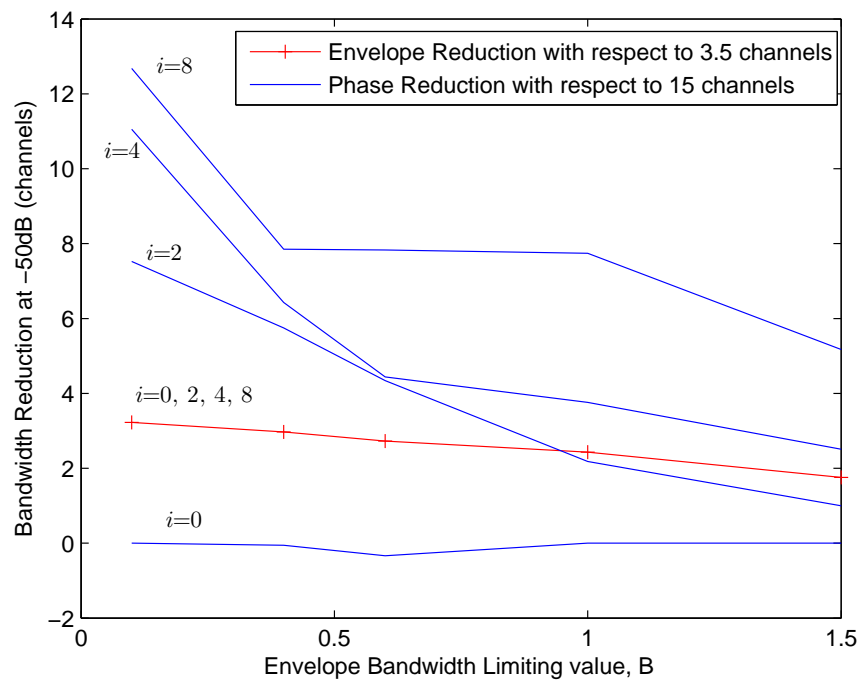


Figure 3.15: Bandwidth improvement in envelope and phase spectrum at -50 dB for different i repetitions from original phase bandwidth of 15 channels and envelope bandwidth of 3.5 channels.

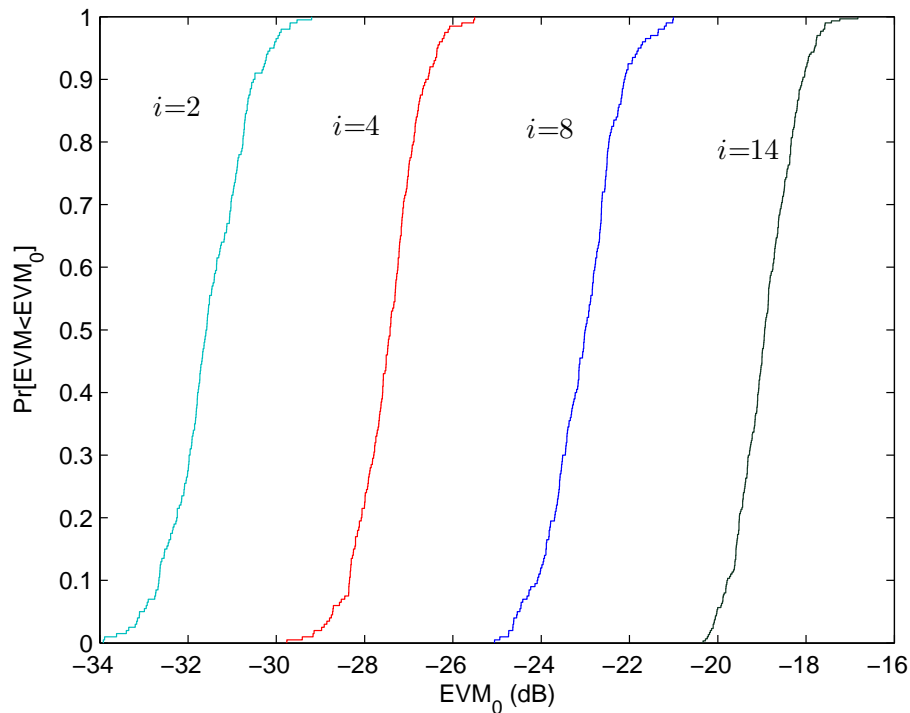


Figure 3.16: CDF of EVM for different i repetitions at envelope bandwidth limiting value of $B = 1$ channel bandwidth

i . The improvements are compared at -50 dB power level. The reduction in bandwidth is proportional to the number of repetition loops with diminishing return for $i > 8$. For $i = 8$ and for up to 0.5 channel bandwidth reduction, the phase bandwidth improves by 8 channels (53.3%) at -50 dB power level.

With every repetition, the OFDM-RF's adjacent channel power is removed. The overall spectral power of the signal is thus reduced. However, the distortion caused by the bandwidth limitation still increases the EVM. Figure 3.16 shows the CDF of the EVM for different i . As the i increases the EVM becomes worse. For $i = 8$ repetitions the EVM value is -23 dB @50 percentile. Figure 3.17 shows the spectral improvement of the RF signal. The spectrum of the

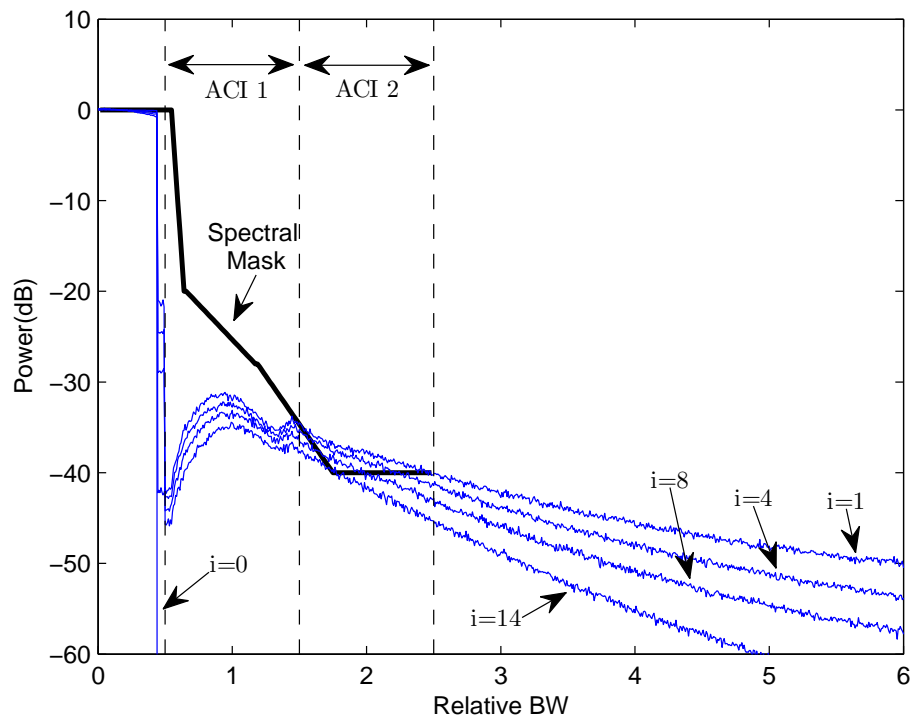


Figure 3.17: Spectrum of OFDM RF signal after $i = 0, 1, 4, 8$ & 14 repetitions

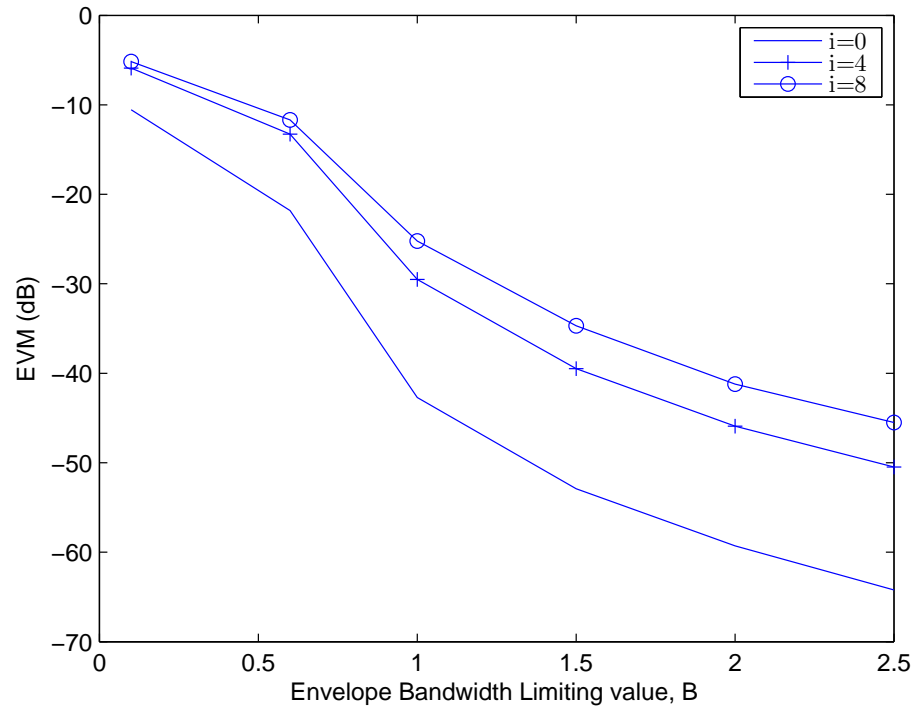


Figure 3.18: EVM vs bandwidth limitation values for different i repetitions

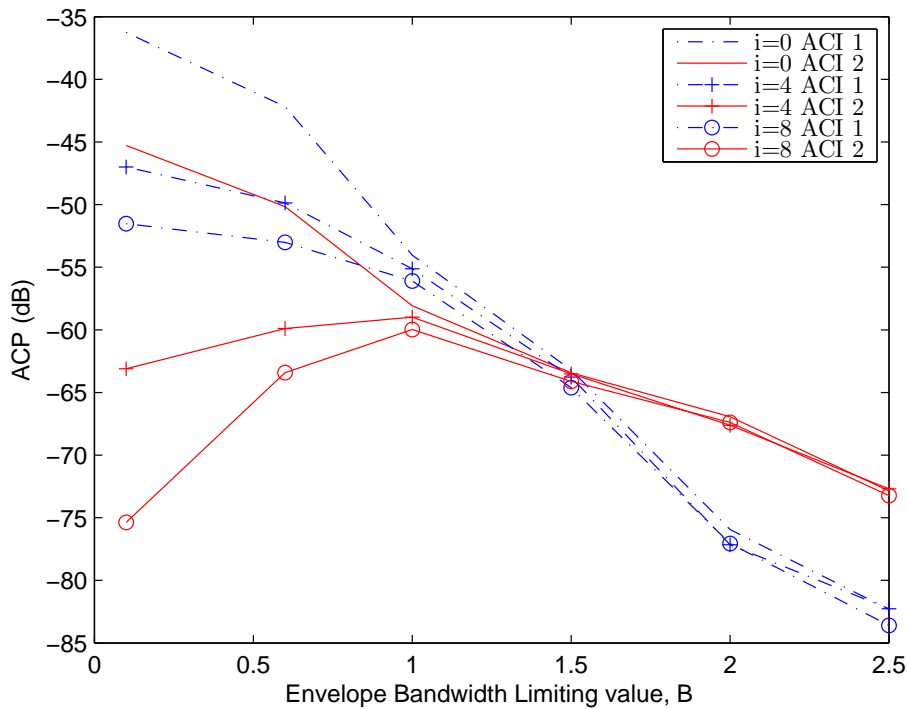


Figure 3.19: ACI 1 and ACI 2 vs bandwidth limitation values for different i repetitions

RF signal gets better with every repetition because of the ACP reduction. For this simulation, $i = 0, 1, 4, 8$ and 14 and a bandwidth limiting value of $B = 1$ are used. It is interesting to see that, with a higher number of repetitions, the RF signal follows the spectral mask.

Due to repetitions, the improvement in RF adjacent channel interference (ACI) has a direct trade-off with EVM buildup. In Figure 3.18 and Figure 3.19, the EVM and ACI are plotted against envelope bandwidth limitation values for different i . It has been already established that the EVM gets worse with repetition (Figure 3.16); so it is interesting to see for which bandwidth limiting value, B , the EVM is more. From the figure, it can be seen that

the difference in EVM is more prominent for bandwidth limitation greater than 0.6 channel bandwidth. Bandwidth limitation needs to be > 1 channel bandwidth if the WLAN EVM specification (-25 dB) is to be met with $i = 8$ repetitions. In Figure 3.19, the dot-dash line represents the ACI 1 and the solid line represents ACI 2. For bandwidth limiting values of 0.6 channel bandwidth and lower, there is a greater improvement in ACI with increasing i values. This shows that there is a trade off between EVM and ACI. The complexity of this technique is much less than IBL and IBL-PTS. The complexity of this technique is $C_{RBL} = iC_{bl}$ (Appendix A). A technique to stop EVM buildup is now introduced in the next sub-section.

3.5.1 QAM Correction

The repetitive bandwidth limitation technique achieves spectral efficiency not only for both envelope and phase signals, but also for the resulting OFDM signal. However, the process results in deteriorated EVM of the signal. In order to rectify this limitation, a QAM correction technique is introduced. In this scheme a square boundary of length 2α is defined around each original constellation point, where α corresponds to the desired EVM threshold. To achieve this EVM, only the scattered points outside the boundary are pulled back on it. This process is shown in Figure 3.20. In this figure, the original constellation point is taken as a reference. The repetitive bandwidth limited data is at $x + jy$ point due to the distortion. The point is then moved back

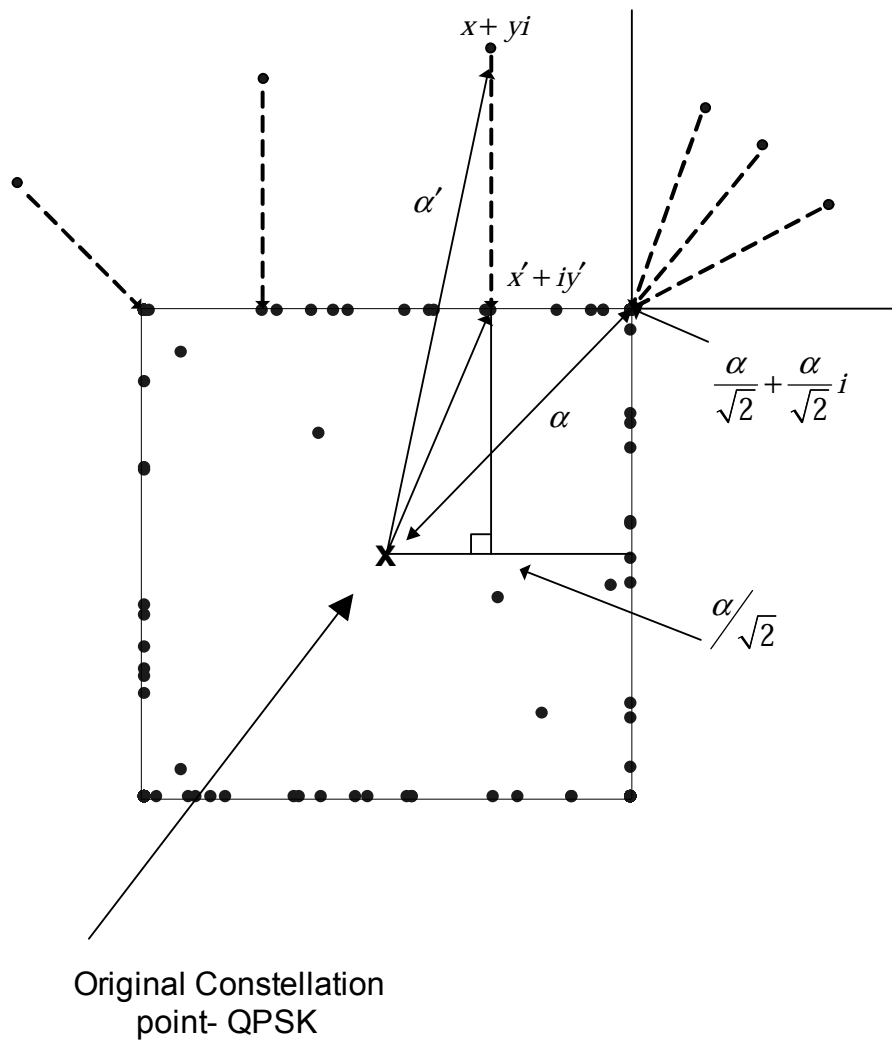


Figure 3.20: QAM correction process for EVM limitation. The original constellation point is (x_d, y_d)

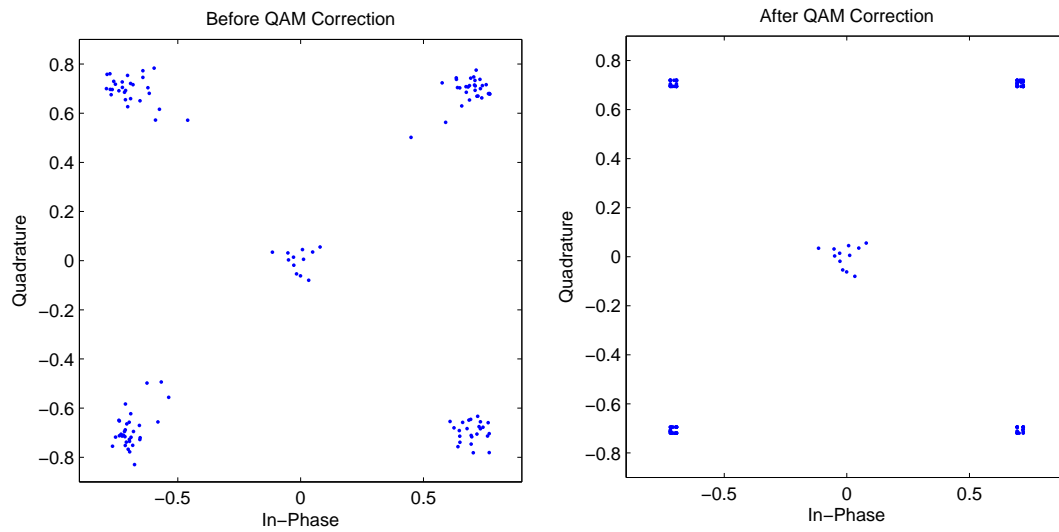


Figure 3.21: Constellation points before and after QAM correction

on the boundary $(x' + jy')$ of the square. The points are moved back on the boundary by the horizontal and/or vertical distance which reduces the distortion power.

$$\begin{aligned}
 &\text{IF } x - x_d > \alpha/2 \text{ then } x' = x_d + \alpha/2 \\
 &\text{IF } x - x_d < \alpha/2 \text{ then } x' = x_d - \alpha/2 \\
 &\text{IF } y - y_d > \alpha/2 \text{ then } y' = y_d + \alpha/2 \\
 &\text{IF } y - y_d < \alpha/2 \text{ then } y' = x_d - \alpha/2 \\
 &\text{ELSE } x' = x \text{ and } y' = y
 \end{aligned} \tag{3.9}$$

where x_d and y_d are the original signal constellation points.

As it is the transmitter side, the locations of the constellation points are already known. As such, a QAM correction technique can be performed on the constellation points. Figure 3.21 shows the constellation points before and after the QAM correction process is performed. The QAM correction is performed on all constellation points except the inactive tones (don't care bins). This is why the $(0,0)$ co-ordinate points are not corrected. For this

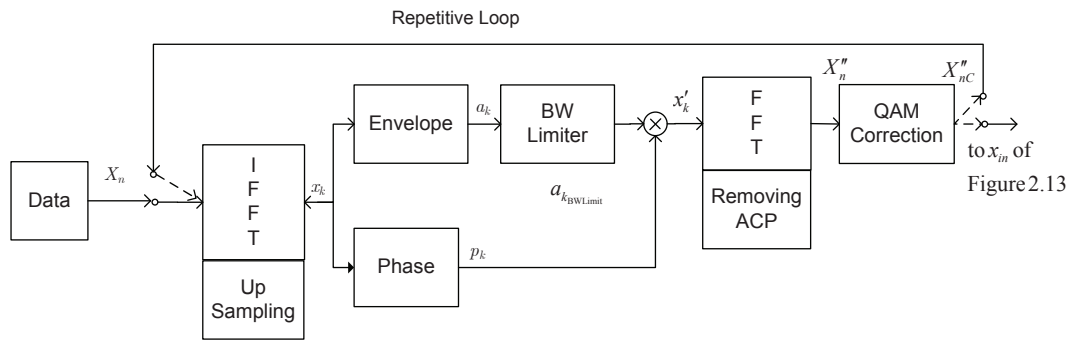


Figure 3.22: Revised block diagram of Repetitive BW limit process with QAM correction included in the loop

simulation, an EVM threshold of -25 dB is used, which results in $\alpha = 0.0562$.

The drawback of the QAM correction process is: as the constellation points are corrected, there is spectrum regrowth for the envelope and phase component. However, if the QAM correction is performed inside the repetitive loop, the spectrum regrowth can be partially corrected. The revised block diagram is shown in Figure 3.22: with the QAM correction block inside the loop. Figure 3.23 shows the spectrum of the OFDM signal and the envelope and phase components when the QAM correction is performed as a repeated process. With $i = 10$ repetitions, the envelope bandwidth reduces to 2.6 channels (from the original envelope bandwidth of 3.5 channels) and the phase bandwidth reduces to 10 channels (from the original phase bandwidth of 15 channels). In addition, the OFDM RF spectrum does not deteriorate except for the ‘dont care’ bins. As such, the signal stays within the spectral mask. Figure 3.24 shows the CDF of EVM for the OFDM RF signal when the QAM correction is employed for $i = 10$ repetitions.

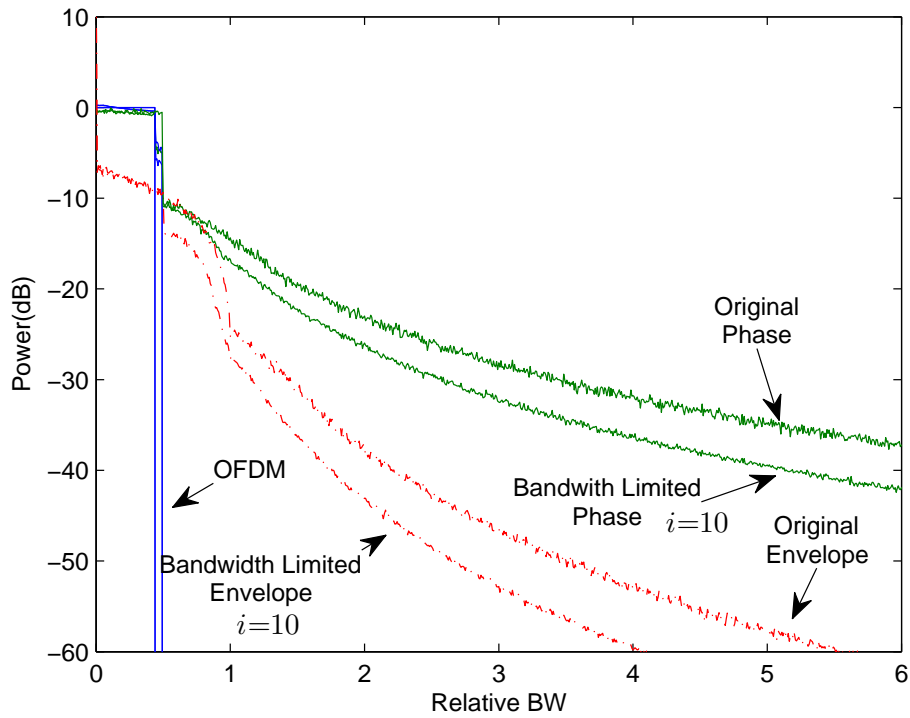


Figure 3.23: Bandwidth improvement in envelope and phase spectrum at -50 dB for $i = 10$ repetitions with QAM correction enabled in the loop.

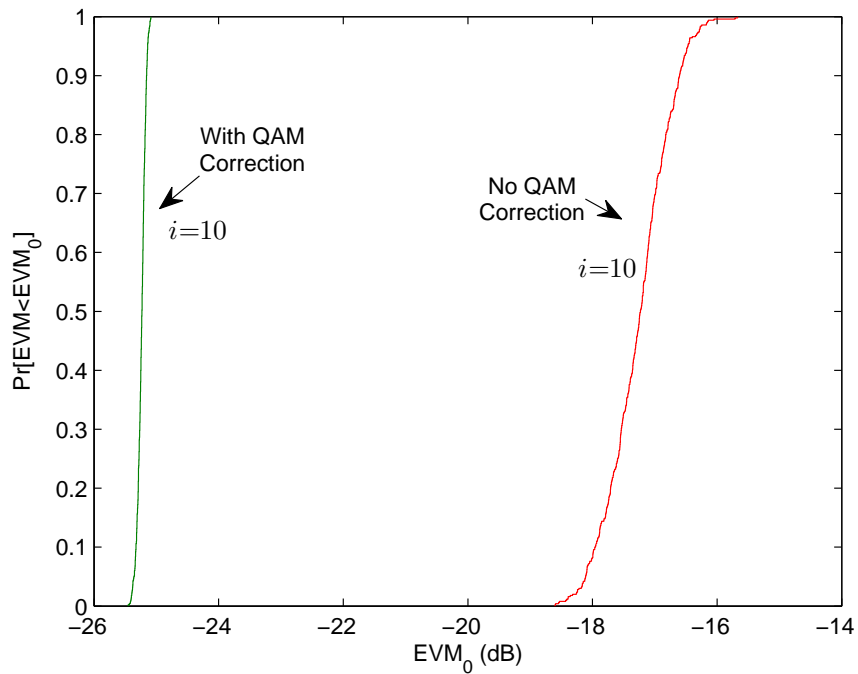


Figure 3.24: CDF of EVM for $i = 10$ repetitions at envelope bandwidth limiting value of $B = 1$ channel bandwidth and QAM correction enabled.

In this section, a new repetitive bandwidth limitation technique has been introduced. The technique manages to reduce both envelope and phase bandwidths. The process also minimizes the RF spectrum of the OFDM signal. In addition, a trade-off is shown between EVM and ACI. From the simulated diagrams, an optimum bandwidth limiting value and number of repetitions can be chosen depending on spectral mask and design criteria. The repetition causes high EVM buildup. This is solved using a new QAM correction scheme which constrains the constellation points to a desired EVM value.

3.6 Bandwidth Limiter with RF drive compensation (BLDC)

So far in this chapter, both distortionless and distortion based schemes have been considered. Although the distortion based schemes provide better bandwidth reduction for the polar components, they result in added EVM buildup. In this section, a novel technique is proposed that combines a small amount of RF drive modulation with the EER architecture. If the amplitude modulation of the RF drive signal is to effect the output, then the amplifier should be linearly biased (e.g. Class B). Switching amplifiers are not so sensitive to small amplitude variations on their input pulse signals, but can be made responsive by converting any amplitude variation into a pulse width modulation (PWM). The process can be viewed in Figure 3.25. The dotted box marked $\Sigma\Delta$ is responsible for converting the amplitude and phase modulated signal, s_p , into

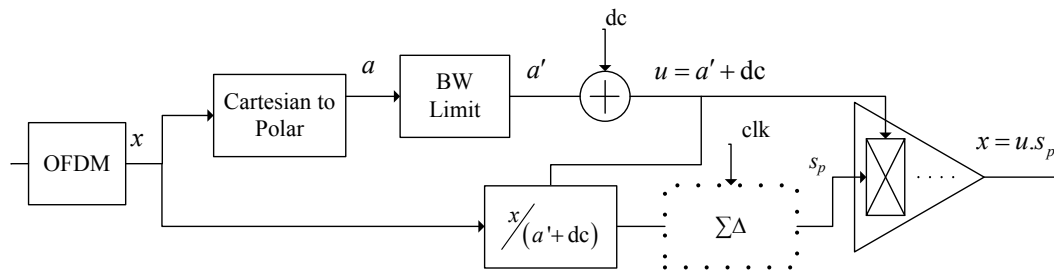


Figure 3.25: Block diagram of bandwidth limiter with amplitude compensation of the RF drive signal, s_p .

a pulse position modulation (PPM)/PWM signal for driving the SMPA input. The SMPA's PPM/PWM signals are square pulses with amplitude equal to V_{dd} . The V_{dd} voltage is controlled by the envelope from the EER separator, which effectively scales the amplifier's PWM/PPM output. This scaling effect also applies to linearly biased amplifiers. The EER power amplifier can therefore be modelled (to a good first order approximation) as a multiplier. The new architecture portions the responsibility for the amplitude modulation between the EER envelope signal and the amplifier RF input signal. The latter is achieved by changing the amplitude (or pulse width) of the RF drive signal, s_p . The idea is to handle the low frequency envelope components through the V_{dd} drive and use the RF input signal with its higher bandwidth capability to account for the high frequency envelope components.

The process first limits the envelope BW in a low pass filter (using the technique described in Section 3.2) to give a' and then adds a dc^4 value to stop the amplifier from clipping. Amplifier clipping occurs when $a' + dc < |x|$

⁴The dc level is set to give a clipping threshold of 8 dB above the average power level. The 8 dB figure represents the PAPR of a typical transmit signal from a basestation.

or if $s_p > 1$. The first constraint occurs when the supply voltage is not high enough for the required instantaneous output power, and the second constraint is when the required input signal goes over saturation⁵. The $u = a' + dc$ signal acts as the supply modulator for the amplifier. Here, $s_p = x/(a' + dc)$ is the drive signal for the PA. In the case of no BW limitation (i.e. $B = \infty$ channels and $a' = a = |x|$), the input drive, s_p , is a constant magnitude signal containing phase information only, $s_p = \angle x$. The architecture then works as ideal EER. On the other hand, if there is maximum bandwidth limitation ($B = 0$ channel), u contains only a fixed DC value and s_p is the original input signal, x . Partially limiting the envelope BW and introducing some envelope variation into the phase drive signal, s_p , results in reduced BW expansion for both envelope and phase drive signals compared to the ideal EER system. The input drive, s_p , is scaled (multiplied) by the envelope signal, u , within the power amplifier to recreate, x_{out} , at the amplified output.

Figure 3.26 and Figure 3.27 show the effect of BW limiting the envelope signal to $B = 0.1$ and $B = 4$ channel bandwidths. The u becomes more like a gently varying dc signal with almost no envelope signal content at the low bandwidth. The envelope signal u must contain a dc component to stop the amplifier from clipping on the signal peaks (Figure 3.26). Conversely the drive signal, u has a much closer match to the ideal signal ($|x|$) at the higher bandwidth, and needs less dc offset to avoid the clipping (Figure 3.27). The

⁵The signal levels have been normalised such that input saturation is 1.0 and the amplifier gain is 1.0.

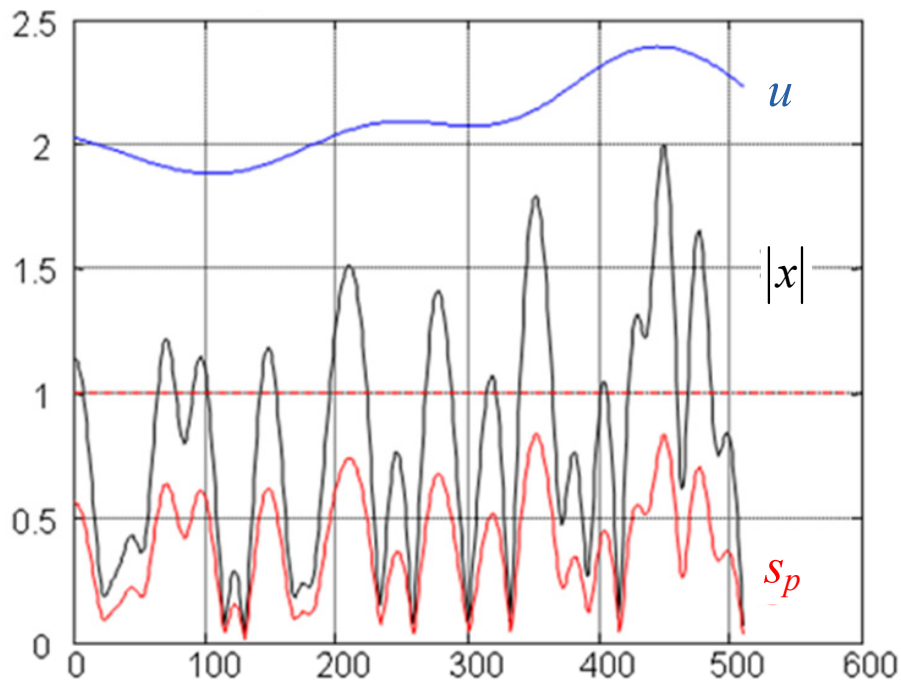


Figure 3.26: The effect of bandwidth limiting the envelope signal to 0.1 channel bandwidth

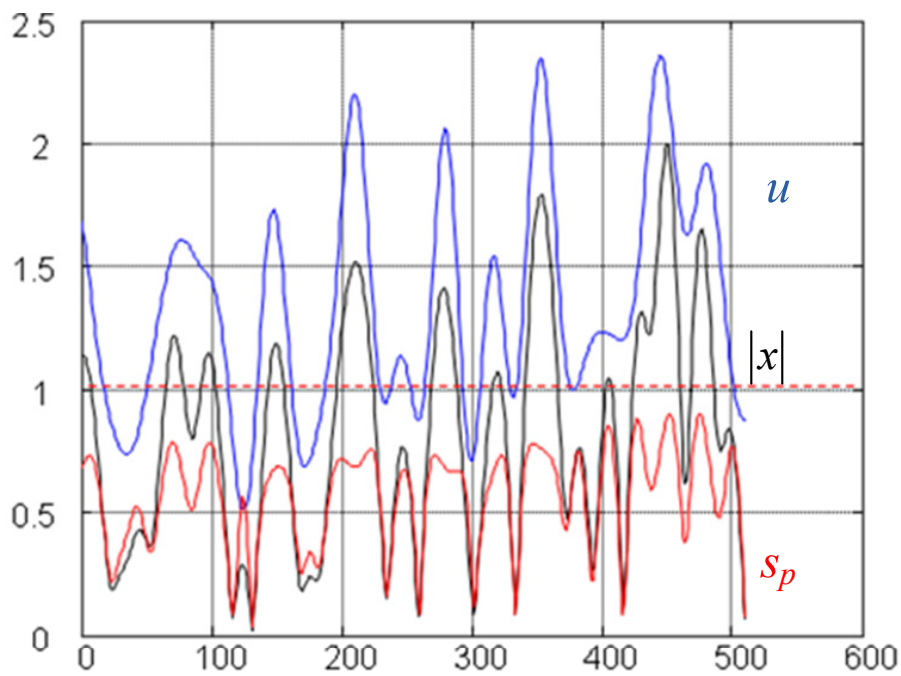


Figure 3.27: The effect of bandwidth limiting the envelope signal to 4 channel bandwidth

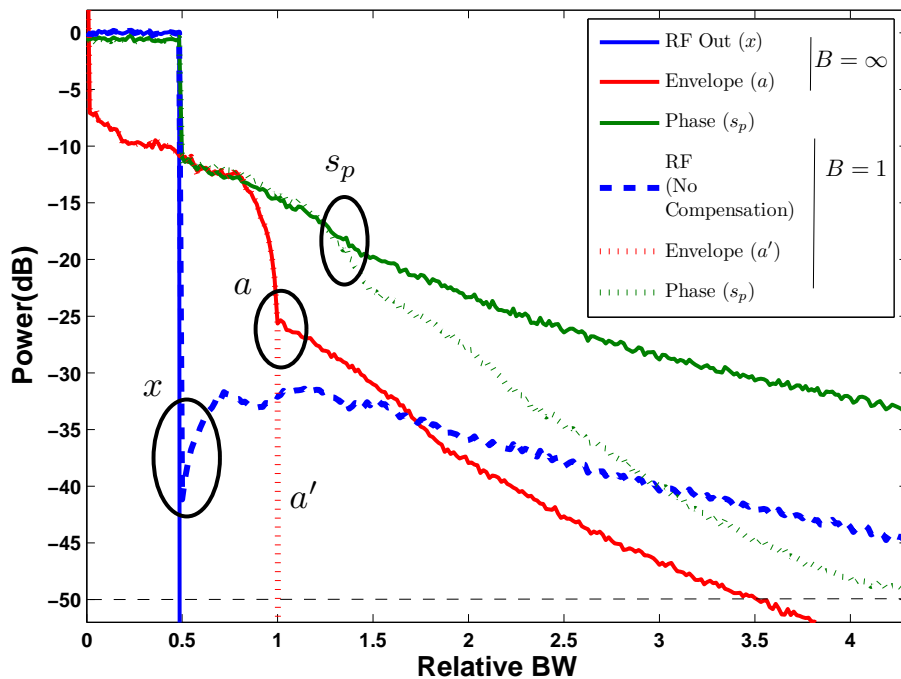


Figure 3.28: Spectra of the input drive signal, s_p envelope signal, a , and OFDM RF signal, x .

power dissipated in the amplifier is related to the voltage drop across the amplifier, which is the difference between the u and $|x|$. The advantage of the small dc-offset is that the envelope signal can follow the desired signal more closely resulting in lower power dissipation.

Figure 3.28 shows the spectra of the OFDM RF signal, x , and its polar drive components s_p and a . The effect of envelope bandwidth limitation is shown with and without compensation of the phase drive signal. The thin solid lines show the RF and polar components, when there is no BW limitation. The dotted line, x , shows the blowout of the RF spectrum when the envelope (a' , shown dotted) is BW limited, to one OFDM channel ($B = 1$) without applying the corresponding compensation. This is the same situation as in Section 3.2.

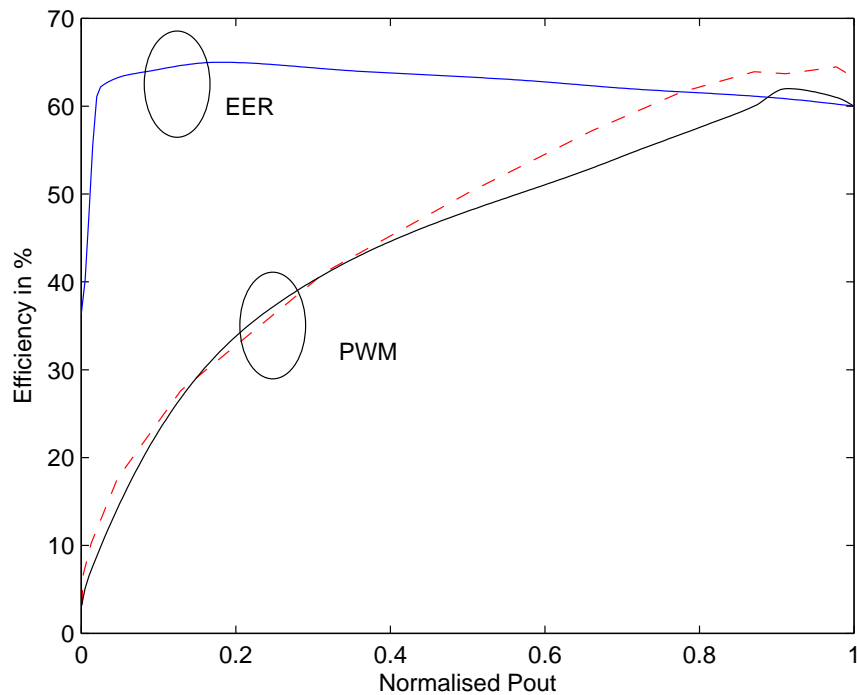


Figure 3.29: Efficiency against power output. PWM curves are for $V_{dd} = 30V$ (solid) and for $V_{dd} = 10V$ (dashed) and EER (solid) [63]

When the compensation is applied to the input signal, s_p , its BW reduces (Figure. 3.28 green, dotted), and the blowout in the RF spectrum is repaired, as is the EVM. The new architecture leads to envelope and phase BWs being reduced to 1 channel and 4.5 channel respectively, when measured at a -50 dB threshold. This is an improvement of 71.4% for the envelope and 70% for the phase signal. Even though the RF signal suffers no EVM or ACI, when the envelope bandwidth is limited, the amplifier efficiency is compromised.

The measured efficiency vs. output power curves from a class E Gallium Nitride HEMT amplifier design given in [63] is used to predict the amplifier efficiency when it passes an OFDM signal. The curves are reproduced in Figure (3.29) and show the amplifier operation in EER mode, with a constant

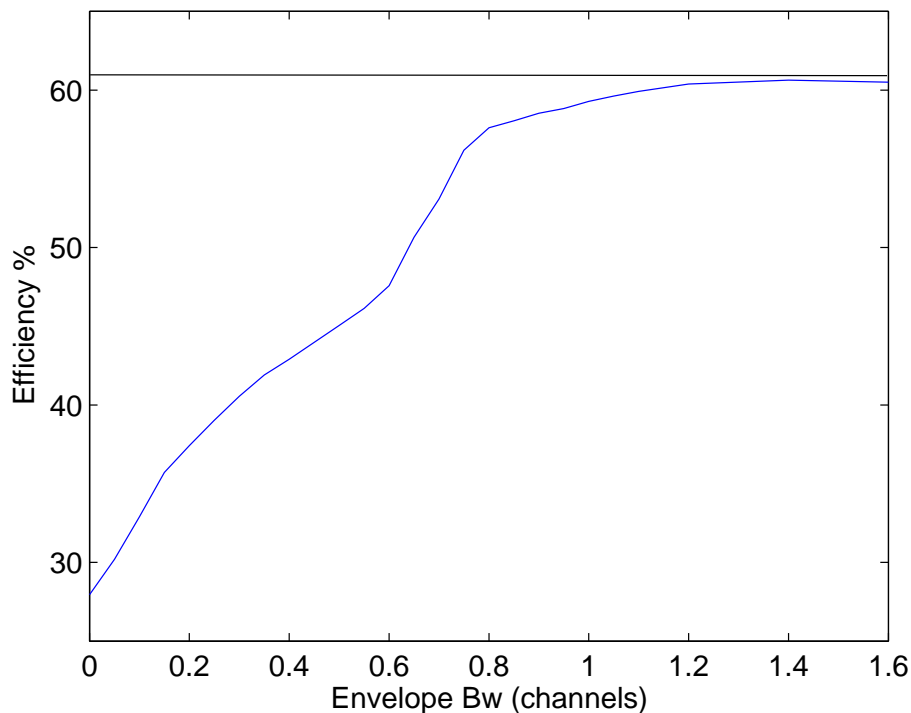


Figure 3.30: Predicted efficiency versus envelope bandwidth for an OFDM signal using BLDC and the measured amplifier of Figure 3.29.

input signal, as well as in PWM mode with a constant V_{dd} supply. The noise-like OFDM signal has a wide dynamic range and in the simulations amplifier clipping occurs when $a' + dc < |x|$, or if $|s_p| > 1$. Low dc values increase clipping but are best for efficiency. For each BW limit we choose the dc offset value to give the same clipping energy as a normal OFDM signal clipped to 8 dB PAPR. The clipping noise for each simulation is therefore the same.

Figure 3.30 shows the predicted efficiency versus envelope bandwidth plots for OFDM simulation. The ideal amplifier would have high efficiency and low envelope bandwidth; therefore an operation close to the top left hand corner is preferable. When there is no envelope BW limitation ($B = \text{inf}$) the amplifier

structure works as EER and the efficiency is at 62% (see the horizontal line in Figure 3.30). However, when the BW limitation is at 0Hz, that is, the envelope has only a fixed dc value, the efficiency is 28% which is the efficiency of the PWM amplifier itself. A further 10% efficiency can be gained with the envelope filtered to 0.25 channel bandwidths. The optimal point lies at the knee of the curve at $B = 0.75$ channels BW which yields 57% efficiency. Expanding the bandwidth beyond this value leads to diminishing returns in efficiency. 57% efficiency is only 5% less than the theoretical EER optimum of 62%. It is a very good tradeoff for the large 78.5% reduction in envelope bandwidth to $B = 0.75$ channels.

3.7 Summary

In this chapter, two types of techniques have been introduced to reduce the bandwidth expansion of the polar drive signals in the EER architecture. Here we concentrate on the envelope signal as it is more critical in practical applications. The distortion-less technique called minimum power PTS shows only a small improvement of 22.2% in bandwidth for a large cost of complexity of 64 trials and the requirement of sending additional side information. One of the interesting observations is that there is no correlation between sequences that are good for PAPR reduction and the sequences that are good for bandwidth reduction. It is therefore possible to obtain both PAPR and polar bandwidth reduction by selecting from a set of Q_s lowest PAPR sequences out

of $S = Q^{M-1}$ trials and choosing the sequence with the lowest bandwidth from the set of Q_s .

The distortion based techniques are all based on some form of bandwidth limitation of the polar drive signals. A low pass filtering operation is performed on the envelope signal. The iterative BW limitation (IBL) scheme incrementally reduces the envelope bandwidth until the reconstituted OFDM signal exceeds the spectral mask. The technique managed to reduce the envelope bandwidth to 2.55 channels (27.1% improvement at -50 dB level) and keeps the OFDM signal within the spectral mask criteria. However, the phase bandwidth did not improve. These results were further enhanced by additionally incorporating the sequences from the PTS scheme and choosing the lowest one with the IBL bandwidth. The resulting bandwidth of the envelope was further reduced to 2.21 channels (27% improvement) and the phase bandwidth also improved to 13.6 channels at -50 dB level with a very low EVM cost of -43 dB. The time complexity equations for IBL and IBL-PTS is shown in Appendix A.

The repetitive bandwidth limitation technique limited the envelope signal repeatedly and allowed the don't care bins to distort. It managed to reduce both envelope and phase signal bandwidth at the cost of large EVM buildup. This was partially fixed using the QAM correction technique. The technique managed to reduce the envelope bandwidth to 2.6 channels (25.7%) and the phase bandwidth to 10 channels. The complexity in this scheme is much less

compared to the three previous schemes (Appendix A).

The last section of the chapter showed a novel bandwidth reduction scheme. The technique used PWM and PPM signals with the EER architecture. It showed that allowing some envelope variation on the phase modulated input signal helped to reduce both envelope and phase bandwidth without distorting the OFDM spectrum or EVM buildup. This technique yielded the best result in this chapter, but came at the expense of a small loss in efficiency. If the envelope bandwidth was reduced to 1 channels the efficiency loss is only 4%. In addition, the RF drive signal (s_p) bandwidth improves to a very respectable 4.5 channels. The methods that satisfy the spectral mask criteria are summarized in Table 3.1.

The complexity figures are found from using $N = 128$ subcarriers with $L = 64$ oversampling rate and for PTS with $S = 64$ trials. The $N \log_2 N$ operations of the FFT/IFFT process dominates and so only these are included in the Table.

Table 3.1: Summary of bandwidth reduction techniques on polar drive signals for the EER architecture. Bandwidths are normalized to 1 OFDM channel.

Technique	Normalized Bandwidth @-50 dB				EVM @50 per- centile (dB)	Comple- xity (Opera- tions)
	Envelope		Phase			
	ch	Im- prove- ment (%)	ch	Im- prove- ment (%)		
No Band- width limi- tation	3.5	-	15	-	-	-
Minimum Band- width PTS (Section 3.1)	2.72	22.2%	12	20%	No EVM	6.8×10^6
IBL- Envelope (Section 3.3)	2.55	27.1%	14.9	0.6%	-44.4 dB	2.59×10^7
IBL-PTS- Envelope (Section 3.4)	2.21	37%	13.6	9.3%	-43 dB	4.9×10^7
RBL for $i = 10$ (Section 3.5)	2.6	25.7%	10	33.3%	-26 dB	2.1×10^6
BLDC (Section 3.6)	1	71.4%	4.5	70%	No EVM	2.1×10^5

Chapter 4

Theoretical Analysis of Hole Punch Method

In the previous chapter, the bandwidth of the polar drive signals have been reduced by both distortionless and distortion based methods. In this chapter, the ‘hole punch’ method is discussed which was originally introduced by Rudolph [3].

It has been found that the OFDM signal describes an almost random path in the I & Q plane. Any near zero crossings cause large dips in the envelope signal and a large rate of phase change (instantaneous frequency) for the phase drive signal. The coordinate transform of this signal from Cartesian to polar results in signal components that have wider bandwidth than that of the input signal. This principle of hole punch technique: prevents zero crossings in the I & Q plane by adding a bandwidth limited correction signal to keep the signal envelope from going to zero. The paper [3] confirmed that any adjacent channel power generated by the process was minimal. However, inband distortion is still produced which degrades the EVM of the transmitted signal. This was

one of a number of serious omissions in [3]. Others include: non-complete specification of the Gaussian window and choosing a poor reference value for determining the hole size threshold. These problems made the reproduction and verification of [3]’s simulations impossible. In this chapter, we correct these omissions and provide a first time theoretical analysis of the system.

Section 4.1 describes the hole punch method and how it improves the spectrum of polar components. We also provide theoretical expressions for the resulting EVM and ACI and show how a different windowing techniques affects the results (Section 4.2). Most of the work from this chapter has been published in the EURASIP Journal on Wireless Communications and Networking [64].

4.1 Hole Punch

To prevent the zero crossing, an approach similar to [3] is used. The amplitude of the signal is restricted from falling below a minimum threshold level, a_{th} , to give the hole punched signal y_k (Fig 4.1).

$$y_k = \begin{cases} x_k, & a_k > a_{th} \\ a_{th}e^{j\theta_k}, & a_k \leq a_{th} \end{cases} \quad (4.1)$$

where a_k and θ_k are the sampled version of envelope and phase of x_k . In this work, we set the a_{th} relative to the average signal power. We note that, [3] defines the hole size with respect to peak power. However, we chose to use average power because this is a more stable measure for OFDM and multicarrier signals whose peak power varies considerably on a symbol by symbol basis.

The abruptness of the hole in y_k causes spectral splatter. The complementary residue signal, z_k , which contains the distortion components (and spectral splatter), is then calculated by subtracting out the original signal. In order to isolate the peaks, a peak detector is used which results in the residue signal of z'_k . The peak detector finds the zero slope. If the oversampling is high then we get a number of zero slope points on our peak. Therefore the algorithm uses a sliding window and records a peak when the value is maximum over the window. To spectrally fit z'_k into the specified bandwidth, pulse shaping is applied. This produces a bandwidth reduced residue signal, u_k , that can be added to the original signal to give a hole with smoother transitions. For pulse shaping, we considered Hanning (w_h) and Gaussian window (w_g) functions.

$$w_h(k) = 0.5 \left(1 - \cos \left(\frac{2\pi k}{LV - 1} \right) \right) \quad (4.2)$$

$$w_g(k) = e^{-1/2(\alpha \frac{k}{LV/2})^2}, \quad -LV/2 \leq k \leq LV/2, \quad \alpha \geq 2 \quad (4.3)$$

where $LV + 1$ is the window size. The window is convolved with the spiky residue signal z_k , to smooth (shape) the sharp transitions. The signal u_k is added to an appropriately delayed version of the input signal x_k to give (figure 4.1) the hole punched signal x'_k that feeds into the EER transmitter. The process is shown below:

$$\begin{aligned} z_k &= x_k - y_k \\ z'_k &= \begin{cases} z_k & |z_k| > |z_{k+i}| \text{ for } \omega/2 < i < \omega/2 \\ 0 & \text{otherwise} \end{cases} \\ u_k &= z'_k * w \\ x'_k &= x_{(k - \frac{LV}{2})} + u_k \end{aligned} \quad (4.4)$$

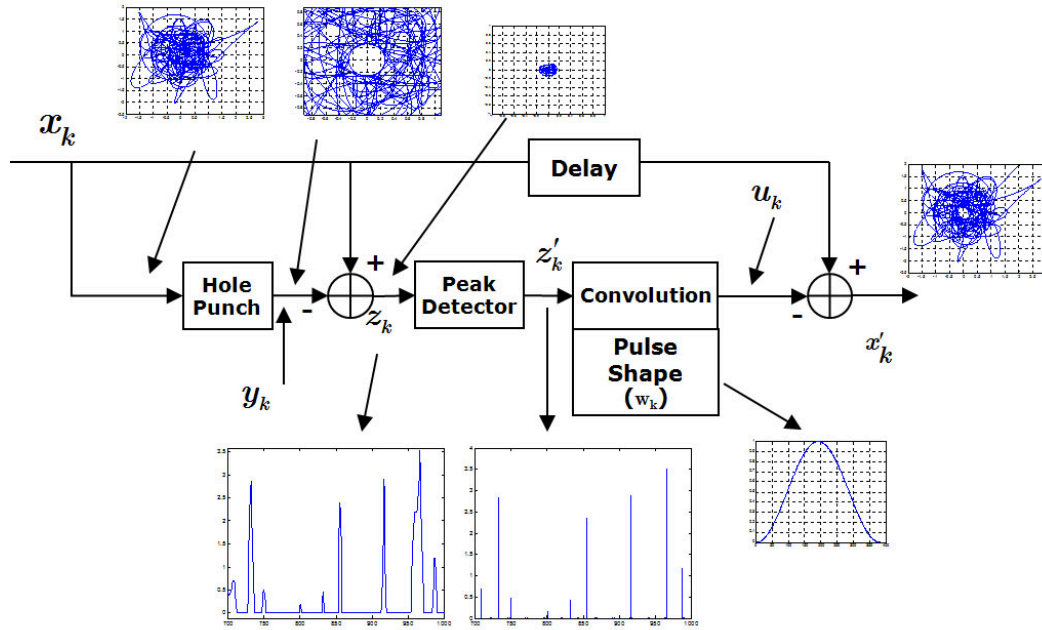


Figure 4.1: Block diagram of hole punch process.

where ω is the length of the running window to determine the peaks. The value of ω depends on the oversampling rate.

The hole punched signal x'_k improves the spectrum of the polar drive signals, but at the expense of the RF distortion. In the next section, we derive theoretical expressions for the in-band and out of band errors as a function of window length (V), window shape and the threshold (a_{th}). For ease of understanding, we use $w(k)$ as a generic window function.

4.2 Error Analysis

4.2.1 Theory

The first goal is to calculate the total distortion power of the correction signal u_k . The second goal is to identify how the power is apportioned in the frequency domain. We make use of the noise like property of OFDM, in particular the Rayleigh probability density function (PDF) of its envelope.

In order to find the power of the correction signal u_k , we need to know the amplitude and rate of occurrence of the correction peaks, z'_k . We make the assumption that, for sufficiently large N , the envelope of the OFDM signal follows Rayleigh distribution [65]. We define N_a as the level crossing rate of the level amplitude, a . If the level is much less than the rms value of the signal ($a \ll a_{rms}$) then each level crossing corresponds to a valley in the envelope signal (figure 4.2). N_a therefore represents the number of valleys/sec with amplitude less than a . The following equation is stated from [10].

$$N_a = \sqrt{\frac{\pi}{3}} \frac{N}{T_s} a e^{-a^2} \quad (4.5)$$

where, T_s is the OFDM symbol period. The rate of change of level crossing rate with respect to the amplitude can be used to determine the number of valleys in the signal between a small range da (figure 4.2). The number of valleys/sec occurring between a and $a + da$ can be represented as

$$N_a - N_{a+da} \quad (4.6)$$

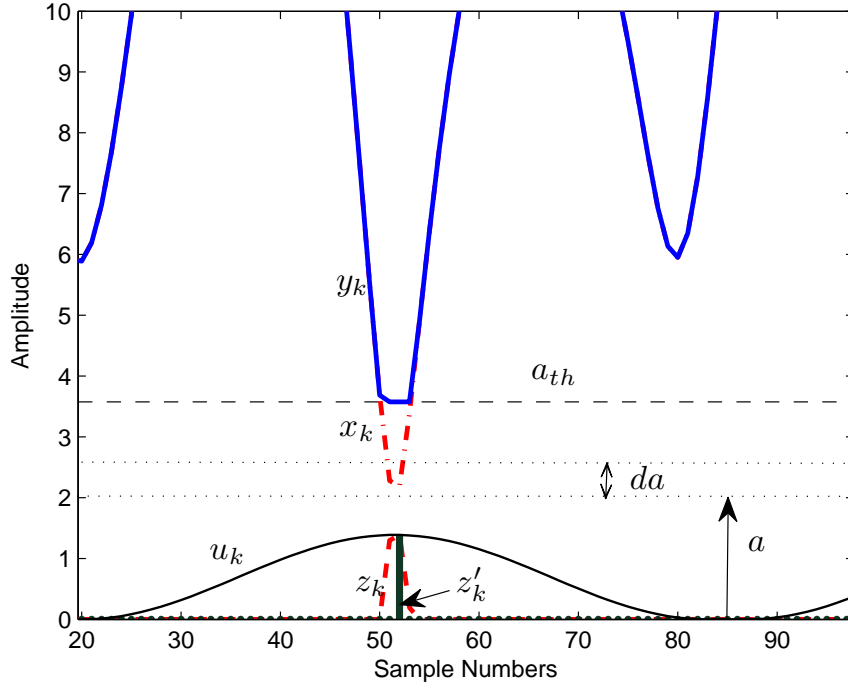


Figure 4.2: The original signal x_k is limited to a minimum amplitude a_{th} by adding a residue signal z_k . The peak of z'_k is used to scale the window function

Hence, we can write the PDF of the valleys as

$$\begin{aligned}
 P(N_a(\hat{a})) &= \frac{N_a - N_{a+da}}{da} = \left(\frac{dN_a}{da} \right) \\
 &= \sqrt{\frac{\pi}{3}} \frac{N}{T_s} e^{-a^2} [1 - 2a^2]
 \end{aligned} \tag{4.7}$$

The power of the correction peaks associated with these valleys can be represented as

$$P_{z'_k} = \frac{dN_a}{da} (a_{th} - a)^2 \tag{4.8}$$

Energy of the window function can be expressed as

$$E_{w_k} = \frac{1}{L} \sum w_k^2 \tag{4.9}$$

Using (4.7), (4.8) and (4.9), the power of u_k can be derived as

$$\begin{aligned}
P_{u_k} &= \int_0^{a_{th}} \frac{dN_a}{da} (a_{th} - a)^2 E_{wk} da, \\
P_{u_k} &= \sqrt{\frac{\pi}{3}} \frac{N}{T_s} \sum w_n^2 t_{ss} \int_0^{a_{th}} e^{-a^2} [1 - 2a^2] (a_{th} - a)^2 da \\
&= \sqrt{\frac{\pi}{3}} \frac{N}{T_s} \sum w_n^2 t_{ss} \left[\int_0^{a_{th}} a_{th}^2 e^{-a^2} (1 - 2a^2) da - a_{th} \int_0^{a_{th}} 2a e^{-a^2} (1 - 2a^2) da \right. \\
&\quad \left. + \int_0^{a_{th}} a^2 e^{-a^2} (1 - 2a^2) da \right] \\
&= \sqrt{\frac{\pi}{3}} \frac{N}{T_s} \sum w_n^2 t_{ss} \left[a_{th}^3 e^{-a_{th}^2} - a_{th} \left(-1 + e^{-a_{th}^2} + 2a_{th}^2 e^{-a_{th}^2} \right) \right. \\
&\quad \left. + \frac{1}{2} \left(2a_{th} - \sqrt{\pi} \operatorname{erf}(a_{th}) \right) e^{a_{th}^2} + 2a_{th}^3 \right] e^{-a_{th}^2} \\
&= \sqrt{\frac{\pi}{3}} \frac{N}{T_s} \sum w_n^2 t_{ss} \left[a_{th} - \frac{\sqrt{\pi}}{2} \operatorname{erf}(a_{th}) \right]
\end{aligned} \tag{4.10}$$

where $\operatorname{erf}(a_{th}) = \frac{2}{\sqrt{\pi}} \int_0^{a_{th}} e^{-t^2} dt$ is the error function. The error function is twice the integral of the Gaussian distribution with 0 mean and variance of 1/2.

The threshold, a_{th} , determines the hole size and the effectiveness of the hole punching scheme. A larger a_{th} reduces the bandwidth expansion but increases distortion and vice versa.

The EVM can be theoretically calculated by finding the fraction of the correction signal (u_k) power that falls in-band (between the frequencies $\frac{-N}{2T_s}$ and $\frac{N}{2T_s}$). This quantity is obtained by integrating under the window energy spectrum curve (figure 4.6).

$$\text{EVM} = \frac{P_{u_k}}{P_{x_k}} \cdot \frac{E_{W_{ib}}}{E_{W_f}} \tag{4.11}$$

Here, $E_{W_{ib}}$ is the in-band energy of the window spectrum and E_{W_f} is the total energy of the window spectrum. The P_{x_k} is the total energy of the input signal. The calculations of the in-band, out of band, total energy and the adjacent channel interference (ACI) of a Hanning window function is shown in the next subsection. Other window functions can be treated in a similar fashion.

4.2.2 Derivation of In-band and Out-of-band Power of Hanning Window Function

In this subsection we derive the in-band and out of band energy of the Hanning window function in the frequency domain. We first calculate the Fourier transform of the continuous time domain Hanning window and later find the energy of it for the in-band and out of band regions.

The continuous time domain expression of Hanning window is

$$f(t) = 0.5 \left(1 - \cos \left(\frac{2\pi \left(t + \frac{VT}{2} \right)}{VT} \right) \right) \quad (4.12)$$

where, $T = \frac{T_s}{N}$ is the critically sampled period of the OFDM symbol. The Fourier transform of the above window function is

$$F(f) = \int_{-\infty}^{\infty} 0.5 \left(1 - \cos \left(\frac{2\pi \left(t + \frac{NT}{2} \right)}{NT} \right) \right) e^{-j2\pi ft} dt \quad (4.13)$$

By expanding the *cos* to exponential functions and simplifying the integrals, we get a sum of 3 sinc functions.

$$F(f) = 0.5NT \frac{\sin(\pi fVT)}{\pi fVT} + \frac{VT}{4} \frac{\sin(\pi VT(f - \frac{1}{VT}))}{\pi VT(f - \frac{1}{VT})} + \frac{Vt_s}{4} \frac{\sin(\pi VT(f + \frac{1}{VT}))}{\pi VT(f + \frac{1}{VT})} \quad (4.14)$$

The total energy of the window function $F(f)$ can be found by integrating the absolute value square over the total spectrum.

$$E_{W_f} = \int_{-\infty}^{\infty} |F(f)|^2 df \quad (4.15)$$

Similarly the in-band energy and the ACI of the out of band energy can be derived as

$$E_{W_{ib}} = \int_{-\frac{1}{2T}}^{\frac{1}{2T}} |F(f)|^2 df \quad (4.16)$$

$$E_{W_{ob}}(n) = \int_{\frac{2n-1}{2T}}^{\frac{2n+1}{2T}} |F(f)|^2 df$$

here, n represents the out of band channels.

Using the same concept, the out of band error or ACI can be derived using

$$\text{ACIn} = \frac{P_{u_k}}{P_{x_k}} \cdot \frac{E_{W_{ob}}(n)}{E_{W_f}} \quad (4.17)$$

here, $E_{W_{ob}}(n)$ is the total energy in adjacent channel n .

4.2.3 Theoretical and Simulation Results

There are two window requirements in the time domain. Firstly, the centre tap, w_0 , is to be unity which is needed to create the hole, and secondly the coefficients should have minimum energy in order to minimize the added distortion within the signal, which shows up as EVM and ACP. Unfortunately it's not possible to set $w_0 = 1$ and have the remaining coefficients set to zero, because the resulting distortion will be splattered across the band and not meet the spectral mask requirements. Some taps are therefore required to

shape the distortion away from critical parts of the spectrum, even though the additional taps increase the distortion. The goal is therefore to reduce the number of additional taps and still meet the spectral mask specifications.

In this section, the Hanning and Gaussian window functions will be compared for spectral shaping. To make the comparison accurate, both windows should have the same coefficient energy. It was found that if the Gaussian window has truncated to the same length as the Hanning window, it produced high spectral side lobes; this is because the Gaussian window does not go to zero and the discontinuity at the end of the window is large. To reduce these side lobes, the Gaussian window length was increased by 20% and the coefficients adjusted (by selecting α) to maintain the same energy. The α can be calculated by solving the following equation for different values of V .

$$\sum_{k=1}^{LV} \left(0.5 \left(1 - \cos \left(\frac{2\pi k}{LV-1} \right) \right) \right)^2 = \sum_{k=1}^{LV} \left(e^{-1/2 \left(\alpha \frac{k}{LV'/2} \right)^2} \right)^2 \quad (4.18)$$

here the $V' = 1.2V$ is the increased length of V .

The spectra of the OFDM signals and their polar components using Hanning and Gaussian windows are shown in Figure 4.3 and Figure 4.4 respectively. The inband distortion, quantified as EVM for both windows is shown in Figure 4.5. The threshold a_{th} values of 10%, 20% and 30% of the average power are used for the EVM plot and 10% and 30% thresholds are used for the spectrum plots (30% of average power is approximately the same as 10% of peak power used in [3]). Window lengths of $V = 6$ and $V' = 1.2V$ are used for Hanning

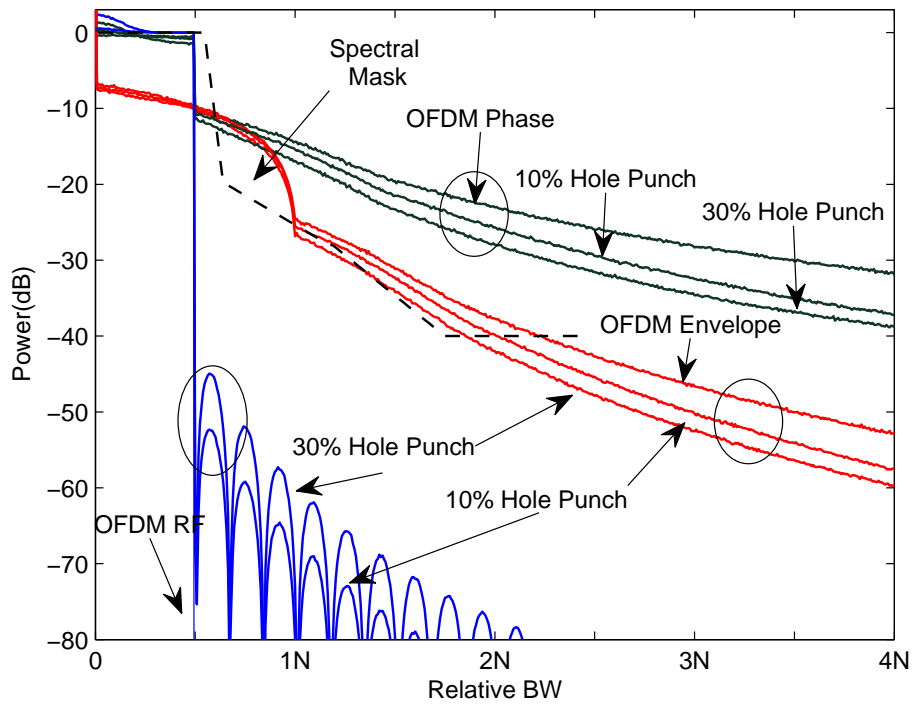


Figure 4.3: Spectrum of amplitude and phase signal with and without hole punching for Hanning window length of $V = 6$.

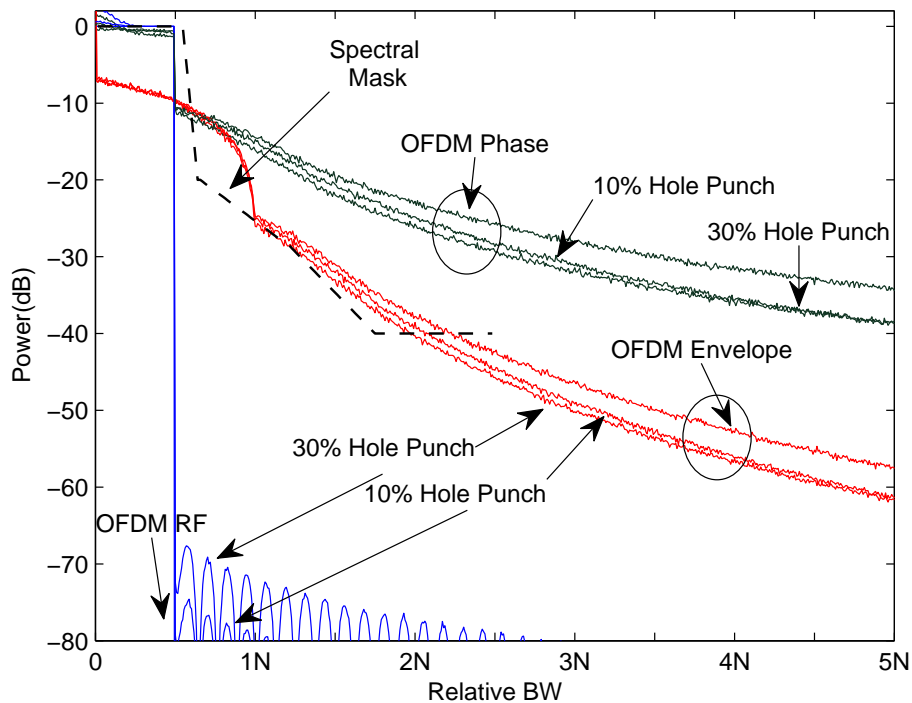


Figure 4.4: Spectrum of amplitude and phase signal with and without hole punching for Gaussian window length of $V = 6$, $V' = 1.2V$

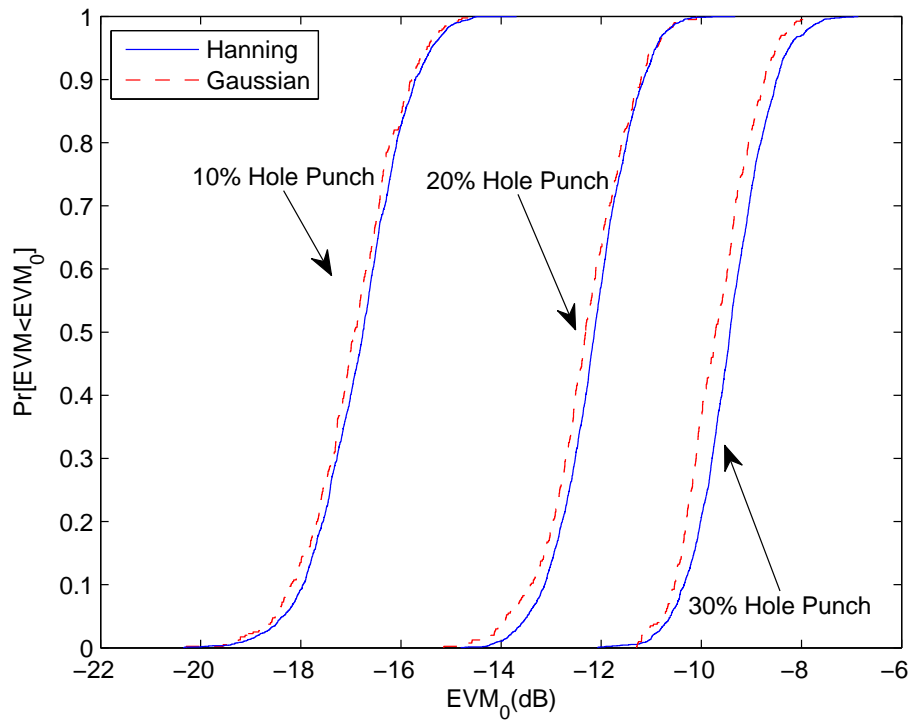


Figure 4.5: CDF of EVM for 10%, 20% and 30% of hole punch for Hanning and Gaussian window of length $V = 6$

and Gaussian windows. The black dashed line is the spectral mask for the WLAN standard of 802.11g. Although the energy in both types of window is kept the same, the spectrum of the signals differs quite significantly. Both window functions achieve spectrum improvement at a cost of EVM loss. The results are summarized in Table. 4.1.

The Hanning window outperforms the Gaussian window in terms of bandwidth reduction of the polar components. However, the Gaussian window has a small advantage in terms of EVM (< 0.2 dB).

In Table. 4.1 the unit of bandwidth is represented as the normalised OFDM channel bandwidth. At the -40 dB level for Hanning window the phase signal

Table 4.1: EVM and Envelope, Phase improvements with respect to channels

	Envelope BW @-40 dB in channels		Phase BW @-40 dB in channels		EVM @98 percentile (dB)	
Original	2.25		7.6		No EVM	
Hole size	10%	30%	10%	30%	10%	30%
Hanning window	2.0 (11%)	1.8 (20%)	4.8 (37%)	4.3 (43%)	-14.9	-7.6
Gaussian window	2.09 (7%)	1.9 (16%)	5.55 (27%)	5.5 (28%)	-15.03	-8.1

bandwidth improves to 4.3 channel BW, which is a respectable 43% reduction and the envelope signal bandwidth reduces to 1.8 channel BW (20% improvement) for the larger a_{th} value. The EVM however is -7.5 dB (@98 percentile). In the case of the Gaussian window the hole punch achieves an improvement of 28% and 16% for phase and envelope signals. For better visibility of these figures, we have not limited the range of the relative bandwidth axes. At -40 dB the relative bandwidth of the original phase signal is 7.6 channel BW. For the Hanning window, a smaller hole size of 10% gives a 27% phase bandwidth reduction and a 11% envelope bandwidth reduction, but improves the EVM to -15 dB, which will limit the modulation to about QPSK (Differential QPSK is used for digital audio broadcast (DAB)). As for the bandwidth limitation of the polar drive signals, the Hanning window provides a better result than the Gaussian window, and so we have used the former as the default window for the next set of simulations and analysis.

It is interesting to see how the performance of the hole punch process changes with varying window lengths. Figure. 4.6 shows the Hanning window

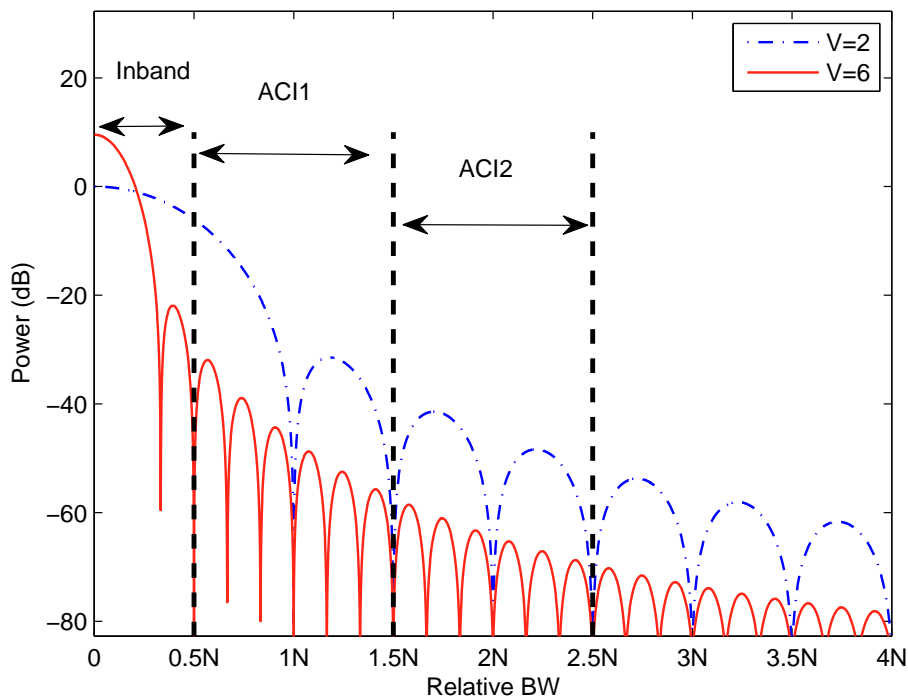


Figure 4.6: In-band and out of band channels of the Hanning window for window lengths of $V = 2$ and $V = 6$ in the frequency domain.

spectrum for window lengths of $V = 2$ and $V = 6$. Smaller window lengths result in less of the distortion power falling in-band and more of it falling out of band in the ACI channels. The larger window size of $V = 6$ concentrates nearly all the distortion power in-band; interestingly the main lobe only effects the inner tones of the OFDM signal. Additionally, as the centre tap of the Hanning window is always scaled to unity, the energy of the window function increases as more coefficients are added resulting in an increase in distortion power shown by the increase of P_{u_k} in Figure 4.7. The solid and the dashed lines show the theoretical results for EVM and P_{u_k} respectively, whereas the markers show the simulation results. For small window lengths, we can observe the EVM to be lower than P_{u_k} . The shortfall is the power residing out of band

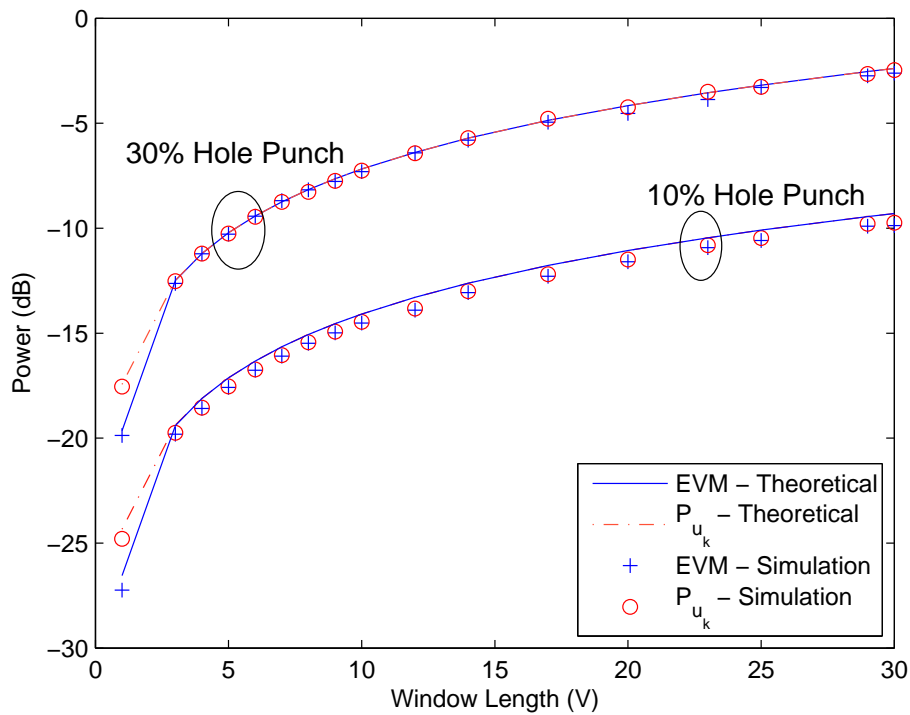


Figure 4.7: P_{u_k} and EVM using Hanning window for 10% and 30% of Hole Punch with increasing window length.

in the ACI channels. Note, the power of the correction signal (P_{u_k}) is the addition of the EVM and ACI. When $V > 3$ the P_{u_k} and EVM lines overlap indicating little energy in the ACI channels (Figure 4.8). The reduction in out of band spectrum is greater than the increase in total distortion power as window lengths increase. For this window the ACI2 channel is approximately 25 dB below the ACI1 channel. A different window shape will allow different ACI behaviours.

Figure 4.9 shows the bandwidth improvement for the polar drive signals with increasing window length. We have found that the bandwidth improvement gradually decreases for $V > 4$. For a higher window length, overlapping

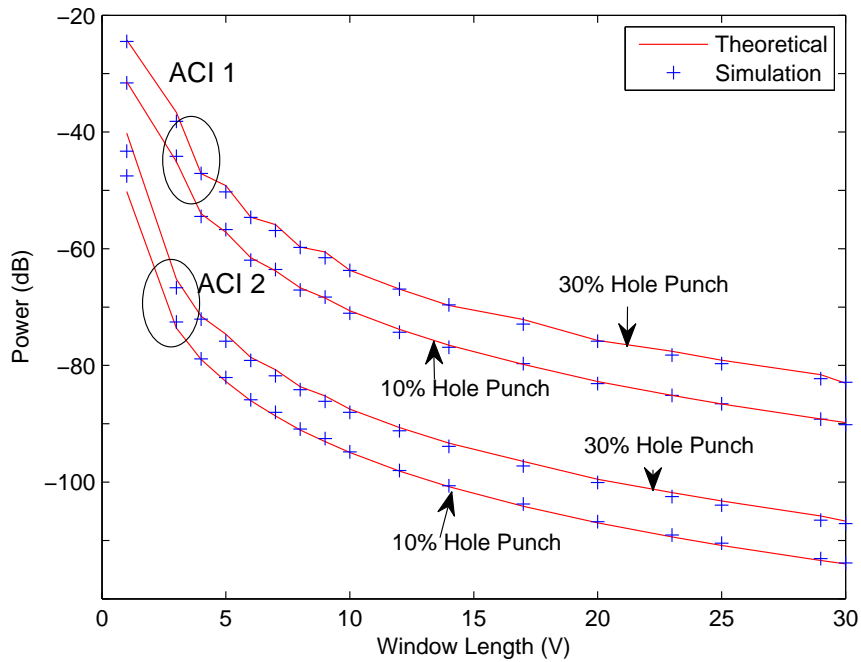


Figure 4.8: ACI 1 and ACI 2 for 10% and 30% of Hole Punch with increasing window length.

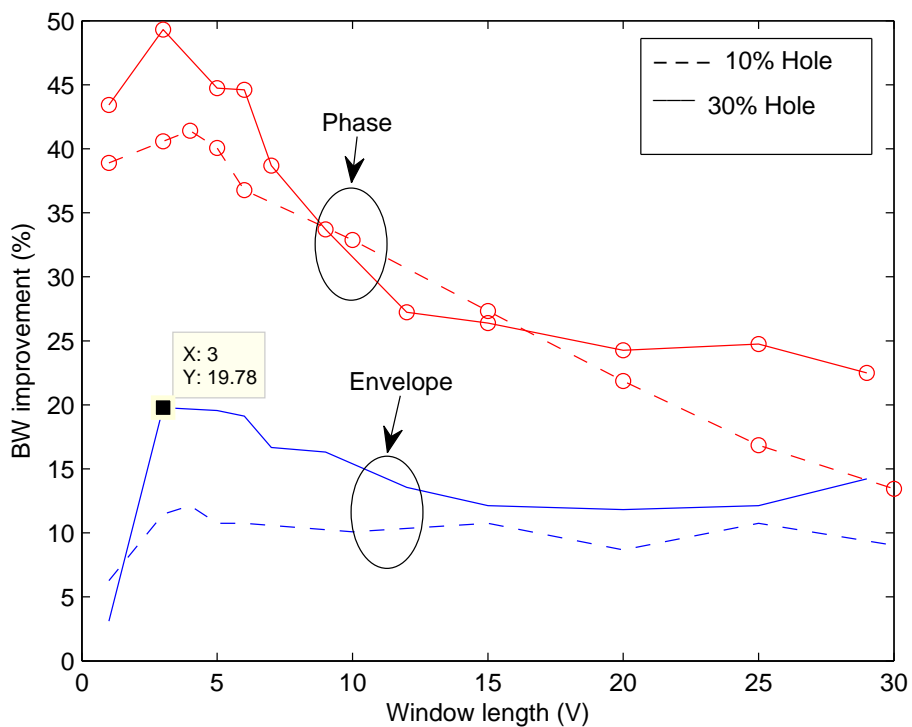


Figure 4.9: Envelope and Phase bandwidth improvement at -40 dB using 10% and 30% hole punch with respect to increasing window length.

Table 4.2: Effect of hole punch on ET, EER and polar CMOS amplifiers

Amplifiers	Bandwidth		Efficiency	EVM	
	Normal (MHz)	30% Hole (MHz)		Normal (dB)	30% Hole (dB)
ET	20	24	28.7%	-26	-14.7
EER	20	24	36%	-31	-14.9
Polar CMOS	20	24	7.2%	-26.8	-14.7

of the window signals occurs and other sections of the signal can fall into the hole. This decreases the hole size and the improvement for the polar signal bandwidth.

Choosing a smaller window length is beneficial for both EVM and the polar drive signal. A window length of $V = 4$ will meet the ACI specification for WCDMA and $V = 2$ for 802.11g WLAN specification. Both window lengths have similar performance for bandwidth reduction.

Based on these results, Table. 4.2 shows the expected effect of a 30% hole ($V = 2$) on three different published polar linearization schemes [38, 66, 67, 68]. The EVM of the hole punch scheme is added (in terms of power) to the reported EVMs of the amplifiers. In all cases the hole punch distortion dominates the EVM, and the bandwidth improvement is 20%. The increased bandwidth is expected to have little effect on the efficiency of the system [60, 62, 66]. Note that the Polar CMOS scheme [68] uses the envelope signal to control the number of parallel transistors and so does not benefit from operating the amplifiers continuously in saturation as do the EER and ET schemes. This explains its lower efficiency.

4.3 Summary

Hole punching is required for many reasons. Polar transmitters have great difficulty in generating high fidelity low level signals. The electronic circuits in Class S amplifiers find difficulty in tracking high rates of change which occur when the signal modulation passes through zero. Hole punching solves some of these problems and can reduce the bandwidth expansion on the polar drive signals.

The expressions for the correction signal (u_k) have been mathematically derived for a hole punching system in a band limited noise input signal: which models the well known OFDM and CDMA modulations. In addition, the expressions for the distortion power caused by the correction signal have been derived and it has been shown how this power is distributed in the frequency domain, by the choice of window function. From this, it has been theoretically obtained: the expressions for the resulting EVM and ACI generated by the hole punch process. The results are confirmed by simulations and shown that the hole punch method originally proposed in [3] leads to considerable distortion most of which falls in-band. This chapter confirms acceptable ACI performance using a Hanning window with lengths between $V = 2$ and $V = 6$ critical sample periods (T). This will cater for most practical situations. The Hanning window proposed here out performs the Gaussian window of [3] in reducing the bandwidth expansion of the polar components. Even so, quite

large holes are needed to make any significant bandwidth reduction. A 30% hole reduces the envelope bandwidth by 20% and the phase bandwidth by 43%. However, for $V = 2$ the hole punch threshold of 30% of average power results in EVM of -15 dB. This limits the constellation clarity of the transmitter modulation to QPSK or BPSK, and is close to what is needed for WCDMA systems. The hole size must be reduced to 10% to improve this to -22 dB. Table 4.3 compares hole punch technique to the best schemes of Chapter 3. Compared with the repetitive bandwidth limitation and the RF drive compensation technique from Chapter 3, the polar bandwidth of the hole punch scheme is similar. However, the EVM suffers 16 dB more than repetitive scheme. This limits the application of the hole punch scheme.

The next chapter will consider bandwidth limitation on the LINC architecture.

Table 4.3: Comparison of hole punch technique with bandwidth limitation schemes from Chapter 3

Technique	Normalized Bandwidth @-40 dB				EVM @50 percentile (dB)
	Envelope		Phase		
	channels	Improve- ment (%)	channels	Improve- ment (%)	
No Bandwidth limitation	2.25	-	7.6	-	-
Hole Punch with Hanning window $V=6$ and 30% Hole	1.8	20%	4.3	43%	-9.5
Repetitive BW limitation for $i = 10$ (Section 3.5)	1.75	22.2%	5.13	32.5%	-26
BW limitation with RF drive compensation (Section 3.6)	1	55.5%	3	60.5%	No EVM

Chapter 5

Bandwidth Reduction Schemes on LINC

5.1 Introduction

In Chapters 3 and 4 we showed that the nonlinear process of Cartesian to polar conversion produces high bandwidth expansion for the EER drive symbols. Various schemes were proposed to reduce the envelope and phase component bandwidths. There is also another class of emerging amplifier architectures that face similar issues. These are known as outphasing amplifiers, two important examples being the LINC and Chierex amplifiers. The outphasing structures take an envelope modulated bandpass waveform and resolve it into two phase modulated constant envelope signals, which are separately amplified and then summed to regenerate the originate amplitude modulated signals. The two constant envelope components allow the use of highly efficient and nonlinear power amplifiers, such as switched amplifiers (e.g. Class D, E and F). The generation of the constant envelope drive signals requires nonlinear processing in the DSP which leads to expanded bandwidth. As in the EER

structure the wider bandwidth causes problems in the analog components following the generation process. DAC's require a higher sampling rate and the wider bandwidth of the reconstruction filters and modulator circuits introduce more noise and make the matching of both paths more difficult. This chapter proposes a number of novel solutions for containing the bandwidth expansion of the outphasing process.

Section 5.2 explains the source of bandwidth expansion for the LINC components. Section 5.3 describes a preconditioning scheme to reduce the bandwidth. Section 5.4 and 5.5 explains two post conditioning schemes on the phase part of the LINC components. Section 5.6 shows measurement results of the best technique using software defined radios. The chapter is summarized in the last section. The post conditioning schemes from this chapter are being prepared for a journal submission.

5.2 Explanation

The LINC block diagram can be found from Figure 2.12. The LINC processing generates an orthogonal vector, $e(t)$, that is added and subtracted from the desired signal vector to generate the two drive signals $s_1(t)$ and $s_2(t)$. $e(t)$ is designed such that the drive signals are constant envelope signals lying on a circle in the I & Q plane. The phase angle of $s_1(t)$, $s_2(t)$ consists of two parts: one part represents the phase of the input signal $\arg(x_{in})$, while the other part is an outphasing component that controls the amplitude of the combined

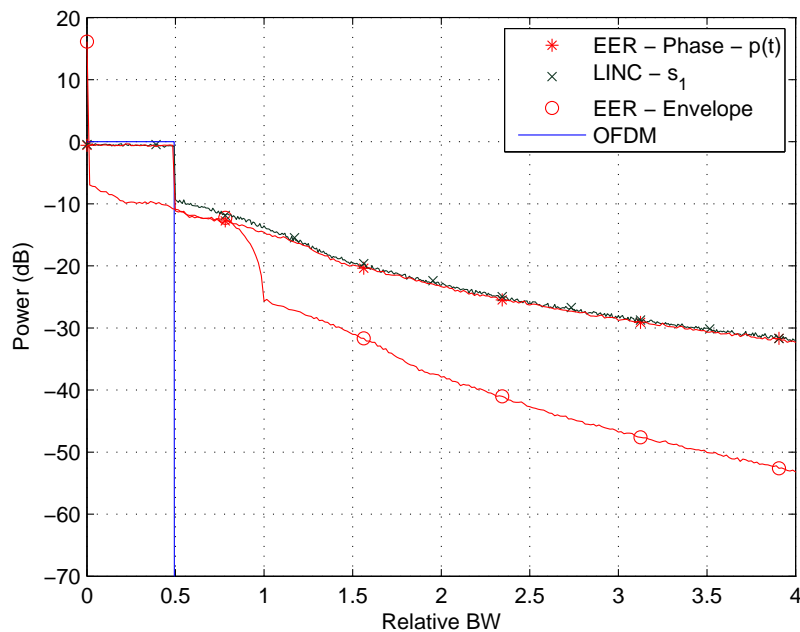


Figure 5.1: Spectrum of EER and LINC components.

output signal x_{out} . The RF drive signals are therefore phase modulated, and their spectrum will be defined by the resulting phase variations. It is interesting to compare the spectrum of the LINC component drive signals with the EER polar component drive signals. Figure 5.1 shows the component drive signals for an OFDM modulated RF input signal. The spectrum of s_1 and s_2 are the same, so only $s_1(t)$ is plotted. It is interesting to note that $s_1(t)$ has almost the same spectrum as $p(t)$, the EER phase component. We can theorise that the phase part of the OFDM signal is the dominant cause of bandwidth expansion for the LINC components. We can further strengthen this argument by doing a twostep process. Firstly, we put an envelope signal with no phase component (i.e. $x_{in} = |x_{in}|$) through the LINC separator and then secondly, we do the opposite, where we put a phase signal with no envelope component (i.e.

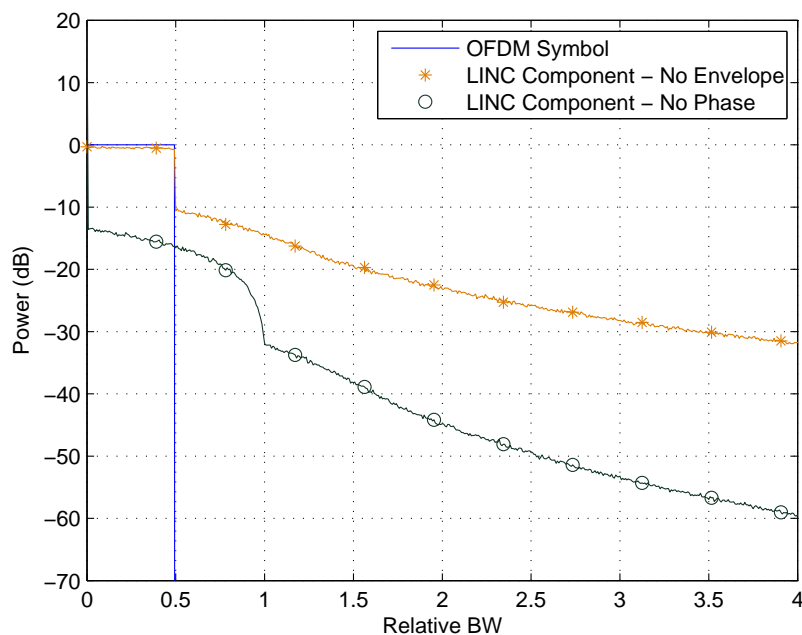


Figure 5.2: Spectrum of OFDM and LINC component with no Phase part and vice-versa

$x_{in} = \angle x_{in}$) through the separator and then compare the resulting spectrums.

In Figure 5.2, the '★' marker line shows the LINC component of $|x_{in}|$ and the 'o' marker line shows the LINC component of $\angle x_{in}$. Clearly it is the phase component of the input signal that dominates the out of band (OOB) spectrum of s_1 being between 17 dB and 30 dB higher than the spectrum derived from the amplitude component (for relative bandwidths greater than one). One potential strategy for bandwidth reduction is therefore to reduce the spectrum of the phase component of the input signal in a pre-conditioning block. This contrasts with bandwidth reduction schemes for EER, which concentrated on reducing the envelope spectrum because of the difficulty in providing switch-mode operation of the V_{dd} drive signal at wide bandwidths.

An alternate structure would be to directly limit the bandwidth of the

$s_1(t)$ and $s_2(t)$ signals after the LINC separator in a post-conditioning block. The LINC architecture poses some difficulties for post-conditioning bandwidth limitation using schemes described in the previous chapters, because the advantages of LINC fail when the $s_1(t)$ and $s_2(t)$ components do not have constant envelope. In the next section, we show a pre-conditioning scheme working on the input signal before entering the LINC separator. This will then be followed by two more schemes working in the post conditioning mode.

5.3 Pre-conditioning: Bandwidth Reduction on the Polar Phase

In the last section it was established that the input signal phase was the main source of bandwidth expansion for the two LINC components ($s_1(t)$ and $s_2(t)$). However, a direct bandwidth limitation can not be performed on the phase signals (s_1 and s_2) as was done in Section 3.2. Figure 5.3 shows the I & Q diagram of LINC component $s_1(t)$ before and after bandwidth limitation. The distortion caused by the bandwidth limitation process violates the constant envelope property. Therefore, we try a pre-conditioning scheme that works on the input signal ($x_{in}(t)$) before the LINC separator. The process can be found from the block diagram at Figure 5.4. The bandwidth limitation scheme is the same as shown in Section 3.2. Firstly, the input Cartesian signal ($x_{in}(t)$) is converted to the polar signals, $a(t)$ and $p(t)$.

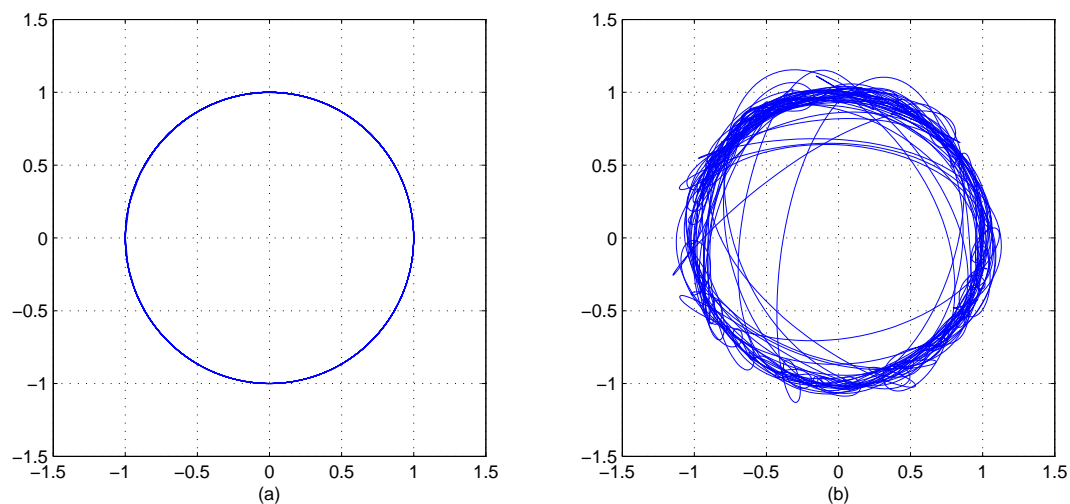


Figure 5.3: I & Q diagram of $s_1(t)$ (a) before and (b) after bandwidth limitation

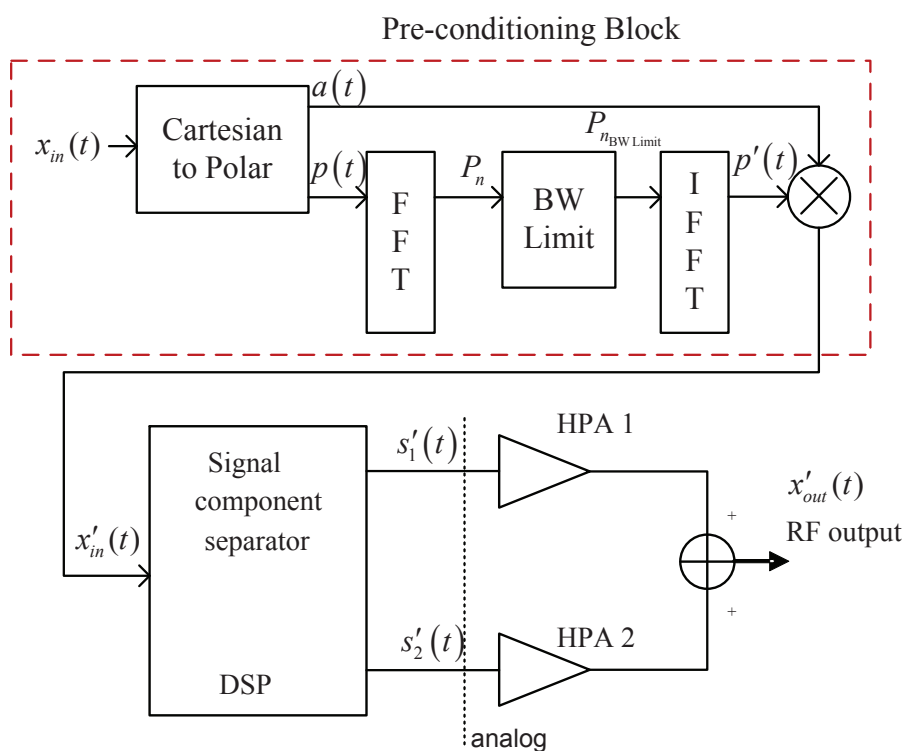


Figure 5.4: Block diagram of the pre-conditioning scheme for BW limitation of LINC architecture

$$\begin{aligned} a(t) &= |x_{in}(t)| \\ p(t) &= e^{j\theta(t)} \end{aligned} \quad (5.1)$$

Bandwidth limitation is then performed on the phase signal. The process can be described from the following equations:

$$\begin{aligned} P_n &= \text{FFT}(p(t)) \\ P_{n_{\text{BWLlimit}}} &= \text{LPF}(P_n) \\ p'(t) &= \text{IFFT}(P_{n_{\text{BWLlimit}}}) \end{aligned} \quad (5.2)$$

where, the $P_{n_{\text{BWLlimit}}}$ operation is same as Equation 3.4. The reconstituted signal $x'_{in}(t)$ is fed back into the LINC separator. The LINC separator produces the constant envelope phase signals of $s'_1(t)$ and $s'_2(t)$.

$$x'_{in}(t) = a(t) \cdot p'(t) \quad (5.3)$$

Figure 5.5 shows the spectrum of the OFDM spectrum before and after preconditioning as well as the LINC component. For this simulation, the normalized bandwidth of the phase component, $e^{j\theta(t)}$ is reduced to one channel bandwidth ($B=1$). The preconditioning scheme manages to lower the bandwidth expansion by a small margin. At -50 dB level the bandwidth of the unaltered $s_1(t)$ is 14.5 channels while the bandwidth of $s'_1(t)$ and $s'_2(t)$ is at 10.1 channels (an improvement of 31%). However, the spectrum of the OFDM signal suffers from a large increase in spectral splatter. When compared with the spectral mask of 802.11g WLAN (black line), the pre-conditioned OFDM signal fails to stay below the spectral mask.

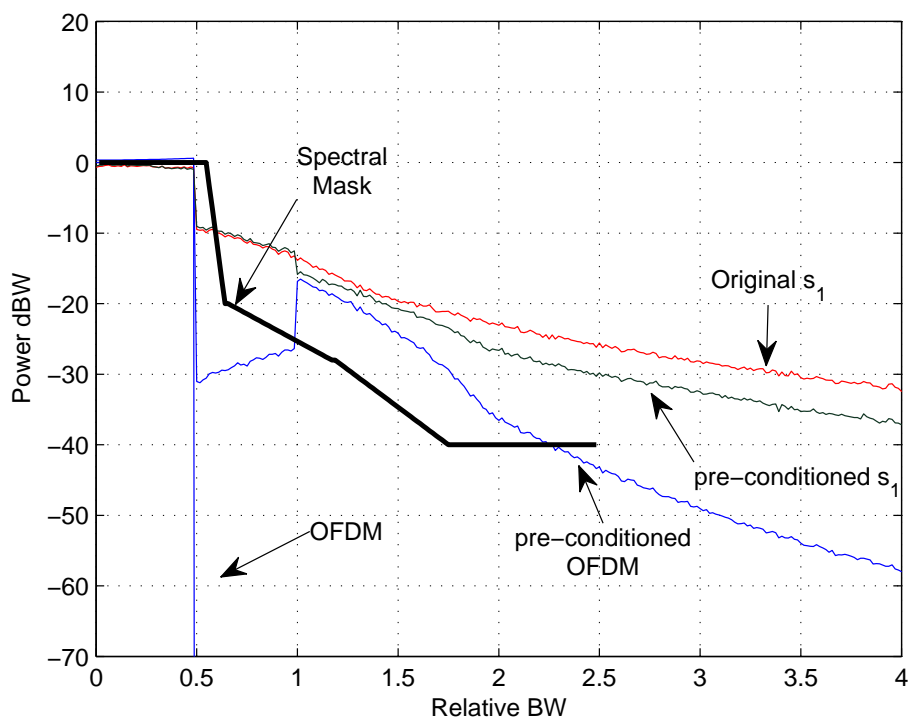


Figure 5.5: Spectrum of OFDM and LINC components with pre-conditioning to reduce bandwidth expansion

We found in previous chapters, the bandwidth reductions schemes lead to EVM build-up. The same trend can be seen here. The EVM is -25 dB at the 50 percentile level (Figure 5.6), which barely satisfies the WLAN specifications.

The pre-conditioning scheme fails to give any significant improvement for the bandwidth of the $s'_1(t)$. In addition the spectral mask criterion for the OOB OFDM signal is not satisfied. In order to get a more substantial reduction the in bandwidth expansion a post-conditioning scheme is necessary.

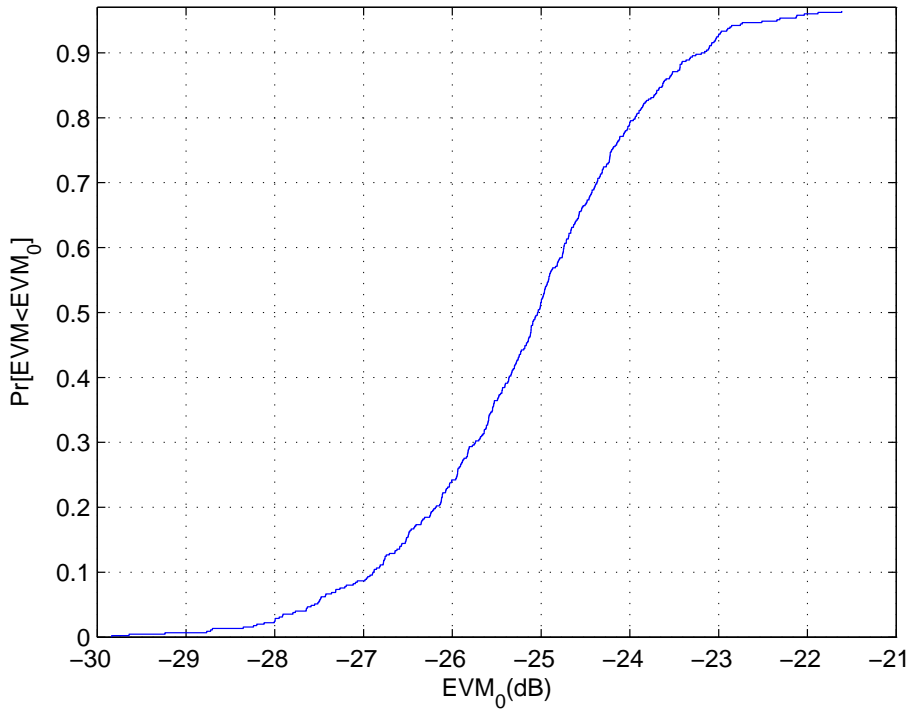


Figure 5.6: CDF of EVM using pre-conditioning scheme

5.4 Post-conditioning: Bandwidth limit on Unwrapped Phase

In this section we perform a bandwidth limitation on the angle ($\theta(t)$) of the $s_1(t)$ and the $s_2(t)$ components. The polar component $\theta(t)$ rotates between $+\pi$ to $-\pi$ and has discontinuity whenever the trajectory crosses the π boundary. In order to bandwidth limit the angle $\theta(t)$, we need to unwrap it prior to the frequency domain filtering. Figure 5.7 shows the time domain samples of the $\theta(t)$ and the unwrapped angle $\theta_u(t)$. The angle $\theta(t)$ is found and unwrapped using the following equations:

$$\begin{aligned}\theta(t) &= \tan^{-1} \frac{\text{Im}(e^{j\theta(t)})}{\text{Re}(e^{j\theta(t)})} \\ \theta_u(t) &= \text{unwrap}(\theta(t))\end{aligned}\tag{5.4}$$

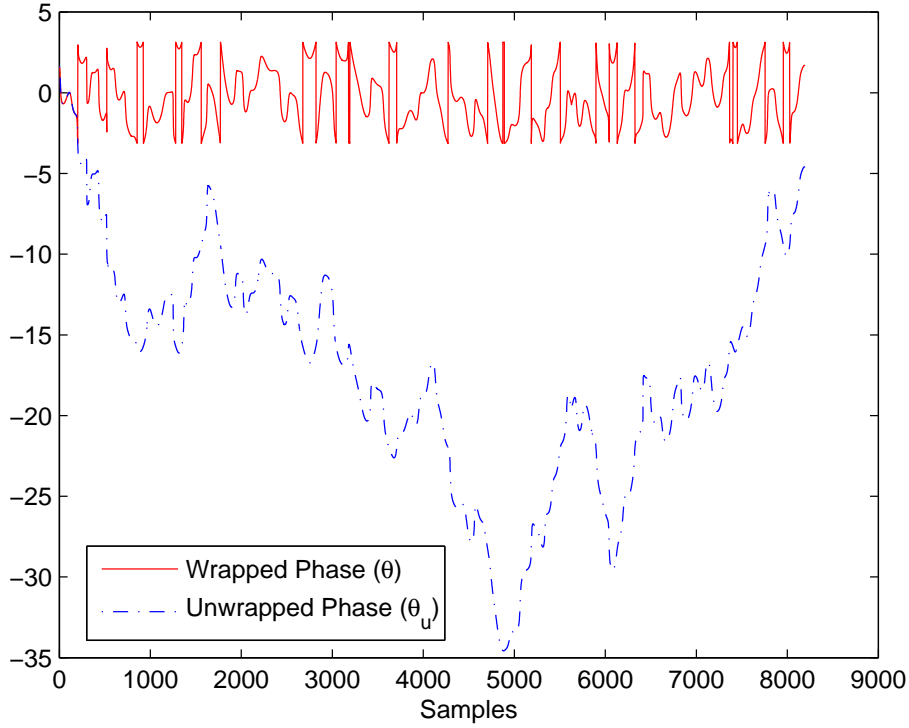


Figure 5.7: Time domain view of wrapped and unwrapped phase of s_1

The θ_u is then converted to the frequency domain to give Θ_u .

$$\Theta_u = \text{FFT}(\theta_u(t)) \quad (5.5)$$

Then the bandwidth limitation is performed that yields $\Theta_{u_{BL}}$ and the component is converted back to time domain.

$$\Theta_{u_{BL}} = \begin{cases} \Theta_u & 0 \leq n \leq B, \\ & NL - B \leq n \leq NL - 1 \\ 0 & B + 1 \leq n \leq NL - 1 - B \end{cases} \quad (5.6)$$

$$\theta'_u(t) = \text{IFFT}(\Theta_{u_{BL}})$$

Figure 5.8 shows the block diagram of the process. In the Matlab simulation, there is no need to perform an explicit re-wrapping operation as the exponential

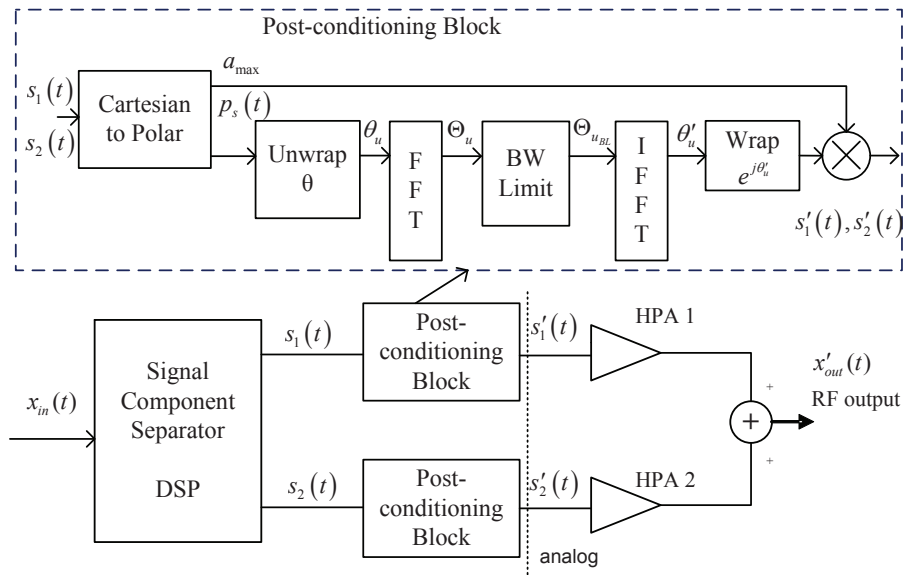


Figure 5.8: Block diagram of the post-conditioning bandwidth limitation scheme with unwrapped phases

function does it automatically.

$$p'_s(t) = e^{j\theta'_u(t)} \quad (5.7)$$

where $p'_s(t)$ is a generic expression for the polar phase component of $s_1(t)$ and $s_2(t)$. The modified phase component then gets scaled with the envelope amplitude, a_{max} . The constant envelope property of signal is preserved here, as the bandwidth limitation is performed on the angle $\theta(t)$ rather than the complex signal $e^{j\theta(t)}$ as in EER (Section 3.2).

$$s'_1(t) = p'_s(t) a_{max} \quad (5.8)$$

As the postconditioning bandwidth limitation scheme is performed on both LINC components s_1 and s_2 , the resulting bandwidth limited s'_1 and s'_2 have

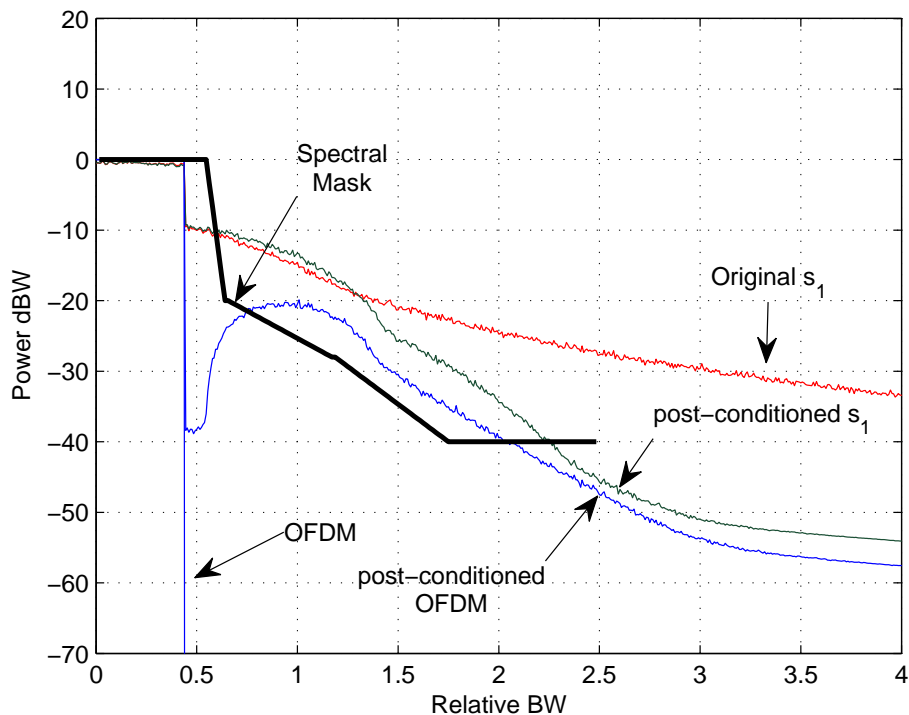


Figure 5.9: Effect of bandwidth limitation on unwrapped θ - spectrum of OFDM ($x_{in}(t)$), modified OFDM ($x'_{out}(t)$), $s_1(t)$ and $s'_1(t)$

same bandwidth. As such, for the rest of this chapter, when referring to bandwidth limited LINC component, only s'_1 is mentioned.

Figure 5.9 shows the spectrum of OFDM ($x_{in}(t)$) and the LINC component before ($s_1(t)$) and after ($s'_1(t)$) the bandwidth limitation. We can notice that the LINC component has achieved significant bandwidth reduction. For this simulation, the bandwidth was limited to two ($B = 2$) channel bandwidths. At the -50 dB level, the bandwidth of $s'_1(t)$ is a respectable 2.9 relative channel bandwidths, which is an improvement of 80%. Figure 5.10 shows the CDF of the EVM. At the 50 percentile the EVM is at -38 dB, which is well within the specification of the WLAN standard.

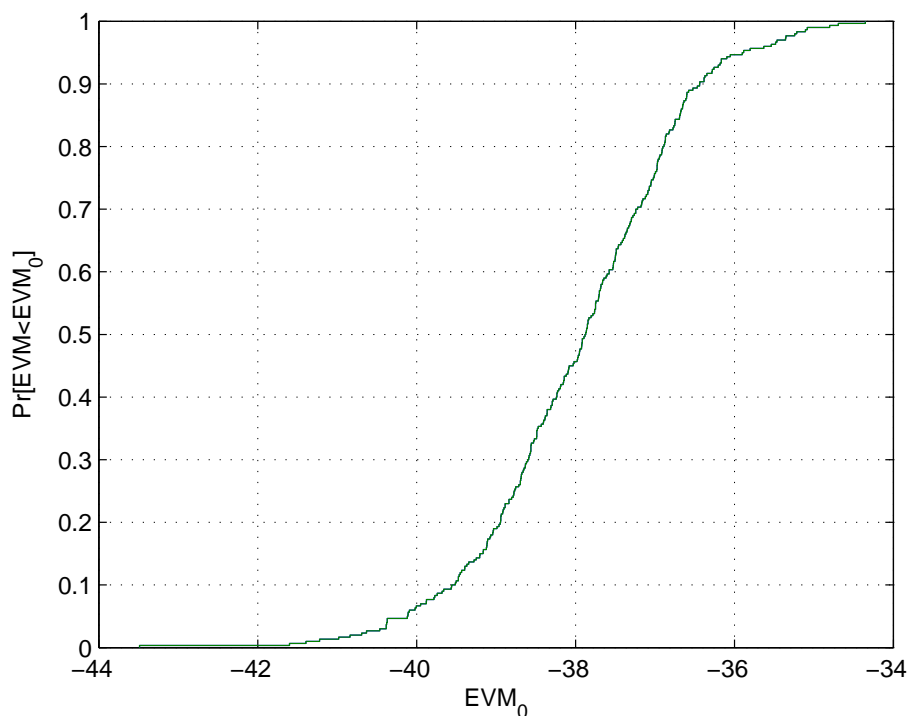


Figure 5.10: Effect of bandwidth limitation on unwrapped $\theta(t)$ - CDF of EVM for modified OFDM ($x'_{out}(t)$)

Although, the bandwidth reduction is quite significant, a large portion of the modified OFDM signal, $x'_{out}(t)$, fails to stay below the spectral mask. In order to address this issue, an OOB correction scheme is proposed here. In this scheme, any spectral components that lie above the spectral mask are forcefully pushed below it in an "OOB Correction" algorithm. The new signal $x'_{in}(t)$ passes through LINC separator and the HPA1 and HPA2 amplifiers. There is almost no change in EVM as the inband bins are not modified, but as expected, the bandwidth improvement of $s'_1(t)$ and $s'_2(t)$ is reduced. Figure 5.11 shows the effect of OOB correction on the $x'_{out}(t)$. The bandwidth of $s'_1(t)$ goes to 7 channel bandwidth, which is still an improvement of 51.7% and

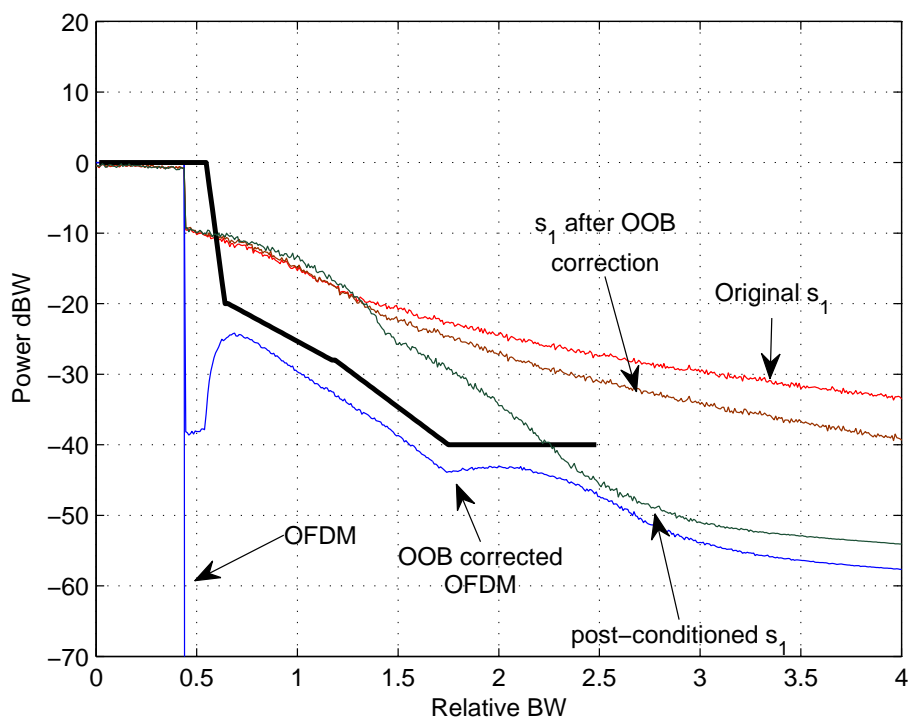


Figure 5.11: Spectrum of OFDM and s'_1 with bandwidth limitation and OOB correction

the EVM is virtually unaffected.

In Section 3.5, it was found that the results from bandwidth limitation can be further improved by repeating the process and allowing the don't care bins to distort. We employ a similar technique for this simulation. The revised block diagram can be found at Figure 5.12. It is a three step procedure. Firstly the modified LINC components $s'_1(t)$ and $s'_2(t)$ are summed and then OOB correction is performed on the resultant signal as a second step. Lastly, the corrected signal is fed back into the first LINC separator and it goes through the bandwidth limit block. The process is repeated i times.

The bandwidth of $s'_1(t)$ improves with the number of repetitions (i). Figure

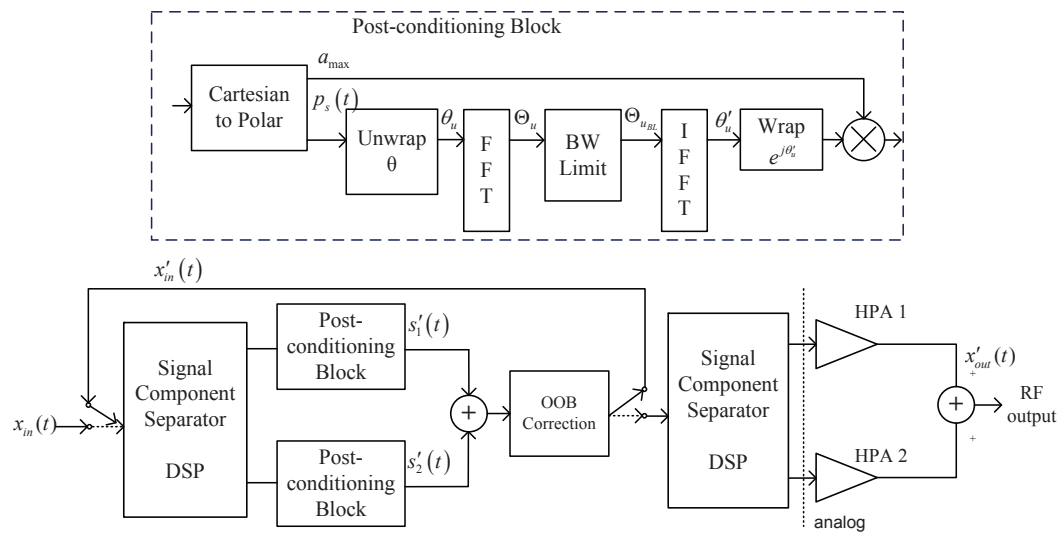


Figure 5.12: Revised block diagram of post-conditioning bandwidth limitation scheme with unwrapped phases and OOB correction

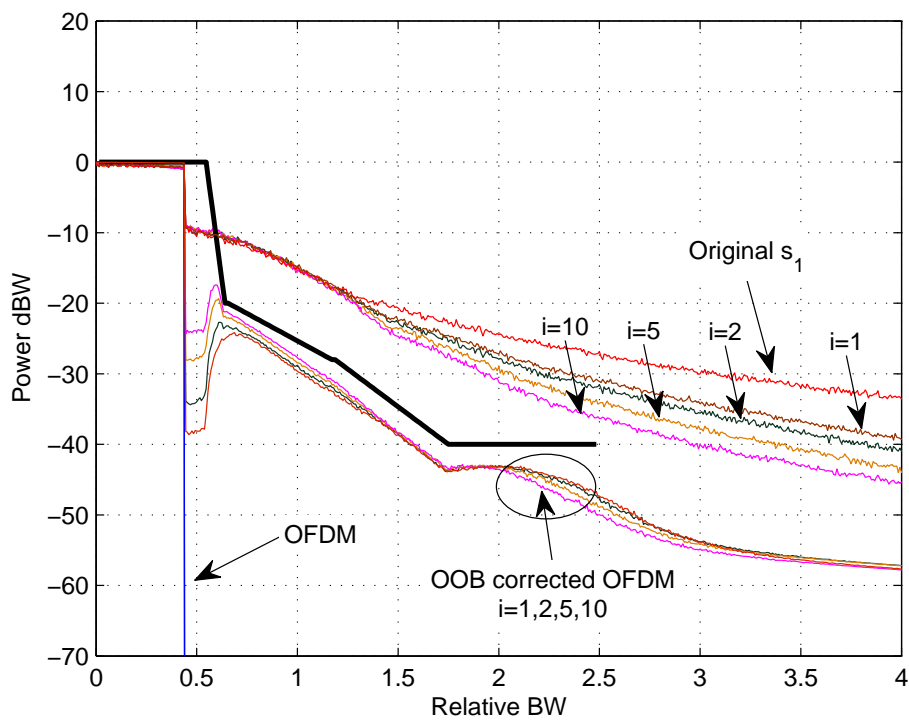


Figure 5.13: Spectrum of OFDM and s'_1 for different i values

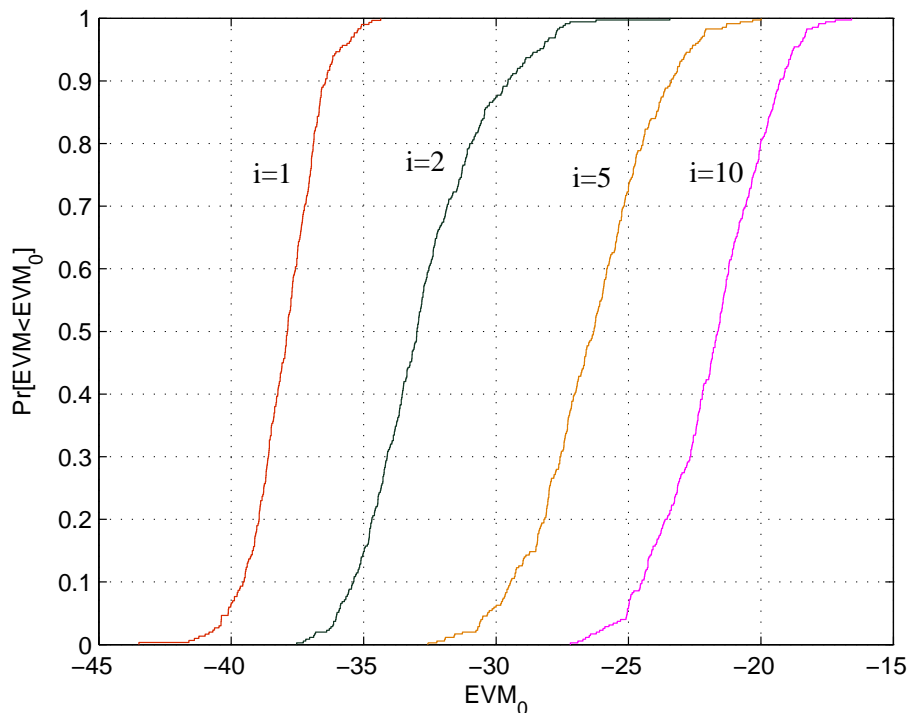


Figure 5.14: CDF of EVM for x'_{out} for different i values

5.13 shows the spectrum improvement for values of i up to 10. With a second repetition, the channel improvement of $s'_1(t)$ increases to 57.2% from 51.7%. With 5 and 10 repetitions, the relative channel bandwidth comes down to 5.6 ch and 5.1 ch respectively. Figure 5.14 shows the CDF of EVM for the aforementioned i values; and all the results are summarized in Table 5.1.

A trade off can be seen from these simulations. A single loop OOB correction did not yield any added EVM buildup, but with the repeating loop, the signal goes through the LINC separator and a frequency domain filtering block. This causes some of the distortion to fall inband and as such we can see a degradation in EVM with increasing i . For $i = 5$, we find an optimum point which gives a reasonable bandwidth reduction with acceptable EVM.

Table 5.1: Effect of bandwidth limit on unwrapped phase with OOB correction for different values of i

No of Iteration i	Bandwidth @-50 dB		EVM @50 percentile (dB)
	in (channels)	Improvement (%)	
0	14.5 ch	-	-
1	7 ch	51.7%	-38 dB
2	6.2 ch	57.2%	-33 dB
5	5.6 ch	61.4%	-26.5 dB
10	5.1 ch	65%	-21.6 dB

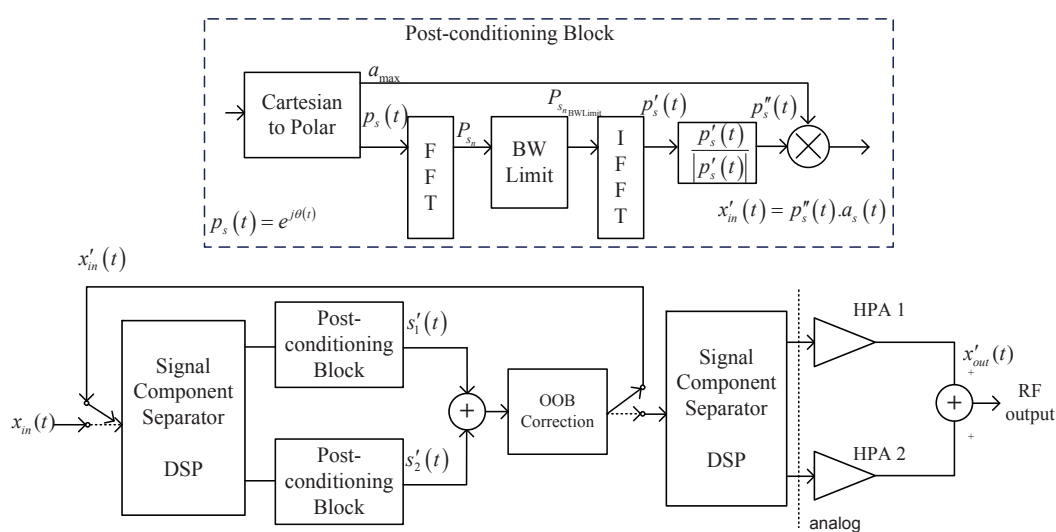


Figure 5.15: Block diagram of bandwidth limitation on the phase polar component with OOB correction

5.5 Post-conditioning: Bandwidth Limit on Polar phase component

In the last section we bandwidth limited the angle ($\theta(t)$) of the LINC component $s_1(t)$ and $s_2(t)$. In this section, we modify the process and bandwidth limit the complex phase signal, $p_s(t)$. There is now no requirement for unwrapping. The block diagram can be viewed in Figure 5.15. The bandwidth

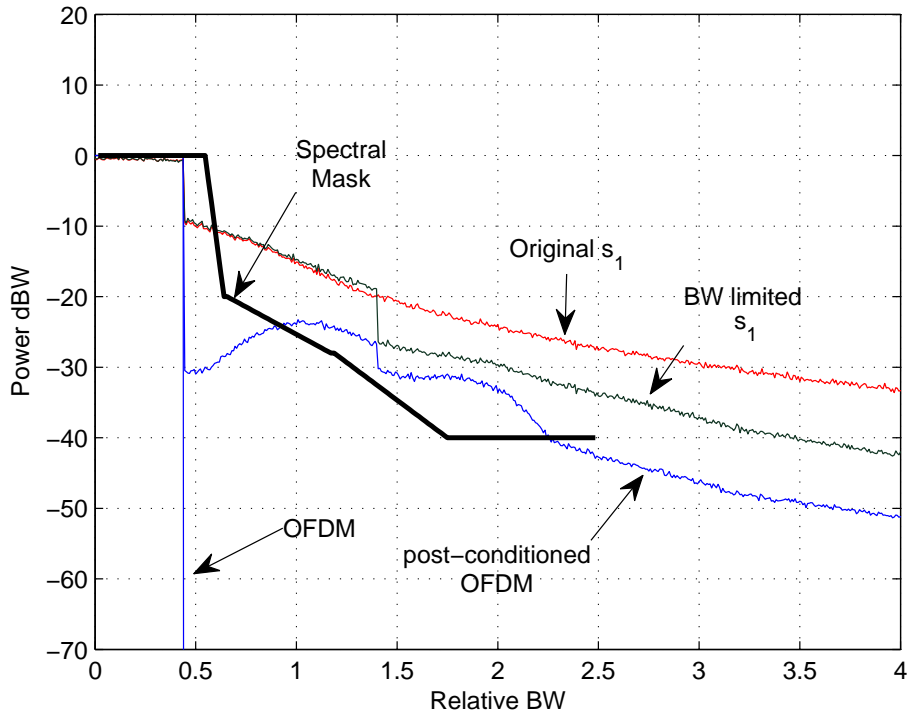


Figure 5.16: Effect of bandwidth limitation on the polar phase of LINC component. Spectrum of LINC component s_1 , BW limited LINC component s'_1 , input OFDM x_{in} and resulting BW limited OFDM x'_{out} .

limited signal $p'_s(t)$ is no longer constant envelope. We restore the constant envelope property without further altering the phase, to give the signal $p''_s(t)$.

$$p''_s(t) = \frac{p'_s(t)}{\text{abs}(p'_s(t))} \quad (5.9)$$

This method of bandwidth limitation gives similar results to that of the last section. The phase bandwidth of $s_1(t)$ and $s_2(t)$ is improved but the reconstituted OFDM fails to stay below the spectral mask (Figure 5.16). We employ the same OOB correction technique with i repetitions. Figure 5.17 shows the effect of bandwidth limit on the component spectrums with up to four repetitions. The bandwidth of $s'_1(t)$ reduces quite significantly as i increases. After 4th repetition, the improvement goes into diminishing returns and the EVM

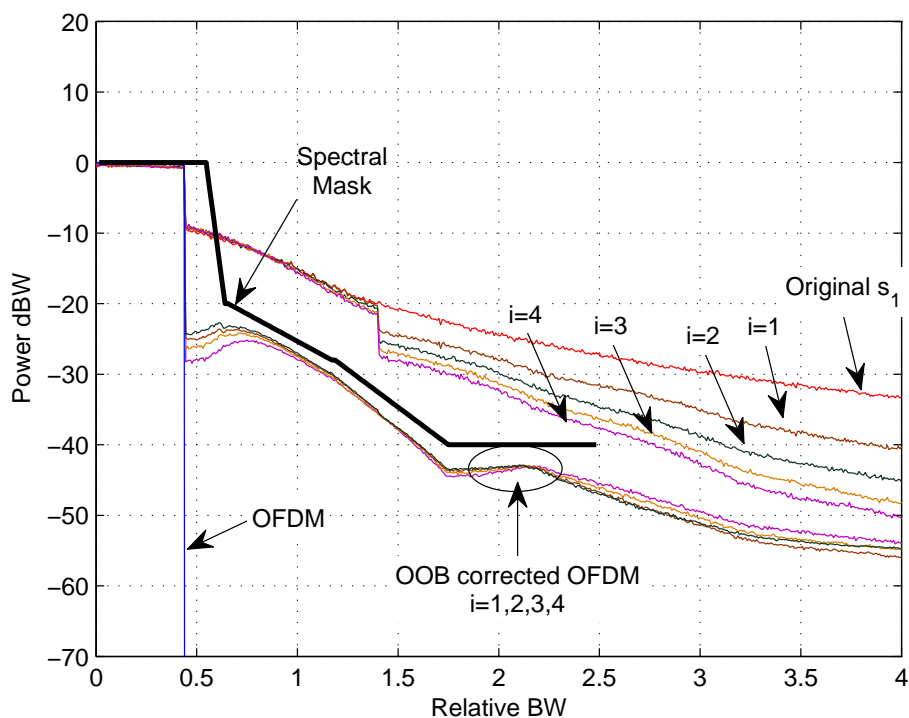


Figure 5.17: Effect of repetitive bandwidth limitation on polar phase of LINC component with OOB correction for resulting OFDM signal. Spectrum of s_1 , x_{in} , s'_1 and x'_{out} for $i = 1, 2, 3, 4$.

continues to degrade. Figure 5.18 shows the CDF of EVM for $i = 1, 2, 3, 4$.

The results from these two figures are summarized in Table 5.2.

The technique manages to achieve better bandwidth reduction than the previous section with fewer i values. With four repetitions, there is an improvement of 73.1% for the bandwidth of $s'_1(t)$. The EVM also manages to stay within acceptable limit of -25 dB. In the next section, measurement results are shown for the technique shown in this section.

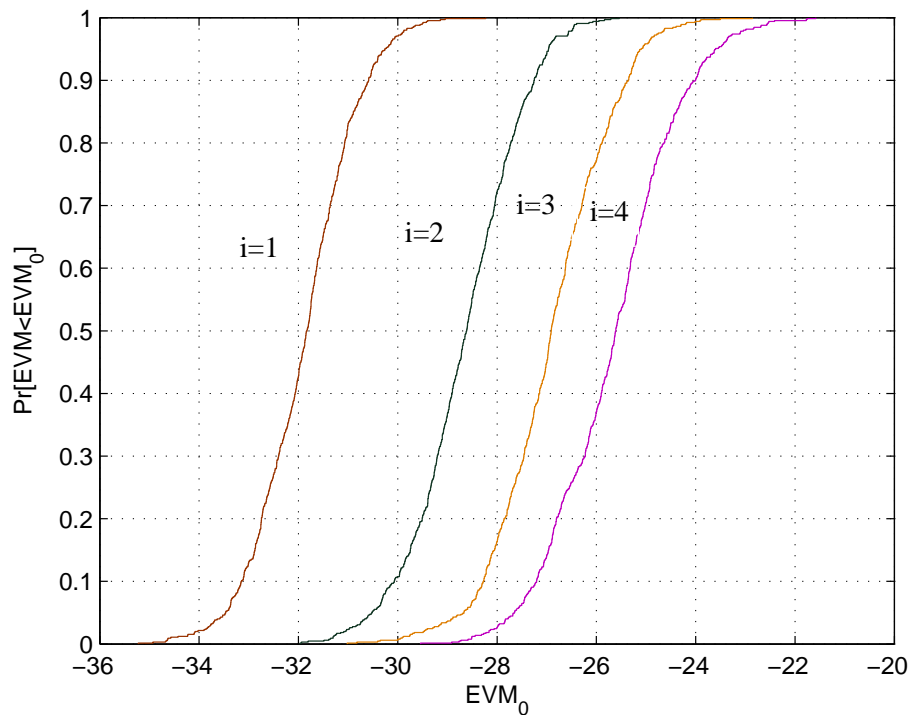


Figure 5.18: CDF of EVM for modified OFDM signal x'_{out} . For repetition values of $i = 1, 2, 3, 4$

Table 5.2: Effect of bandwidth limit on Polar phase component with OOB correction for different values of i

No of Iteration i	Bandwidth @-50 dB		EVM @50 percentile (dB)
	in (channels)	Improvement (%)	
0	14.5 ch	-	-
1	7 ch	51.7%	-32 dB
2	5.4 ch	62.8%	-28.7 dB
3	4.5 ch	69%	-26.9 dB
4	3.9 ch	73.1%	-25.7 dB

5.6 Measurement Results

From previous sections, it is found that the post-conditioning with bandwidth limitation on the polar phase components scheme (Section 5.5) shows the most promising results. In this section, the measurement results for the aforementioned scheme is shown. The following sub-section describes the measurement equipment. The hardware part consists of the universal software radio peripheral (USRP) and the software component is the GNU radio companion (GRC). This will then be followed by measurement results using a signal analyser (Rohde & Schwarz).

5.6.1 USRP and GNU Radio

The hardware part (USRP) is a high speed universal serial bus (USB) board. This was developed as an inexpensive hardware device facilitating the building of a software radio. It serves as a digital baseband and IF section of a radio communication system. The basic design philosophy behind the USRP was to do all of the waveform-specific processing, like modulation and demodulation in a common hardware unit. All of the high speed general purpose operations like digital up and down conversion, decimation and interpolation are done on an FPGA. A large community of developers and users have contributed to a substantial code base and have provided many practical applications using the hardware and software [69]. The USRP has 4 high-speed analog to digital converters (ADCs), each at 12 bits per sample, 64 MSamples/sec. There are

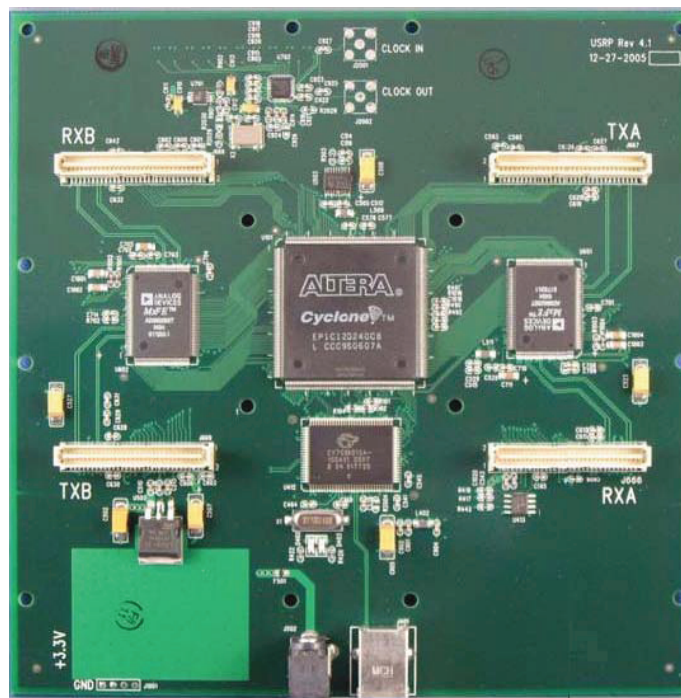


Figure 5.19: Motherboard of USRP1

also 4 high-speed digital to analog converters (DACs), each at 14 bits per sample, resulting a 128 MSamples/sec. These 4 input and 4 output channels are connected to an Altera Cyclone EP1C12 FPGA. The FPGA, in turn, connects to a USB 2.0 interface chip, the Cypress FX2, and on to the computer. The picture of a USRP board is shown in Figure 5.19.

In this measurement setup, the first generation boards (USRP1) are used. The USRP1 can connect two wireless transceiver daughter boards. A number of wireless daughter boards are available for specific bands within the frequency range of 50 MHz - 2.2 GHz. In this work, we have used the 400 MHz boards covering frequency range of 400 MHz - 500 MHz with a transmit power of 100 mW (20 dBm) [70].

The I & Q signals are Tx/Rx on the USB connection to the PC for software processing. The software part (GRC) is an open source platform. The GRC uses a graphical user interface (GUI) for building GNU radio flow-graphs. Users can drag and drop GNU radio blocks into an editable flow-graph, and connect the blocks, and edit various block parameters. Examples of the blocks being various sources, sinks, filters, logical operators and FFT/IFFT blocks. The GRC then takes a flow-graph and generates the equivalent codes in python language. The codes can be easily modified which gives customization options. The python scripts the FPGA and downloads and uploads the data.

5.6.2 Test Setup

Experiment 1: In the first experiment, MATLAB¹ is used to generate the OFDM signal. The signal is then stored to a file. The GRC reads the file and outputs the signal from daughter board, D1 (Figure 5.20). The resulting signal is viewed on the signal/spectrum analyzer.

The Matlab generated OFDM signal in Figure 5.21 has been modified to have low OOB side lobes so the study of the OOB distortions can be done more easily. The modified OFDM signal consists of continuous tones made possible by repeating the same data sequence for each symbol and not using a cyclic prefix. The spectrum shows distortion skirts starting -35 dB down from

¹The GRC could have been used to generate the OFDM code directly using built-in building blocks. However, in later measurement setups, the complexity of the signal processing goes very high and it is more convenient to generate the signal in MATLAB due to the limited range of available building blocks in GRC.

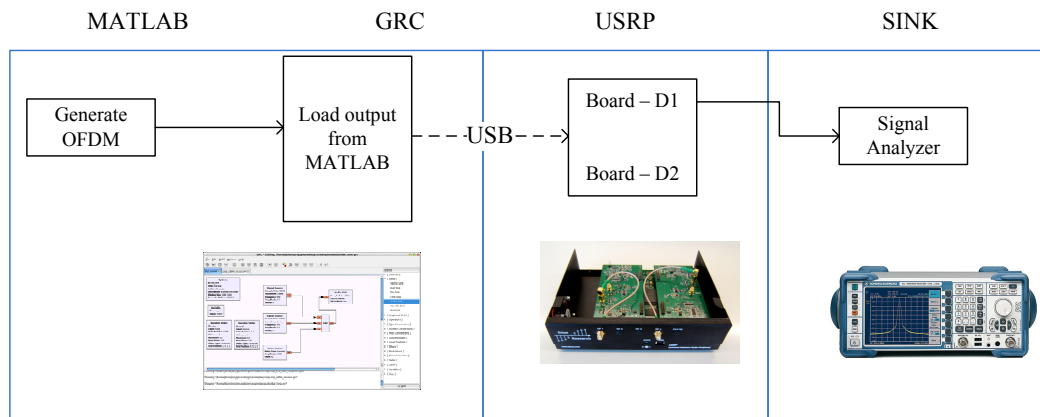


Figure 5.20: Block diagram of test setup 1.

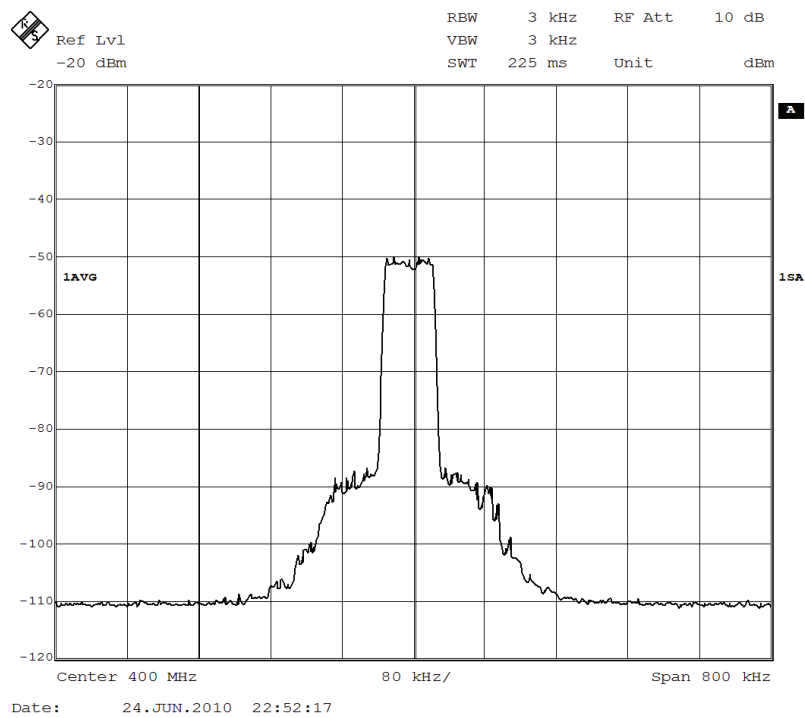


Figure 5.21: Spectrum of OFDM at the signal analyzer generated by a single USRP daughterboard.

the main signal. These distortion skirts are caused by nonlinearities in the RF PA of the USRP board. These are class A amplifiers without any linearization circuitry. The width of the skirt (approximately 1 channel) is indicative of a dominant 3rd order distortion. If the OFDM test signal was not modified, the 3rd order distortion would have been masked by the OFDM side lobes. The signal through the PA must be backed off (reduced) to account for PAPR of the OFDM and to limit the OOB distortions. This means, the transmit power is well below the advertised output power of the daughter board. Since, the output power of the daughter boards are very low and there is already a considerable backoff: only a 30 dB attenuator was used to model the path loss.

Experiment 2: In the second test setup, the LINC components, $s_1(t)$ and $s_2(t)$ are generated in MATLAB and then they are loaded onto the GRC (as previously). Then the signals are transmitted simultaneously from the two daughter boards, $D1$ and $D2$. The USRP built-in amplifiers are used instead of SMPAs. This sacrifices some power efficiency. however it does allow the gain and phase balances to be adjusted using the GRC building blocks. The signals are added using a Wilkinson power combiner and the output can be seen at the signal analyzer. The process can be visualized in Figure 5.22.

For this test setup, some gain and phase correction is required. The latter is very important as each amplifier has its own local oscillator (LO)/synthesizer. The frequency reference is the same for both synthesizers since it comes from

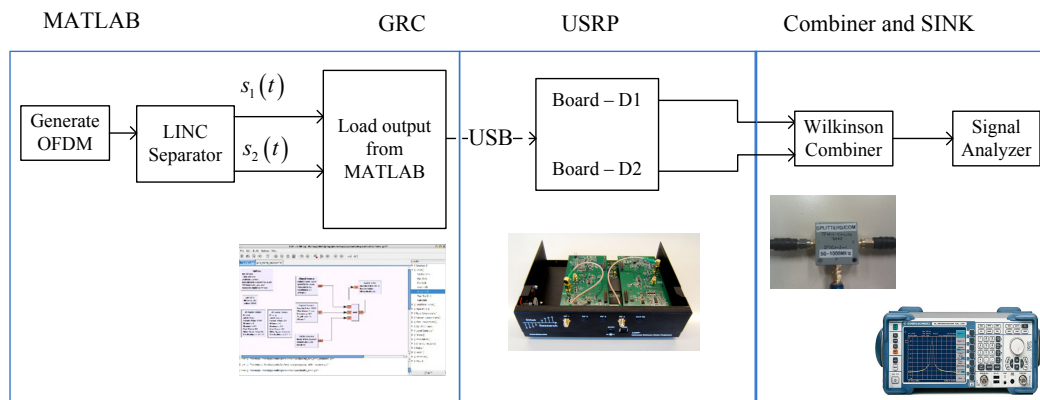


Figure 5.22: Block diagram of test setup 2.

the USRP board. The transmit LO frequencies are therefore exactly equal. However, the starting phase of the synthesizers is not controlled. Each time the USRP is switched on, the phase difference between the two LOs alters. Therefore, a manual phase imbalance correction unit is introduced in the GRC. Any phase and gain imbalance between the two transmitted signals s_1 and s_2 result in spectral splatter because their OOB components do not exactly cancel out. The issue is corrected by manually rotating the phase of the s_1 component. The GRC flowgraph is shown in Figure 5.23. Amplitude imbalance causes a similar effect; but the gain of both transceiver boards are quite well managed, so the required adjustment was less than 2%.

Figure 5.24 shows the spectrum of the same OFDM signal coming out of the Wilkinson combiner. The yellow line shows the OFDM signal when there is no phase correction employed. The blue line represents the OFDM signal when phase correction of -0.328 radian was used. It is not possible to totally eliminate the skirts because of a number of small factors that start to dominate

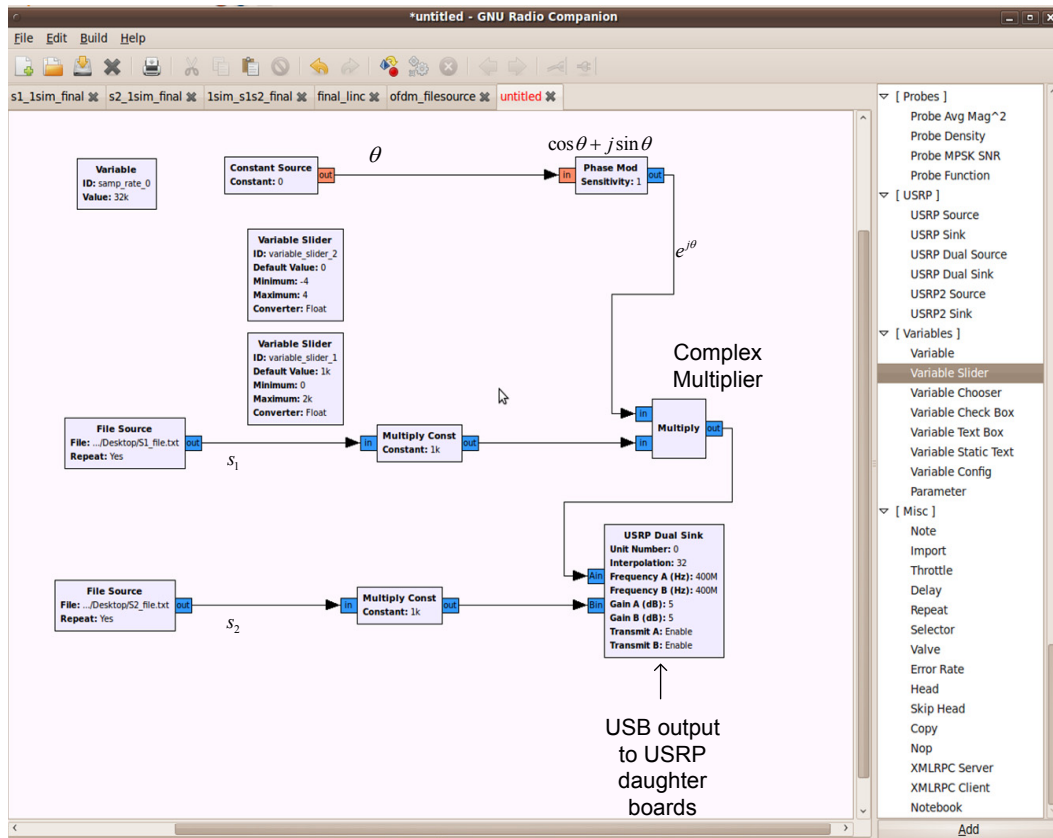


Figure 5.23: A screenshot of the GRC GUI showing the process of transmitting s_1 and s_2 simultaneously.

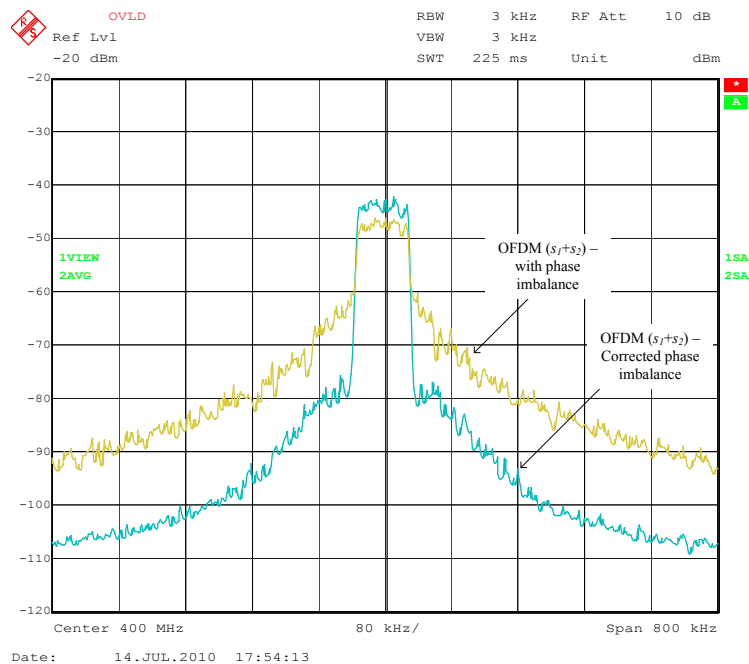


Figure 5.24: Spectrum of OFDM ($s_1 + s_2$) at the signal analyzer. Yellow line showing output from the combiner with no phase correction. The blue line is when the phase imbalance is corrected.

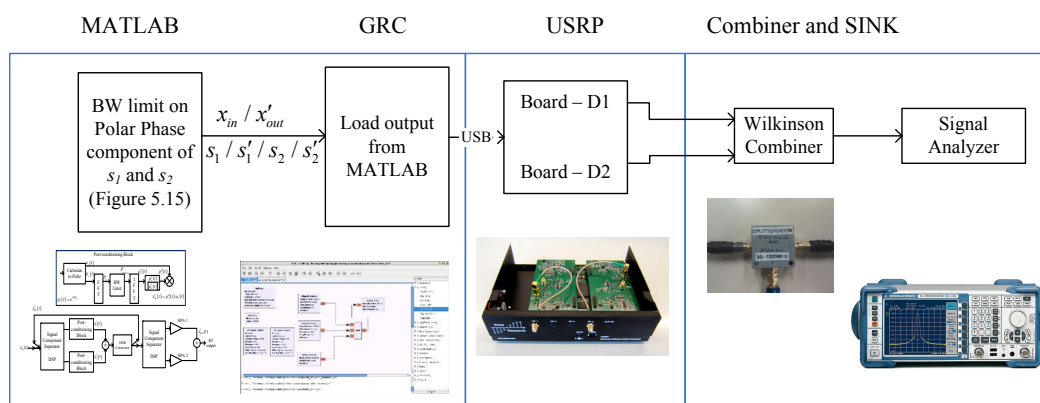


Figure 5.25: Block diagram of test setup 3.

at low spectrum values. These include:

- path delay mismatches caused by non-matched analog frequency responses of both transmitter chain.
- a non-perfect isolation of the hybrid combiner: particularly if impedances are not exactly matched (50Ω).
- the nonlinear behaviour of the amplifiers if the s_1 and s_2 signals are not exactly constant envelope².

Experiment 3: The third experiment measures the LINC component s_1 and the BW limited LINC component s'_1 in the signal analyzer. In addition, the resulting OFDM signal from the bandwidth limitation process is measured and a comparison of x_{in} and x'_{out} is shown. Figure 5.25 shows the block diagram of the process.

²As previously described in Section 2.1, the dominant cause of amplifier distortion is AM to AM conversion and AM to PM conversion. Any envelope variation in the signal will therefore generate distortion.

An I & Q plot of s_1 is shown in Figure 5.26. The signal is almost constant envelope as indicated by the circular shape. However, the width of the annulus in which the points are constrained indicates the presence of noise, distortion or an out of band signal. The width of the blurring is around 10% of the trajectory diameter. This indicates a signal to interference, noise or distortion ratio of about 20 dB. Since the signal is quite strong, noise is discounted. Therefore, there are two probable explanations for the problem. Distortion occurs if the bandwidth of s_1 is restricted as shown in the simulations of Figure 5.3b. Potential causes are the USRP interpolation/upconversion process or filtering in the signal analyzer itself. However, since the bandwidth restriction on s_1 required to generate this much distortion is quite significant ($B = 1$ channel) it is unlikely to be caused by the hardware setup which has many MHz bandwidth.

It was also noticed that the USRP operates in a ‘low IF’ mode and has a significant carrier leak component (Figure 5.27), some 4 MHz away from the desired LINC component s_1 and approximately 20 dB down. Since the Signal Analyser bandwidth was set at 5 MHz (the 3GPP standard), the carrier leak was most likely the cause of the blurring of the circular trajectory.

Figure 5.28 compares the spectrum of the constant envelope LINC component s_1 with the bandwidth limited and OOB corrected LINC component s'_1 . The data files used for this measurements are the same as those used to generate Figure 5.17 with $i = 4$ repetitions. The postconditioning reduces the

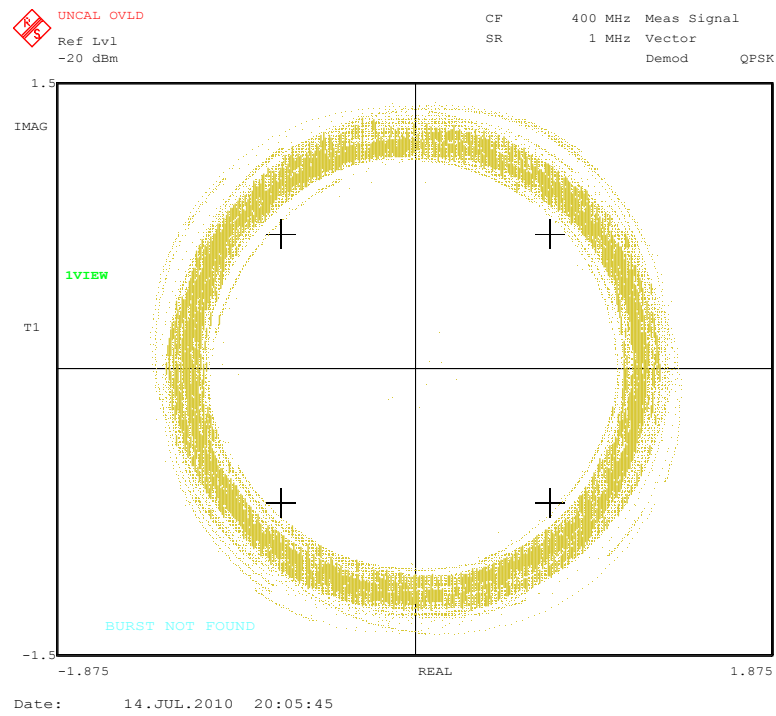


Figure 5.26: I & Q plot of s_1 on the signal analyzer.

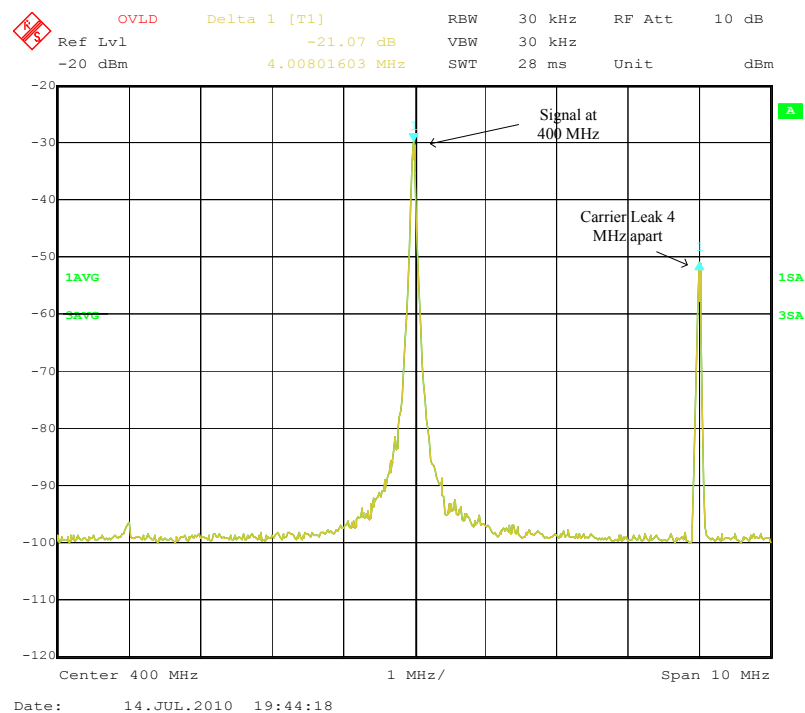


Figure 5.27: Spectrum of a signal at 400 MHz and the carrier leak caused by USRP which is 4 MHz away from the centre.

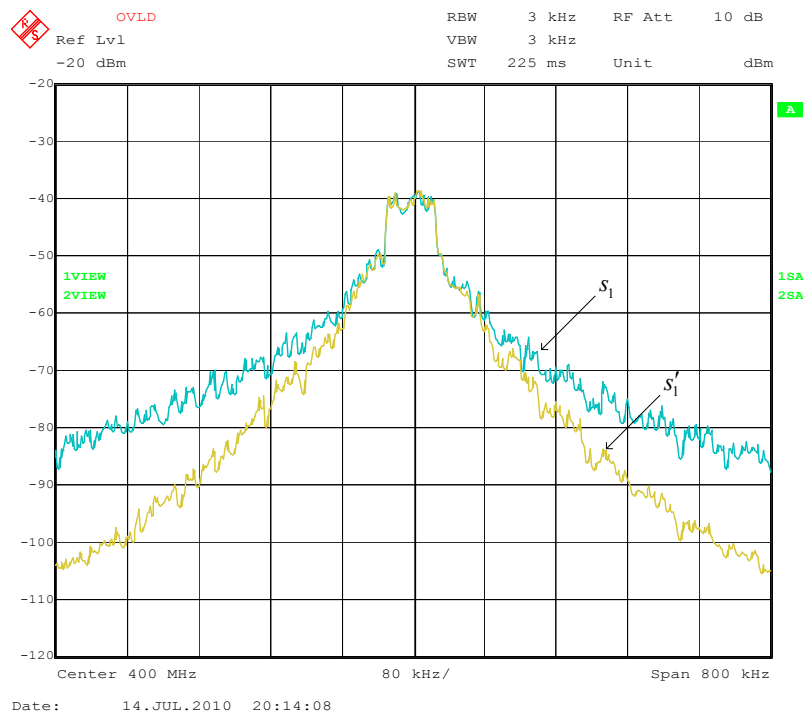


Figure 5.28: Spectrum of s_1 (blue line) and s'_1 (yellow line) at the signal analyzer.

OOB spectral components by almost 20 dB at a normalised bandwidth of 4 channels. This agrees with the simulations of Figure 5.17 to within < 2 dB. Of course the improvement is at the expense of EVM and Spectral Splatter of the recovered signal after the combiner. The modified OFDM signal deteriorates in the spectrum but still stays below the IEEE 802.11g WLAN spectral mask. The spectrum of the OFDM signal, x'_{out} , obtained from the bandwidth limited LINC components, $s'_1 + s'_2$, is shown in Figure 5.29. The spectral splatter in the x'_{out} (yellow line) is the unwanted byproduct of the bandwidth limitation process of the LINC components. It can be seen that, the spectrum starts to break around -28 dB down from the peak. Similar behaviour is seen in Figure

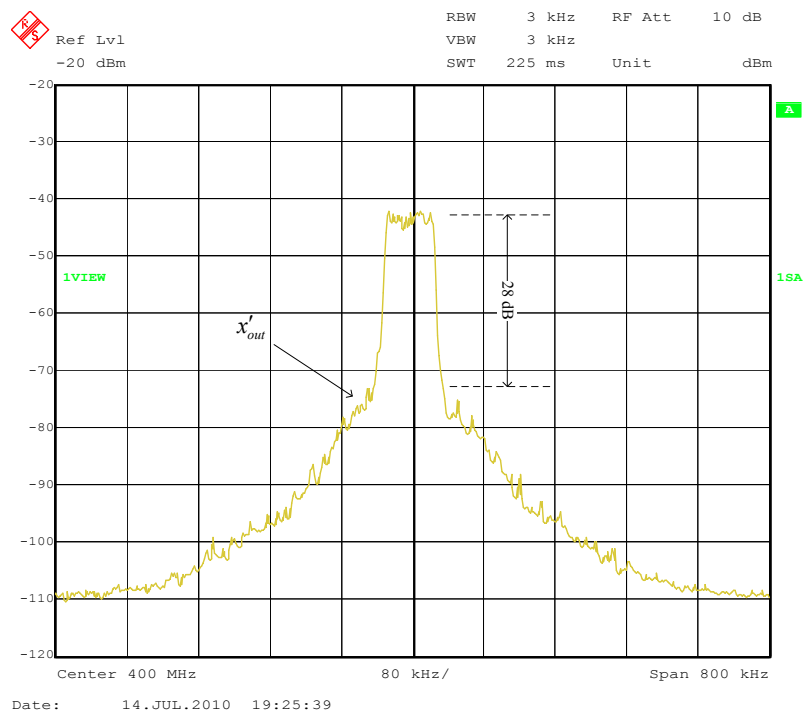


Figure 5.29: Spectrum x'_{out} at the signal analyzer showing the distortion caused by the bandwidth limitation process.

5.17 for $i = 4$. Although the shoulder is not as distinct as the simulations probably due to data dependence since the simulation results were an average over a large number of data symbols.

5.7 Summary

In this chapter, three bandwidth limiting schemes have been proposed for the constant envelope LINC components. All the schemes performed some form of bandwidth limitation on both LINC components s_1 and s_2 . The resulting bandwidth limited components were s'_1 and s'_2 respectively. As the same operations were performed on both components, the bandwidth of s'_1 and s'_2 are same. As such, when referred to the bandwidth limited components, only s'_1

is mentioned.

The first bandwidth reduction scheme: a preconditioning technique that reduces the bandwidth of the polar phase component of the input signal before entering the LINC separator. The technique managed to reduce the bandwidth of the LINC component, s_1 , to 10.1 channels from 14.5 channels at the -50 dB level, which is an improvement of 31%. However, the spectrum of the OFDM signal failed to match the spectral mask of the IEEE 802.11g WLAN standard. The distortion caused by the bandwidth limitation process resulted in -25 dB EVM, which barely satisfies the specification of the aforementioned standard.

In this second technique, bandwidth limitation was performed on the unwrapped phase of the s_1 . The signal was limited to 2 channels ($B = 2$). The technique managed to reduce the bandwidth of s_1 considerably. The bandwidth of the modified LINC component s'_1 reduced to 2.9 channels at the -50 dB level, which is an improvement of 80%. Although the EVM was at an acceptable value of -38 dB at the 50 percentile, the OFDM spectrum failed to follow the spectral mask. In order to solve this issue, an "OOB correction" algorithm was proposed. The algorithm compares the OOB spectrum of OFDM signal with that of the spectral mask and corrects it accordingly. When corrected, the bandwidth of s'_1 gets expanded. As such, the process was repeated a number of times. For $i = 5$ repetitions, the bandwidth of s'_1 was now 5.6 channels with an EVM value of -26.5 dB, and the OOB spectrum 3 dB below the spectral mask.

Table 5.3: Summary of bandwidth reduction techniques on constant amplitude signals of LINC architecture. Bandwidths are normalized to 1 OFDM channel.

Name of Technique	Bandwidth @-50 dB		EVM @50 percentile (dB)
	in (channels)	Improvement (%)	
No bandwidth limitation	14.5 ch	-	-
Pre-conditioning (Section 5.3)	7 ch	51.7%	-32 dB
Post-conditioning: BW limit on unwrapped phase (Section 5.4)	5.4 ch	62.8%	-28.7 dB
Post-conditioning: BW limit on polar phase (Section 5.5)	4.5 ch	69%	-26.9 dB

A third technique was introduced to further improve the results. The scheme limited the bandwidth of the polar phase component ($e^{j\theta}$) of the LINC component s_1 . The process showed similar results to the last technique. The bandwidth of s'_1 was improved, but the OFDM signal failed to match the spectral mask. The above mentioned OOB correction algorithm was employed here with i repetitions. For $i = 4$ repetitions, the bandwidth of s'_1 was at 3.9 channels at the -50 dB level with an acceptable EVM of -26.9 dB. Table 5.3 summarizes the results of the three techniques. The third method performed best.

In the second part of the chapter: measurement results were shown for the third technique. Three test setups were shown. In the first setup, an OFDM signal was generated using MATLAB and then loaded onto the GRC using file read/write process. The signal was then transmitted using one of the daughter boards of the USRP and viewed in a signal/spectrum analyzer. For the second setup, The LINC components s_1 and s_2 were generated and then

loaded onto GRC. These two signals were transmitted simultaneously using the two daughter boards of USRP and combined using a Wilkinson power combiner. The resulting signal was viewed in the signal analyzer. It was found that some gain and phase mismatching occurs as the LO of the USRP boards are not synchronized. A phase correction scheme was performed using the building blocks of the GRC software. The effect of mismatching phase was shown with this experiment.

The third setup showed the circular shaped I & Q plot of the LINC components to confirm its constant envelope nature. In addition, it was pointed out that a carrier leak (4 MHz offset) affected the blurring of the circle. The peak of the carrier leak was around 20 dB below the signal peak, which caters for the approximately 10% of the blurring effect. The setup also demonstrated the improvement in bandwidth of s'_1 compared to the original s_1 to within 2 dB of the simulations. The postconditioning technique reduced the OOB spectral components by almost 20 dB at a normalized bandwidth of 4 channels. In addition, the experiment also measured the resulting distortion on the OFDM spectrum, x'_{out} . The distortion shoulder breaks at around 28 dB down from the OFDM peak.

Chapter 6

Conclusion and Future Research

In this thesis, we focused on the bandwidth expansion problem related to the amplifier architectures with high efficiency and linearity. Two such structures were discussed: EER and LINC. It was shown, the polar components of EER architecture (envelope and phase) and the constant amplitude phase variant components of LINC architecture suffer from expanded bandwidth while transmitting multicarrier signals like OFDM. Different solutions to mitigate this issue were proposed in this thesis.

Solutions for the bandwidth expansion problem in EER were shown in Chapter 3 and 4. In Chapter 3, firstly a distortion less scheme was proposed to reduce the bandwidth of the envelope and phase polar components. The scheme used the concept of partial transmit sequence (PTS) to choose the one with the lowest out of band (OOB) bandwidth for the envelope and phase component. The technique managed to reduce the bandwidth expansion by a small margin with no EVM buildup. Then, an iterative bandwidth limitation (IBL) was proposed. The technique reduced the bandwidth of envelope component

in an iterative manner. The spectral mask of IEEE 802.11g WLAN standard was used as a reference for these simulations. The results from IBL technique was further enhanced incorporating the PTS (IBL-PTS) scheme. Although the IBL and IBL-PTS managed to reduce the envelope bandwidth with a very low cost of EVM, the phase bandwidth was mostly unaffected. Also it did not take advantage of the unused tones and this issue was addressed in repetitive bandwidth limitation technique. The technique bandwidth limited the envelope signal using the same bandwidth limiting value (B) and used a QAM correction scheme to minimize the EVM distortion. The scheme in the last section of Chapter 3 used the bandwidth constraint EER architecture with a correction signal superimposed on the RF drive signal. This technique managed to get the envelope bandwidth reduced to a very respectable 0.75 channel (from 3.5 channels) with little complexity and no additional EVM cost. The only drawback is it suffers from a small (5%) efficiency loss.

In chapter 4, an in depth theoretical analysis of the hole punch method was described. The hole punch scheme was originally introduced by Rudolph [3]. The chapter managed to find and correct the important omissions of the scheme described in the aforementioned paper. The hole punch process restricts the envelope value from crossing zero in the I & Q plane by adding a correction signal and thus creates a vector hole. The expressions for the correction signal and resulting EVM and ACI generated by hole punch process was mathematically derived. The effect of using different window function

(Gaussian and Hanning) was also discussed. The chapter confirmed acceptable ACI performance using Hanning window lengths of between 2 and 6 samples.

In chapter 5, the LINC architecture was discussed and it was confirmed the modulation's phase component as the dominant cause of bandwidth expansion in a LINC setup. Three bandwidth limitation schemes for the LINC architecture were shown. Among these, the post-conditioning bandwidth limitation scheme gives the best result. The technique managed to improve the bandwidth of the LINC components (s_1 and s_2) to 4.5 channels from 14.5 channels, which is an improvement of 69% with an EVM cost of -26.9 dB. The chapter also showed measurement results. The hardware results were within 2 dB of the simulations.

6.1 Future Work

Although a number of schemes gave reasonable improvement in bandwidth for the amplifier drive signals. The cost in terms of EVM and ACI margin was high. This applies to both EER and LINC architectures. For the case of EER, the only scheme that had significant improvement: introduced amplitude correction into the constant envelope phase drive signal. This gave a tradeoff with the efficiency rather than EVM and ACI. Based on measured amplifier characteristics the efficiency was predicted to drop from 62% to 57% which is still a competitive figure. A testbed based on such a system is yet to be built and would form part of future work.

Appendix A

Complexity Calculation for IBL, IBL-PTS and RBL Schemes

Iterative bandwidth limitation (IBL), IBL with PTS (IBL-PTS) and repetitive bandwidth limitation (RBL) use the core bandwidth limitation technique from Section 3.2. This operation introduces complexity as it requires two large FFT/IFFT operations. In this appendix we derive an approximate complexity factor for these three schemes.

Let C_{bl} represent the complexity for one envelope bandwidth limitation operation according to Figure 3.4. The IBL technique manages to reduce the bandwidth of the envelope signal to an average of 2.55 channels. The bandwidth limitation process starts from $B = B_{start} = 3.5$. If B is reduced by a step size of 1 subchannel, then there is a total of $(3.5 - 2.55) * N$ number of bandwidth limitation operation. So the average complexity taken by the brute force IBL process is

$$C_{IBL} = 0.95NC_{bl} \tag{A.1}$$

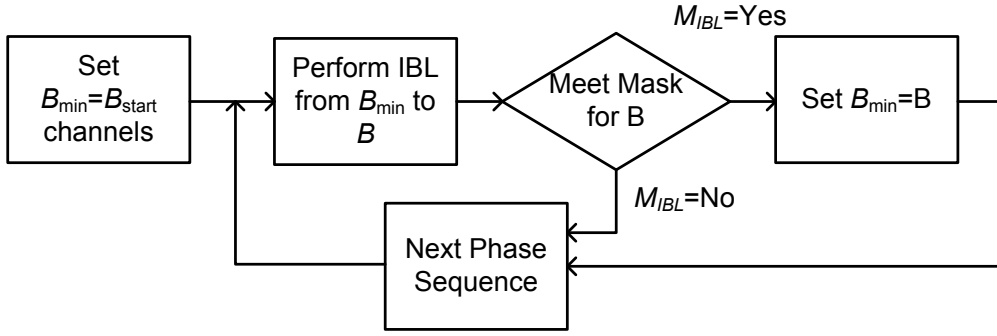


Figure A.1: Detailed flowchart of the IBL-PTS algorithm.

In case of IBL-PTS, the the same process is performed on all PTS sequences. The technique manages to reduce the envelope bandwidth to 2.21 channels. This increases the complexity by the number of total phase sequences, $S = Q^{M-1}$ and the additional bandwidth limitation steps. The flowchart in Figure A.1 shows the detailed algorithm. From the IBL-PTS method we get two outputs

$$[M_{IBL}, B] = \text{IBL (from } B_{min}) \quad (\text{A.2})$$

where, the M_{IBL} gives the condition whether the OFDM-RF signal meets the spectral mask and B gives a minimum envelope bandwidth limiting value which meets the spectral mask criterion.

$$\begin{aligned} C_{\text{IBL-PTS}} &= ((3.5 - 2.21)N + S) C_{\text{bl}} \\ &= C_{\text{IBL}} + ((2.55 - 2.21)N + S) C_{\text{bl}} \end{aligned} \quad (\text{A.3})$$

As such, the total time taken for the IBL-PTS scheme is extended by the second term.

For the repetitive bandwidth limitation (RBL) technique, the complexity is much less compared to IBL and IBL-PTS. The process limits the envelope

bandwidth i number of times for same B value. For RBL with QAM correction and $i = 10$ repetitions: the envelope bandwidth reduces to 2.6 channels. As such the time taken for the RBL process can be derived as

$$C_{\text{RBL}} = iC_{\text{bl}} \quad (\text{A.4})$$

Bibliography

- [1] X. Li and L. J. Cimini jr., "Effect of Clipping and Filtering on the performance of OFDM," *IEEE Commun. Lett.*, vol. 2, no. 5, pp. 131-33, May 1998.
- [2] A. D. Pham, "Outphase Power Amplifiers in OFDM Systems," PhD dissertation, Massachusetts Institute of Technology, Department of Electrical Engineering and Computer Science, Sept. 2005.
- [3] D. Rudolph, "Out-of-Band emissions of digital Transmissions using Kahn EER Technique," *IEEE Trans. Microw. Theory & Tech.*, vol. 50, no. 8, pp. 1979-1983, August 2002.
- [4] M. Hunton, "System and method for eliminating signal zero crosses in single and multiple channel communication systems," U.S. Patent 6931240, Aug. 16, 2005.
- [5] J. Wang; A. Zhu; X. Zhu; T. J. Brazil, "Vector Hole Punching Technique for OFDM Signals Using Circle-Tangent Shift and Unused Tones," *IEEE Transactions on Microwave Theory and Techniques*, vol.57, no.11, pp.2682-2691, Nov. 2009.
- [6] N.S. Jung, N.I. Kim and G.H. Cho, "A New High-Efficiency and Super-Fidelity Analog Audio Amplifier with the aid of Digital Switching Amplifier: Class K Amplifier, *29th Annual IEEE Power Electronics Specialists Conf.*, vol. 1, 1998, pp. 457-63.
- [7] M. Faulkner, "Advanced techniques in Mobile Radio Technology," PhD Dissertation, University of Technology Sydney, June 1992.
- [8] S. H. Han and J. H. Lee, "An overview of Peak-to-average Power Ratio Reduction Techniques for Multicarrier Transmission," *IEEE Wireless Commun.*, vol. 12, no. 2, pp. 56-65, Apr. 2005.
- [9] S. Merchan, A. G. Armada and J. L. Garcia, "OFDM performance in amplifier nonlinearity," *IEEE Trans. On Broadcasting*, vol. 44, no. 1, pp. 106-114, Mar. 1998.

- [10] H. Ochiai and H. Imai, "On the distribution of the peak-to-average power ratio in OFDM signals," *IEEE Trans. Commun.*, vol. 49, pp. 282-289, Feb. 2001.
- [11] Y. Wu and W. Y. Zou, "Performance Simulation of COFDM for TV Broadcast Application," *SMPTE Journal*, pp. 258265, May 1995.
- [12] J. Armstrong, "Peak-to-Average Power Reduction for OFDM by Repeated Clipping and Frequency Domain Filtering," *Elect. Lett.*, vol. 38, no. 9, pp. 246-47, Feb. 2002.
- [13] A. E. Jones, T. A. Wilkinson, and S. K. Barton, "Block Coding Scheme for Reduction of Peak to Mean Envelope Power Ratio of Multicarrier Transmission Schemes," *Electron. Lett.*, vol. 30, no. 25, pp. 2098-2099, Dec. 1994.
- [14] A. E. Jones and T. A. Wilkinson, "Combined Coding for Error Control and Increased Robustness to System Nonlinearities in OFDM," in *Proc. IEEE VTC '96*, Atlanta, GA, pp. 904-08, Apr.-May 1996.
- [15] R. W. Baml, R. F. H. Fischer and J. B. Huber, "Reducing the peak-to-average power ratio of multicarrier modulation by selected mapping," *Elect. Lett.*, vol. 32, no. 22, pp. 2056-2057, 1996.
- [16] M. Breiling, S. H. Mller-Weinfurtner, and J.B. Huber, "SLM peak-power reduction without explicit side information," *IEEE Comm. Lett.*, vol.5, no.6, pp.239-241, June 2001.
- [17] G. R. Hill, M. Faulkner, and J. Singh, "Reducing the peak-to-average power ratio in OFDM by cyclically shifting partial transmit sequences," *Elect. Lett.*, vol. 36, no. 6, pp. 560-561, 2000.
- [18] S. H. Han and J. H. Lee, "PAPR Reduction of OFDM signal using a reduced complexity PTS technique," *IEEE Sig. Process. Lett.*, vol. 11, pp. 887-890, Nov. 2004.
- [19] L. J. Cimini Jr. and N. R. Sollenberger, "Peak-to-average power ratio reduction of an OFDM signal using partial transmit sequences," in *Proc. IEEE. ICC'99*, vol. 1, pp. 511-515, 1999.
- [20] S. H. Muller and J. B. Huber, "OFDM with reduced peak to average power ratio by optimum combination of partial transmit sequences," *Elect. Lett.*, vol. 33, no. 5, pp. 368-369, 1997.
- [21] S. H. Muller and J. B. Huber, "A novel peak power reduction scheme for OFDM," in *Proc. PIMRC'97*, pp. 1090-1094, 1997.

- [22] J. Heiskala and J. Terry, "OFDM Wireless LANs: *A Theoretical and Practical Guide*," Sams Publishing, 2002.
- [23] B. S. Krongold, D. L. Jones, "PAR reduction in OFDM via active constellation extension," *in Proc. ICASSP '03*, vol. 4, pp. 525-528, 2003.
- [24] J. Tellado, "Peak to Average Power Reduction for Multicarrier Modulation," Ph.D. dissertation, Stanford Univ., 2000.
- [25] H. Breiling, S. H. Muller-Weinfurtner and J. B. Huber, "SLM peak-power reduction without explicit side information," *IEEE Comm. Lett.*, vol. 5, no. 6, pp.239-241, 2001.
- [26] H. S. Black, "Inventing the Negative Feedback Amplifier," *IEEE Spectrum*, pp. 55-60, Dec. 1977.
- [27] J. L. Dawson, T. H. Lee, "Automatic Phase Alignment for a Fully Integrated CMOS Cartesian Feedback Power Amplifier System," *IEEE Intl. Solid-State Circ. Conf.*, San Francisco 2003.
- [28] S. Cripps, "RF Power Amplifiers for Wireless Communications," Artech House Publishers, 1999.
- [29] T. J. Bennett, R. F. Clements, "Feedforward an Alternative Approach to Amplifier Linearization," *Radio and Elect. Engg.*, vol. 44, no. 5, pp 257-262, May 1974.
- [30] R. M. Bauman, "Adaptive Feedforward System," U.S. patent 4389618, June 21, 1983.
- [31] A. S. Sappal, M. S. Patterh and S. Sharma, "Digital Pre-distortion of Power Amplifiers using look-Up Table Method with Memory Effects," *in Proc. ICGST-PDCS*, vol. 8, Dec. 2008
- [32] D. Bondar, D. Budimir and B. Shelkovnikov, "Linearization of power amplifiers by baseband digital predistortion for OFDM transmitters," *in Proc. CriMiCo 2008*, pp. 270-271, 8-12 Sept. 2008.
- [33] F. Raab, P. Asbeck, S. Cripps, P. B. Kennington, Z. Popovic, N. Potheary, J. F. Sevic and N. Sokal "Power Amplifiers and Transmitters for RF and Microwave," *IEEE Trans. on Microw. Theory and Tech.*, vol. 50, no. 3, pp. 814-826, March 2002.
- [34] L. R. Kahn, "Single sideband transmission by envelope elimination and restoration," *in Proc. IRE*, vol. 40, pp. 803-806, July 1952.

- [35] G. Hanington, P. Chen, P. M. Asbeck, and L. E. Larson, "High efficiency power amplifier using dynamic power-supply voltage for CDMA applications," *IEEE Trans. Microw. Theory and Tech.*, vol. 47, no. 8, pp. 1471-1476, Aug. 1999.
- [36] F. Wang, A. H. Yang, D. F. Kimball, E. Larson, P. M. Asbeck, "Design of Wide-Bandwidth Envelope-Tracking Power Amplifiers for OFDM Applications," *IEEE Trans. on Microw. Theory and Tech.*, vol. 53, no. 4, April 2005.
- [37] J. Staudinger, B. Gilsdorf, D. Newman, G. Norris, G. Sadowiczak, R. Sherman, and T. Quach, "High efficiency CDMA power amplifier using dynamic envelope tracking technique," in *IEEE MTT-S Intl. Microw. Symp. Dig.*, pp.270-271, 8-12 Sept. 2008.
- [38] F.Wang, D. Kimball, D. Lie, P. Asbeck, and L. Larson, "A monolithic high-efficiency 2.4-GHz 20-dBm SiGe BiCMOS envelope-tracking OFDM power amplifier," *IEEE J. Solid-State Circuits*, vol. 42, no. 6, pp. 1271-1281, Jun. 2007.
- [39] H. Chireix, "High power outphasing modulation," in *Proc. IRE*, vol. 23, pp. 1370-1392, Nov. 1935.
- [40] D. C. Cox, "Linear Amplification with Nonlinear Components," *IEEE Tran. on Comm.*, vol. COM-22, pp. 1942-1945, 1974.
- [41] L. Couch and J. L. Walker, "A VHF LINC amplifier," in *Proc. IEEE Southeastcon'82*, pp. 122-125, 1982.
- [42] S. A. Hetzel, A. Bateman, and J. P. McGeehan, "LINC transmitter," *Elect. Lett.*, vol. 27, no. 10, pp. 844-846, May 1991.
- [43] K. Y. Chan, A. Bateman, and M. Li, "Analysis and realization of the LINC transmitter using the combined analogue locked loop universal modulator CALLUM," in *Proc. IEEE 44th Veh. Techn. Conf.*, vol. 1, pp. 484-488, June 8-10, 1994.
- [44] K. Y. Chan and A. Bateman, "Linear modulators based on RF synthesis: Realization and analysis," *IEEE Trans. Veh. Tech.*, vol. 42, pp. 321-333, June 1995.
- [45] C. Conradi and J. McRory, "Predistorted LINC transmitter," *Electronics Lett.*, vol. 38, pp. 301-302, Mar. 2002.
- [46] A. Birafane and A. Kouki, "Distortion free LINC amplifier with Chireix-outphasing combiner using phase-only predistortion." in *Proc. 34th EMC* , pp. 1069-1072, 2004.

- [47] L. Sundstrom and M. Johansson, "Effect of modulation scheme on LINC transmitter power efficiency," *Elect. Lett.*, vol. 30, no. 20, pp. 1643-1645, Sept. 1994.
- [48] L. Romano, L. Panseri, C. Samori, A. L. Lacaita, "Matching requirements in LINC transmitters for OFDM signals," *IEEE Trans. on Circ. and Syst.*, vol. 53, no. 7, pp. 1572- 1578, July 2006.
- [49] M. A. Elaal and F. Ghannuchi, "A Modified LINC Amplification System for Wireless Transceivers," in *Proc. VTC-2006 Fall*, pp.1-3, 25-28 Sept. 2006.
- [50] E. Toulouse, "LDMOS FETs Power Efficient Doherty Amps". [Online]. Available: <http://mwrf.com/Article/ArticleID/21643/21643.html>
- [51] K-J. Cho, J-H. Kim, S. P. Stapleton, "A highly efficient Doherty feedforward linear power amplifier for W-CDMA base-station applications," *IEEE Tran. on Microw. Theory and Tech.*, vol.53, no.1, pp. 292- 300, Jan. 2005.
- [52] J-Y. Lee, J-Y. Kim, J-H. Kim, K-J. Cho, S. P. Stapleton, "A High Power Asymmetric Doherty Amplifier with Improved Linear Dynamic Range," *IEEE MTT-S Intl. Microw. Symp. Digest, 2006*, pp.1348-1351, 11-16 June 2006.
- [53] Y. Yang, J. Cha, B. Shin and B. Kim, "A fully matched N-way Doherty amplifier with optimized linearity," *IEEE Trans. on Microw. Theory and Tech.*, vol. 51, no. 3, pp. 986- 993, Mar 2003.
- [54] K. J. Cho, W. J. Kim, S.P. Stapleton, J. H. Kim, B. Lee, J. J. Choi, J. Y. Kim, J. C. Lee, "Design of N-way distributed Doherty amplifier for WCDMA and OFDM applications," *Elect. Lett.*, vol. 43, no. 10, pp. 577-578, May 10 2007.
- [55] K. W. Eccleston and O. Kyaw, "Analysis and design of class-B dual fed distributed power amplifiers," *IEE - Microw., Anten. and Propag.*, vol. 151, no. 2, pp. 104- 108, Apr 2004.
- [56] U. K. Mishra, P. Parikh, Y-F. Wu, "AlGaN/GaN HEMTs-an overview of device operation and applications," in *Proc. of the IEEE*, vol. 90, no. 6, pp. 1022- 1031, Jun 2002.
- [57] F. H. Raab, P. Asbeck, S. Cripps, P. B. Kenington, Z. B. Popovic, N. Pothecary, J. F. Sevic and N. O. Sokal, "RF and microwave power amplifier and transmitter technologies - part 5," *High Freq. Elect.*, vol. 3, no. 1, pp. 46-54, 2004.

- [58] A. K. Mustafa, V. Bassoo, M. Faulkner, "Reducing the Drive Signal Bandwidths of EER Microwave Power Amplifiers," in *Proc. Intl. Microw. Symp. 2009*, pp.1525-1528, 7-12 June 2009.
- [59] A. K. Mustafa, M. Faulkner, "Iterative Bandwidth Limitation for High Efficiency EER Power Amplifier," in *Proc. ISWPC 2009*, pp.1-5, 11-13 Feb. 2009.
- [60] A. K. Mustafa, M. Faulkner, "Repetitive Fixed Bandwidth Limitation and QAM correction for EER Power Amplifier," *2010 IEEE Wireless Commun. and Networking Conf. (WCNC)*, pp. 1-5, 18-21 April 2010.
- [61] V. Bassoo, K. Tom, A. K. Mustafa, E. Cijvat, H. Sjoland, M. Faulkner, "Potential Architecture for Future Generation 'Green' Wireless Base Station," in *Proc. ISWPC 2009*, pp.1-5, 11-13 Feb. 2009.
- [62] V. Bassoo, K. Tom, A. K. Mustafa, E. Cijvat, H. Sjoland, and M. Faulkner, "A Potential Transmitter Architecture for Future Generation Green Wireless Base Station," *EURASIP J. on Wireless Comm. and Networking*, vol. 2009, Article ID 821846, 2009.
- [63] K. Tom, M. Faulkner, T. Lejon, "Performance Analysis of Pulse Width Modulated RE Class- E Power Amplifier," in *Proc. VTC-2006*, vol. 4, no. 7-10, pp. 1807 - 1811, May 2006.
- [64] A. K. Mustafa and Mike Faulkner, "Theoretical Analysis of Hole Punch Signal Conditioning for High Efficiency EER Power Amplifiers," *EURASIP Journal on Wireless Commun. and Networking*, vol. 2010, Article ID 250949, 2010.
- [65] A. Diet, C. Berland, M. Villegas and G. Baudoin, "PWM Coding and Filtering of an OFDM Envelope Signal in a C Band EER Transmitter Architecture," in *Proc. PIMRC 2004*, vol. 3, pp. 2087-2091, Sep. 2004.
- [66] F. Wang, D. Kimball, J. Popp, A. Yang, D. Y. C. Lie, P. Asbeck, and L. E. Larson, "Wideband envelope elimination and restoration power amplifier with high efficiency wideband envelope amplifier for WLAN 802.11g applications," in *Proc. IEEE MTT-S Int. Microw. Symp. Dig.*, pp. 645-648, Jun. 2005.
- [67] B. W. Walker and J. Ilow, "Spectral Regrowth Reduction for Digital Audio Broadcasting Using EER Amplifiers," in *Proc. Comm. Networks and Service Research Conf.*, May 2008.
- [68] A. Kavousian, D.K. Su and B.A. Wooley, "A Digitally Modulated Polar CMOS PA with 20MHz Signal BW," in *Proc. IEEE Solid-State Circuits Conf.*, pp. 78-79, 2007.

- [69] —, USRP, GNU radio WIKI - [Online]. Available: <http://gnuradio.org/redmine/wiki/1/UsrpFAQIntro>
- [70] —, Transceiver data sheet for USRP daughter boards. [Online]. Available: http://www.ettus.com/downloads/ettus_ds_transceiver_dbrds_v6c.pdf